UNIVERSITÀ DEGLI STUDI DI PADOVA

Sede Amministrativa: Università degli Studi di Padova
Sede Consorziata: Università degli Studi di Trieste

Dipartimento di Ingegneria Industriale

SCUOLA DI DOTTORATO DI RICERCA IN: INGEGNERIA INDUSTRIALE
INDIRIZZO: INGEGNERIA DELL'ENERGIA
CICLO XXVI

MEDIUM VOLTAGE DC INTEGRATED POWER SYSTEMS FOR LARGE ALL ELECTRIC SHIPS

Direttore della Scuola: Ch.mo Prof. Paolo Colombo

Coordinatrice d'indirizzo: Ch.ma Prof.ssa Luisa Rossetto

Tutor: Ch.mo Prof. Giorgio Sulligoi

Co-tutor: Ch.mo Prof. Giovanni Giadrossi

Dottorando: Daniele Bosich

31 gennaio 2014

To my family and Anna

Abstract

Sommario

La distribuzione in media tensione continua (Medium Voltage Direct Current, MVDC) rappresenta una tecnologia promettente per i sistemi elettrici navali del futuro. A tal riguardo, negli ultimi anni, università e centri di ricerca hanno proposto soluzioni tecniche tali da raggiungere gli obiettivi propri della tecnologia MVDC: fra gli altri, risparmio di carburante, riduzione del peso/ingombro dell'impianto elettrico, riconfigurabilità a fronte di guasti e miglioramento della power quality. D'altra parte, la più grande sfida da affrontare riguarda la regolazione della tensione che deve risultare in grado di garantire il requisito fondamentale della stabilità. Relativamente a questo aspetto, una possibile instabilità si manifesta in presenza di convertitori di carico a banda elevata, modellizzabili come carichi a potenza costante (Constant Power Loads, CPLs). Tali carichi non-lineari vengono visti dal sistema come resistenze incrementali negative, le quali rappresentano la causa dell'instabilità della tensione a fronte di un disturbo (per esempio connessione di carico, disconnessione di un sistema di genenerazione).

La tesi è stata realizzata presso il Laboratorio Grid Connected and Marine Electric Power Generation and Control (EPGC Lab.), presso l'Università degli Studi di Trieste. Lo scopo è quello di sviluppare strategie per il controllo della tensione in grado di risolvere la questione CPL, considerando un possibile impianto elettrico integrato (multi-convertitore) in MVDC, convenientemente progettato a partire dalla distribuzione reale MVAC di una nave da crociera. Nel sistema visto, l'instabilità di tensione può essere affrontata secondo diversi approcci, sfruttando soluzioni impiantistiche (aggiunta di filtraggio dedicato, aggiunta di energy storage) oppure soluzioni controllistiche. Il secondo approccio è quello seguito nella presente tesi: gli attuatori di tensione (convertitori DC/DC) vengono usati in questo caso per compensare l'instabilità di tensione. Quindi, da una parte (lato carico) i convertitori sono responsabili del problema dei carichi non-lineari, dall'altro (lato generatori) possono essere utilizzati per contribuire alla sua soluzione, garantendo un comportamento stabile. L'approccio stabilizzante previsto prevede l'utilizzo di diverse tecniche di controllo, analizzate nella tesi dal punto di vista teorico. A partire dalla tecnica semplice State Feedback (SF), altre due tecniche sono state studiate per il caso di sistema multi-converter, ovvero l'Active Damping (AD) e il Linearization via State Feedback (LSF).

L’AD è un metodo di controllo per incrementare transitorialmente la resistenza dei filtri, in modo tale da smorzare le oscillazioni di tensione: uno dei principali vantaggi è quello relativo alla semplice ingegnerizzazione su controllori digitali, mentre lo svantaggio riguarda la limitata azione stabilizzante. Pertanto, strategie basate sull’AD devono considerarsi valide per stabilizzare sistemi non critici. D’altra parte, LSF è una tecnica molto valida per ottenere una buona cancellazione delle non-linearità dei CPL, per mezzo dell’azione di convertitori DC/DC in grado di applicare un’opportuna funzione di controllo non-lineare. A fronte di una notevole capacità nello stabilizzare sistemi critici, grande attenzione va posta nella stima della funzione di controllo: conoscenza inaccurata dei parametri o errori nei feedback ai controllori possono invalidare l’approccio LSF, causando una parziale cancellazione, quindi un sistema risultante non-lineare. Le simulazioni finali hanno lo scopo di testare le tecniche AD e LSF, implementate in strategie di controllo locale e globale: la prima strategia ha lo scopo di risolvere l’instabilità direttamente sui CPL, mentre la seconda assicura la stabilità del bus.

Summary

The Medium Voltage Direct Current (MVDC) distribution represents a promising technology for future shipboard power systems. In such a topic, during the last years, universities and reserch centers have proposed technical solutions to achieve the important targets of MVDC technology, for instance fuel saving, reducing power system weight/space, reconfigurability in case of fault and enhanced power quality. Conversely, the main challenge to face regards voltage control, which has to be capable for guaranteeing the paramount requirement of stability. In regards to this aspect, a possible instability may arise due to the presence of high-bandwidth controlled load converters, modeled as Constant Power Loads (CPLs). Such non-linear loads are seen from the system as negative incremental resistances which are the cause of voltage instability in presence of a perturbation (e.g. load connection, generating system disconnection).

The thesis has been realized in the Laboratory of Grid Connected and Marine Electric Power Generation and Control (EPGC Lab.), at the University of Trieste. The aim is to develop voltage control strategies to solve the CPL issue in a realistic multi-converter MVDC Integrated Power System, which is conveniently designed considering a real cruise line MVAC distribution. In such a system, voltage instability may be engage by different approaches, exploiting plant solutions (addition of dedicated filters, addition of energy storage devices) or control solutions. The latter is followed in this thesis: in this case voltage actuators (DC/DC power converters) are used to compensate for the voltage instability: therefore, on one hand (load side) power converters are responsible for the non-linear loads’ issue but, on the other (generators side), they may be utilized to contribute in its solution, thus ensuring a stable behavior. The stabilizing approach foresees the employment of different control techniques, whose theory is focused in the thesis. Starting from the simplier State Feedback (SF), two techniques are

mostly studied in the multi-converter arrangement, i.e the Active Damping (AD) and the Linearization via State Feedback (LSF).

The AD is a control method to transiently increase the filter resistances in order to damp the voltage oscillations: one of the main pros is the simple implementation on digital controllers, whereas the drawback regards its limited stabilizing action. Therefore, strategies based on Active Damping are to be used to stabilize non-critical systems. Conversely, LSF is a well-performing technique to obtain a notable cancellation of the non-linearities related to CPLs, by exploiting the DC/DC converters to apply a proper non-linear control function. Against the notable capability in stabilizing critical systems, great attention is to be paid in control function's estimation: inaccurate system parameters or errors in controller' feedbacks may invalidate the LSF approach, determining a partial loop-cancellation, therefore a non-linear resulting power system. Final simulations are aimed in testing AD and LSF, implemented in global and local control strategies: the former strategy has the purpose to solve the instability directly on CPLs, whereas the second one ensures the bus stability.

Acknowledgements

Alla fine di un percorso durato tre anni, mi sento innanzitutto in dovere di ringraziare il mio tutor, *Professor Giorgio Sulligoi*, per la bellissima occasione di crescita e per la fiducia riposta nelle mie capacità. Il secondo ringraziamento va al mio co-tutor, *Professor Giovanni Giadrossi*: per me è stato un grande onore poter lavorare al suo fianco in questi anni.

Un pensiero speciale va alla mia *famiglia*, a quelli che mi hanno sempre seguito e a quelli che orgogliosi mi guardano da lassù. Un grazie di cuore va ai miei *genitori* per l'infinito sostegno in questa avventura e ai miei fratelli *Davide e Roberto* per gli importanti consigli che da veri fratelloni mi avete sempre dato.

Un enorme ringraziamento ad *Anna*, per il modo in cui mi guardi e per l'infinita pazienza che hai sempre dimostrato. Ti voglio tanto bene!

Particolare riconoscenza va data a *zio Giorgio*, che ha sempre dimostrato grande interesse per la mia carriera universitaria.

Infine veniamo agli amici e ai colleghi di laboratorio, troppo numerosi per essere elencati. Vi ringrazio tutti di cuore, per le serate passate assieme, per i concerti (mitraglia!), per le feste e per l'importante sostegno nei momenti duri.

Trieste, 31 gennaio 2014

Contents

List of Figures

List of Tables

Glossary

AC	Alternating Current
AD	Active Damping
AES	All Electric Ship
AVM	Average Value Model
AVR	Automatic Voltage Regulator
COTS	Commercial-Off-The-Shelf
CPL	Constant Power Load
DC	Direct Current
EPGC	Electric Power Generation and Control
FESR	Fondo Europeo di Sviluppo Regionale
HF	High Frequency
HFAC	High Frequency Alternating Current
ICR	Interface Converter Regulator
IPS	Integrated Power System
LSF	Linearization via State Feedback
MV	Medium Voltage
MVAC	Medium Voltage Alternating Current
MVDC	Medium Voltage Direct Current
NAVSEA	Naval Sea Systems Command
NGIPS	Next Generation Integrated Power System
NP	Naval Package
ONR	Office of Naval Research
PBSC	Passivity-Based Stability Criterion
PEBB	Power Electronics Building Block
PI	Proportional Integral
PID	Proportional Integral Derivative
PMSG	Permanent Magnet Synchronous Generator
PSS	Power Signal Stabilizing
PWM	Pulse-Width Modulation
QoS	Quality of Service
R&D	Research and Development
SF	State Feedback
SG	Speed Governor
S&T	Science and Technology
WFSG	Wound-Field Synchronous Generator
ZEDS	Zonal Electrical Distribution System

Introduction

Objectives

The thesis studies control solutions to solve the CPL instability in multi-converter Medium Voltage Direct Current (MVDC) power system. Such a technology appears as a good opportunity to improve the Integrated Power System (IPS) functionalities, offering important advantages for military and civilian vessels. Conversely, the main drawback regards voltage instability, which may be solved by proper control approaches. Two different control techniques are mostly analyzed in the work (Active Damping and Linearization via State Feedback). Their application allows to realize global and local control strategies, in order to guarantee the voltage stability both on the load side and on the bus.

Outline of the thesis

The work developed during the PhD has been realized in the Laboratory of Grid Connected and Marine Electric Power Generation and Control (EPGC Lab.), at the University of Trieste. It is included into an important research project, which is based on a tight integration between the knowledge of a top company (Fincantieri, the fifth shipyard all-over the world) and the reaserch expertise of two italian universities (Università degli Studi di Trieste, Politecnico di Milano). The project is called MVDC Large Ship and it is co-funded by Regione Friuli-Venezia Giulia, thanks to European funds FESR. The project target regards the study of an Integrated Power System based on Medium Voltage Direct Current distribution, in order to focus the main pros of such a technology. The activity of Large Ship project may be divided in seven different topics, singularly analyzed by a skilled team in order to provide a very extensive research. The topics are defined as follows: Prime Movers, Generating Systems, Voltage Control, Energy Storage, Power Distribution, Power Electronics and Dependability. In particular, some results proposed in this thesis are consequence of the work fulfilled for the Voltage Control’s topic.

The first Chapter of the thesis will underline the characteristics of MVDC technology, by starting from a brief introduction about All Electric Ships (AESs) and Integrated Power Systems (IPSs). Therefore, the IEEE standard recommendations and the development roadmap (NGIPS), hypothesized by the U.S. Naval Sea Systems Command, will provide a first overview on MVDC power systems.

Besides the several positive aspects that are featured in MVDC distribution (e.g. fuel saving, reducing power system weight/space, enhanced power quality), serious attention is to be paid in a critical point, i.e. the voltage instability due to the presence of Constant Power Loads (CPLs). By starting from the origin of the problem, this topic will be treated in Chapter 2, where analytical developments will provide valuable tools to conclude about the small or large-signal stability.

The third Chapter will discuss the voltage actuator approach and the control techniques to improve the voltage stability of a single converter power system. The control analysis will consider basic techniques as the State Feedback (SF) or the Active Damping (AD), and the well-performing Linearization via State Feedback (LSF) technique. In particular, the notable dynamics offered by this more accurate approach (LSF) will be carefully studied, togheter with possible negative aspects (saturation of interface converter). This Chapter is very interesting because it offers the control basis for the multi-converter implementation proposed in the following.

By starting from an actual MVAC shipboard power system, a possible power system scheme for an MVDC distribution will be proposed in Chapter 4. The topology of such a power system will depend on interface converters, whose typologies will be compared in order to evaluate the most feasible solution. By developing a first linear test, voltage dynamics results will confirm the choice of buck converters as voltage actuators in the on-board MVDC power system. Indeed, remarkable voltage dynamics represent a mandatory requirement to face the CPL voltage instability (Chapters 5 and 6).

The chosen MVDC distribution (Chapter 4) will consider two types of controllable voltage actuators to interface the bus: generating DC/DC buck converters and load DC/DC buck converters. In order to exploit the resources of each converter typology, Chapter 5 will propose an integrated voltage control, based on two strategies, global AD and local LSF. Each strategy will be aimed in realizing a different target, controlling the voltage on the bus (generating converters commanded by global AD) or on impacting loads (load converters governed by local LSF). Proper simulations will be useful to analyze the action of implemented voltage control, highlighting critical interactions between strategies.

The last Chapter will present a voltage control design procedure. To solve the CPL issue, the control design will be based on the global LSF strategy, modeling the CPLs set as an equivalent non-linear load. The determination of a suitable control function will follow a system model simplification able to represent the entire multi-converter MVDC power system as an equivalent non-linear 2^{nd} order model. By applying the LSF technique, the power system will become linear, so the traditional linear systems theory may be utilized to impose the desired dynamics.

1. Medium Voltage DC Integrated Power System IPS

1.1 Introduction

The first Chapter would focus on All Electric Ships and on the development of future shipboard power systems. Starting from a basic treatise about actual AESs and achievable technological transfer, a promising Medium Voltage Direct Current (MVDC) distribution will be presented, together with a detailed description of advantages, challenges to face and requirements. After the presentation of feasible distribution schemes, a complete discussion about stability, key issue in MVDC power system design, will be offered.

1.2 All Electric Ships

Almost 25 years ago, the development of power electronics has made it possible to endow large passenger cruise liners with electrical propulsion systems, thus achieving the concept of All Electric Ships (AESs) [1,2]. The realization of such a new ship paradigm has been driven by the increasing power demand in modern large ships, along with a growing pressure on energy conservation and environmental protection. In this context, Italian Shipyards have played a considerable role in such innovation process, both in terms of accepting this challenge and in terms of proposing innovative solutions. Important contributions in the power system integration and in the architectural definition have been the significant result of a remarkable work, fulfilled by a generation of engineers, both from the naval and the electric sectors.

As a result, 100% of modern cruise ships are electrically propelled and equipped with an Integrated Power System (IPS). The IPS is conceived to feed propulsion system and ship service loads, providing a common flexible electrical platform to guarantee system efficiency, fuel savings and an enhanced quality of service. Therefore for the realization of an efficient AES, the design of a well-performing IPS is of paramount importance. For this reason, the following Subsections will describe main AES subsystems (electrical propulsion and IPS) in order to highlight the characteristics and to force the imagination towards a possible technological transfer.

1.2.1 Propulsion system

The conversion of the Queen Elizabeth II (1986 and 1987) represents the initial point of the modern electric ships era [3]. To refit this ship by means of AES paradigm, the original steam power plant has been substituted by a diesel-electric propulsion system featuring dual machines. The electrical propulsion of an AES is therefore realized by dovetailing each propeller shaft to a large power (15-25 MW) electric motor, usually a synchronous motor (dual three-phase stator winding and wound rotor).

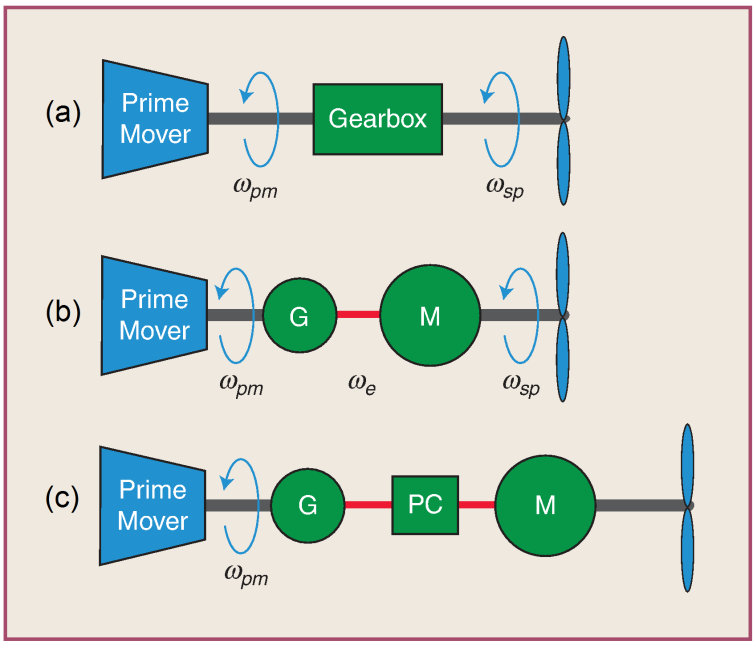

Figure 1.1 Naval propulsion systems [3].

The primary motivation for using electrical propulsion systems has been fuel savings in ships that must operate over a wide speed range, whereas the presence of electrical applications for which power quality requirements are quite high has been the second driver. AES concept is successful when the ship is expected to act with several operational scenarios over a wide speed range.

For instance icebreakers, drilling ships, cruise ships, and warships spend a considerable quantity of time at relatively low speeds, but they also operate at high speeds (large power demand) for short periods of time. In these cases, the expected fuel economy may be obtained thanks to a substantial change in the topology of electric ship propulsion (Figure 1.1). In the Figure, label G is used for the electric generator, PC represents the power converter and M the electric motor.

A classical mechanical drive (a), operating in this scenario, requires either an expensive and problematic high-power, variable-speed transmission or operation of the prime mover far from its most efficient operating speed. This negative situation is mitigated by the electrical propulsion arrangement (b), while the newest electrical drive (c) is able to completely solve it. In effect, in this case the electrical drive arrangement

acts as a continuously variable transmission, therefore the prime mover can operate at its most efficient speed regardless of the ship's speed. In topology (c), motors are fed by means of power converters, which are controlled to supply variable voltage and frequency. Three families of converters have been mostly used in combination with synchronous motors to realize electrical propulsion: cyclo-converters, synchro-converters (or synchro load-commutated inverter) and PWM voltage-source converters.

In order to complete the description of the electrical propulsion it is necessary to mention the main advantages. A list of the reasons for which naval architects prefer electric propulsion [4] may include:

1) Better dynamics performance than diesel engines.
2) Optimization of the vessel weight distribution, by positioning diesel generators in a rational way.
3) Rapid start-up of electric motors.
4) Fuel saving, keeping on duty a number of diesel generators loaded at their minimum specific consumption.
5) Augmented overall vessel comfort, being lower the vibrations of electric motors compared to diesel ones.
6) Practical absence of limits on the electric motor power.
7) On-board space optimization, by using high power-density aeronautic turbines.
8) Elimination of rudders and related mechanics, by the employment of outboard rotating pods.

1.2.2 Integrated Power System IPS

In an AES, electrical generators working in parallel and dedicated control systems (e.g. frequency/active power control, voltage/reactive power control) are to be integrated in order to constitute the shipboard power station. The latter can be considered the cornerstone of the entire ship because it supplies the Medium Voltage AC distribution system, assuring power availability and quality to the IPS. Due to the complexity of the power station and to the presence of highly impacting loads [5,6], guaranteeing high standards of power quality may represent a hard task.

Considering that no "infinite bus" exists on-board an AES, the IPS design has to seriously take into account particular conditions (such as generator trip), which may cause strong transient variations in active and reactive power, power unbalancing, thus critical issues in power quality. Therefore IPS control systems is to be designed [7] to rapidly distinguish between normal and casualty transients, dynamically reconfiguring power distribution under failure conditions to meet changing load priorities. It must be capable of supporting the reconfiguration of the power electronics functionality and network topology. Future ship power systems will require improved methods to achieve the objectives of flexible/reconfigurable power delivery, robust fault management and improved power quality for loads: IPS will have to be capable in guaranteeing these aims.

Talking about control systems, traditionally speed governors regulate generators in frequency/active power, whereas AVRs are responsible of voltage/reactive power control. The former setting is competence of the prime mover manufacturer, while the

latter regards electric design of the power station. It is remarkable to notice the importance of the second control, which impose the main busbar voltage determining the quality of IPS functioning. In an all electric cruise liner, voltage/reactive power control is achieved by endowing each AC generator with an AVR. This regulator realizes the machine's voltage control by acting on excitation, while the secondary busbar voltage regulation is performed by a controller named Master AVR. Paralleled operating generators are designed to control the same bus by their AVRs. The integral action of these regulators [5] may cause uncontrolled reactive power oscillation between generators, leading to actuators saturation and to the voltage instability of busbar. AVRs are therefore to be regulated in droop mode, introducing an equivalent virtual reactance between machine voltage and busbar voltage, in order to decouple the integral actions. Moreover, the droop mode is capable in realizing a steady-state reactive power sharing between generators operating in parallel.

1.2.3 Technological transfer

In the last years, electric propulsion concept has resulted interesting for two new types of ships (pleasure crafts and naval vessels), pointing out real possibility of technological transfer [1]. For instance, the design of an all electric luxury mega-yacht may arise from the need of added value in terms of very specific technical characteristics, whereas in AES naval vessel IPS allows architectural flexibility, improved survivability and stealth, enhancing of the war fighting capability.

The technical characteristics of an innovative mega-yacht (a craft longer than 45 m) must enable for navigation in both tropical and harsh climates. Such an operative profile obliges to fit up equipments that need to work efficiently in very different conditions, consequently with very dissimilar power requirements. A second requirement may regard the employment of new technologies to realize environmental aims, for instance reducing of gas emissions, water/oil pollution, noise. In order to conveniently meet such different needs, installing electrical propulsion can be considered a rational solution, eventually adopting electric podded drives to enhance the characteristics of maneuverability and dynamic positioning [8,9]. On the other hand, the considerable power of hotel and auxiliary justifies the adoption of an IPS, which has to be able to assure fuel saving and adequate power quality. As an all electric cruise line, the control of electro-mechanical quantities (voltage, frequency) plays again a key role.

Major navies in the world have adopted the electric propulsion and the AES architecture in new projects and constructions. Initially, adopted systems have been Medium Voltage Alternating Current (MVAC) IPSs. They has been derived from commercial vessels and applied to military ships, demonstrating that a reduction of the number of marine engineering personnel has been possible. In the very last years instead, the first combatant units in MVAC are being designed, realized or delivered (for example UK Type 45, Italian-French FREMM and US DDG 1000). In particular, the research in such topics [10,11,12] is demonstrating its effectiveness in enhancing new solution: for instance, one of the most promising developments in the field of combatant vessels could be the Medium Voltage Direct Current (MVDC) Integrated Power System (IPS), which will be discussed in the following Subsections.

1.3 Evolution towards MVDC power systems

Future projects in the field of All Electric Ships could be based on Medium Voltage DC (MVDC) Power Systems [13,14,15]. In the last years, this topic has been deeply investigated in the academia, being the MVDC distribution an enabling technology for large ships (cruise liners or military vessels). The advantages given by the new DC distribution are discussed in Subsection 1.4.1, however in this context some aspects (the reduction of power system weight/size, the decrease of fuel consumption, the efficiency enhancement and the enabling of new functionalities) can be highlighted as the most promising attractiveness for civil and military shipyard.

1.3.1 NGIPS roadmap

Although the important discoveries of investigations may be also spent in the civil framework, civil initiatives are still rare and limited to sporadic projects, for instance the MVDC Large Ship project (co-funded by Regione Friuli-Venezia Giulia thanks to European funds FESR). Research system is fundamentally funded by the military sector (e.g. by the ONR Office of Naval research), which can invest in long term ideas. This is the reason why in 2007 the U.S. Naval Sea Systems Command (NAVSEA) has proposed a Next Generation Integrated Power System (NGIPS) Technology Development Roadmap [16]. This document establishes the U.S. Navy's goal of incorporating a Medium Voltage DC (MVDC) Integrated Power System (IPS) in future surface combatants and submarines.

The Navy has been rapidly migrating toward ship designs with electric propulsion and weapon and support systems demanding substantially more electrical power. To address these power demands, ship designs are using integrated power systems that provide electric power either to propulsion or other electrical loads from a common source. Between 1992 and 2007, the U.S. Navy invested significantly in the development of the Integrated Power System (IPS), which integrates the electrical power generation and ship propulsion systems.

The primary aim of the design of an IPS is survivability and continuity (reliability) of the electrical power supply. Survivability relates to the ability of the power system, even when damaged, to support the ship's ability to continue fulfilling its missions to the degree planned for a particular threat. Quality of service (QoS) [17] serves as a metric of the continuity (reliability) of the electrical power supply by measuring the adequacy of distributed systems support for the normal, undamaged operation of its loads.

High power density and enhanced quality of service represent two main goals for a naval shipboard power system: although remarkable investment has made it possible to improve the technology for reaching the success focused on DDG 1000, a great deal of effort has to be paid to realize the final leap ensuring these aims. In this context, MVDC distribution (Section 1.4) may be a good opportunity to improve the Integrated Power System (IPS) functionalities, but the evolution towards MVDC has to start from power architecture which employs mature technology, such as the MVAC distribution. For such a reason, the following Subsections discuss a possible roadmap (Figure 1.2) for maturing different architectures (e.g. HFAC distribution) and providing the technological progress to realize future MVDC IPSs.

	Enhanced Quality of Service Requirements	Standard Quality of Service Requirements
High Power Density Requirements	Power Generation: Goal: Medium Voltage DC (MVDC) Interim: High Frequency AC (HFAC) Enhanced QOS features incorporated into Zonal Electrical Distribution	Power Generation: Goal: Medium Voltage DC (MVDC) Interim: High Frequency AC (HFAC) Standard QOS features incorporated into Zonal Electrical Distribution
Standard Power Density Requirements	Power Generation: Medium Voltage AC (MVAC) Enhanced QOS features incorporated into Zonal Electrical Distribution	Power Generation: Medium Voltage AC (MVAC) Standard QOS features incorporated into Zonal Electrical Distribution

Table 1.1 Power architectures for NGIPS requirement categories [16].

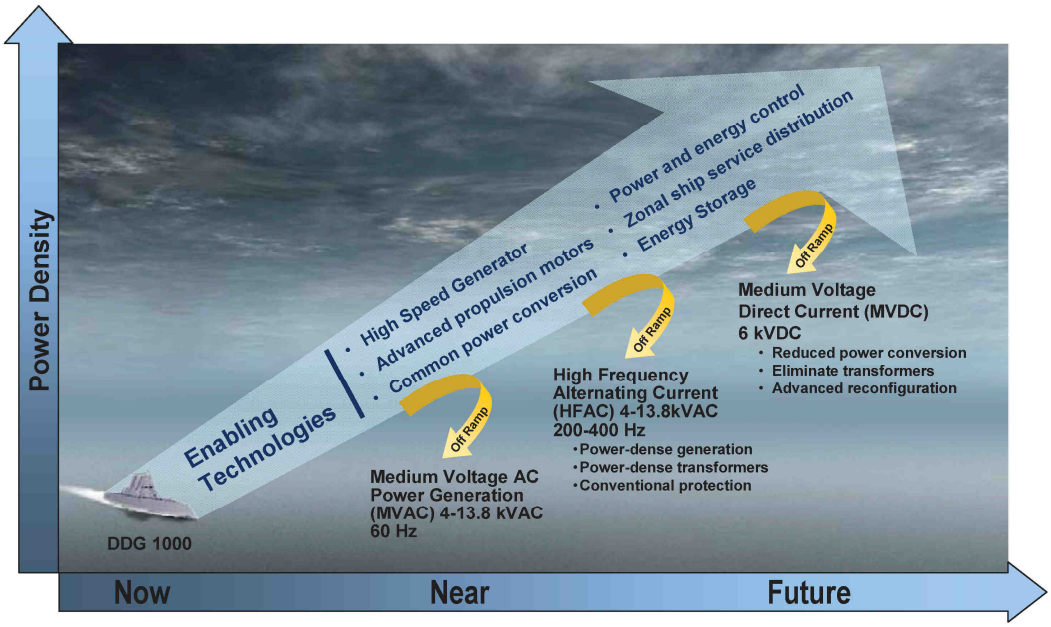

Figure 1.2 NGIPS technology development roadmap [16].

1.3.2 First step: Medium Voltage AC distribution (MVAC)

Medium Voltage AC (MVAC) is the power distribution system utilized in commercial vessels IPS design. This mature technology developed in the last twenty five years has been recently exploited on military AESs: UK Type 45, Italian-French FREMM and US DDG 1000 are the first examples of combatant units.

In an MVAC system [16], power is generated and distributed as three-phase (60 Hz) through a high-impedance grounded power system. The most common voltage levels are 6.6 kV or 11 kV in Europe and 6.9 kV or 13.8 kV in US, depending on the load power and the availability of circuit breakers of sufficient rating both for normal operation and fault current interruptions. An MVAC architecture is compatible with both a radial distribution and an innovative Zonal Electrical Distribution System (ZEDS) [18].

MVAC distribution system constitutes the first safe step towards MVDC Integrated Power Systems, being based on several years of Research and Development (R&D) in the commercial sector. This is the reason why MVAC technical architecture does not need remarkable funds to support R&D, whereas engineering efforts are required to qualify components for military applications and integrate the overall system. Although MVAC distribution has been successfully used to supply huge power amount in cruise lines [19] (e.g. total generators' power of Queen Mary II is 112 MVA), its employment is not recommended in military vessels where high power density is a requirement.

1.3.3 Second step: High Frequency AC distribution (HFAC)

The natural evolution of MVAC system is represented by future High Frequency AC (HFAC) distribution [16], where electric power will be generated at a fixed frequency greater than 60 Hz and less than 400 Hz. In US, the distribution voltage levels will be either 4.16 or 13.8 kV, while grounding could be the same as MVAC distribution (high-impedance solution).

Comparing MVAC and HFAC distributions, a lot of advantages may force the Navy and the academia in studying HFAC, such as:

a. Transformers smaller and lighter than MVAC, being the cross sectional area of a magnetic core approximately inversely proportional to the frequency of operation.
b. Harmonic filters minimized or eliminated, being the current harmonics injected on the power bus substantially reduced to low levels.
c. Galvanic isolation between subsystems, being employed a large number of transformers to isolate all loads from the HFAC high power bus.
d. Improved acoustic performance in seawater, which reduces the ship's detection range.
e. Minimal technology development.

On the other hand, some critical aspects have to be considered and solved to make realistic the high frequency distribution. For example:

a. High number of poles required for generators interfaced with slower prime movers.
b. Constant Power Loads stability issue, as MVDC systems (Chapter 2).
c. Higher ground fault current, being a function of the line to ground parasitic capacitance.
d. Paralleling of Generators at higher frequencies, being reduced the window of time that a generator breaker can close to parallel a generator.
e. Lack of design standards, practices, guides, design tools, and supporting data.
f. Lower power factor in respect to MVAC systems.

1.3.4 Third step: Medium Voltage DC distribution (MVDC)

As seen in the roadmap, MVDC distribution is located at the final stage of the IPS evolution, achievable in the long term (Figure 1.2). This architecture [16] is a direct development of HFAC technology, therefore pros and challenges (Subsection 1.4.1) are quite similar than the high-frequency approach. Nevertheless a great difference exists, being the power distributed in Medium Voltage DC rather than in High Frequency AC.

This radical change deeply impacts on power generation, system management and IPS integration, thus Science and Technology (S&T) and R&D funds are to be considerable to ensure the technological leap. In this context, this thesis wants to focus on this innovative DC distribution providing a contribution in voltage control's topic: therefore in the next Sections and Chapters, a large dissertation on Medium Voltage DC power system will be offered along with methodologies and techniques to study and guarantee the voltage system stability.

1.4 MVDC power systems fundamentals

MVDC distribution represents an opportunity to improve the naval shipboard potentiality [20], assuring the previous two main goals, i.e. high power density and enhanced quality of service. Even though these targets are mandatory for navies, their importance is evident also in case of commercial vessels, where MVDC distribution could guarantee new advanced products to compete with Far East rising economics. In this Section, MVDC fundamentals are clearly explained, whereas system requirements and recommended studies will be treated in the following.

1.4.1 Advantages and challenges

Advantages of a DC power distribution over AC are ensured by the recent successes in the development of fast switching converter for Medium Voltage applications. MVDC pros over MVAC may be summarized [13] as follows:

a. Simplifying connection and disconnection of different types and sizes of power generation and storage devices.
b. Reducing the size and ratings of switchgear.
c. Eliminating large low-frequency (50 Hz or 60 Hz) transformers.
d. Limiting and managing fault currents and enabling reconfiguration.
e. Eliminating reactive voltage drop.
f. Enabling bi-directional power flow.
g. Reducing power system weight by using high speed generators.
h. Enabling higher power ratings for a given cable size.
i. Improving control of power flows, especially in transient and emergency conditions.
j. Reducing fuel consumption by allowing variable speed prime mover operation.
k. Improving efficiency when energy storage and power conversion from batteries, fuel cells, and emergency generators is required.
l. Eliminating the need for phase angle synchronization of multiple sources and loads.

Conversely the main challenges [16] to face are:

a. Difficulty in extinguishing DC arcs in the absence of a voltage or current zero crossing.
b. Constant Power Loads stability issue.
c. Standardized methods for controlling prime mover power guaranteeing load sharing functionality.
d. An effective grounding strategy to provide galvanic isolation.
f. Lack of an established industrial base, being MVDC systems an insignificant commercial market nowadays.

In particular, point b. will be studied and solved in this PhD thesis.

1.4.2 Functional diagram

Figure 1.3 shows the functional block diagram of an MVDC power system [13] for large ships. This notional diagram will be detailed in Subsections 1.4.3 and 1.4.4, depending on the distribution architecture, i.e. radial or ZEDS.

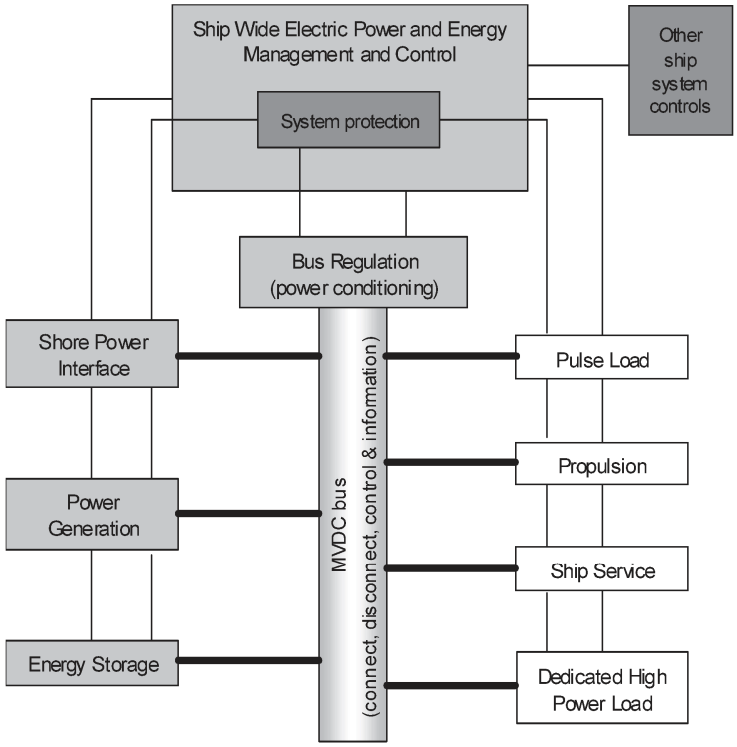

Figure 1.3 Functional block diagram of MVDC power system [13].

The functional blocks are defined [13,16] as follows:

- Shore power interface: a power source that adapts electric energy from the utility system on shore to MVDC power system (e.g. transformer + AC/DC interface converter).

- Power generation: a power source that converts prime energy from fuel into electric energy, hereinafter adapted to MVDC (e.g. prime mover + generator + AC/DC interface converter). Also fuel cell systems are classified as power generation.
- Energy storage: a power source (e.g. super-capacitor, battery, flywheel) that primarily provides power to the system when needed, facing voltage oscillations in MVDC bus caused by step-loads from relevant load devices or the loss of a generator set.
- Pulsed load: a load center that draws intermittent pulses of power from the system in military vessels (e.g. electromagnetic aircraft launch system, rail gun, and free electron laser).
- Propulsion: a load center constitute by electric motors, supplied from the DC distribution bus through variable speed drive inverters.
- Ship service: a load center that primarily draws power from the system to ship services (e.g. hotel load).
- Dedicated High Power Load: a load center that supplies 1 MW or more of power in steady-state operation (e.g. military radar, large thruster, compressor).
- Ship-wide power and energy management control: power controller to maximize the continuity-of-service of vital loads during reconfiguration operations, optimizing the power flows throughout the ship.
- System Protection: AC power subsystems can be protected against damage from faults by the traditional use of circuit breakers, whereas DC system protection is achieved through a combination of converter control and other DC circuit breaking devices (e.g. solid state DC breakers).
- MVDC bus: a functional block that allows interrupting and isolating sections of the MVDC power system.

The MVDC power system theorized in Figure 1.3 foresees extensive use of power converters [20]: every electrical power source and every electrical load are to be interfaced to the MVDC bus via power electronics devices. Interesting functionalities may be enabled by this wide exploitation of power converters: for example energy storage recharge and regenerative power created during ship crash-back maneuvers are achievable by the use of bidirectional devices.

1.4.3 Radial distribution

A functional diagram of MVDC radial distribution is depicted in Figure 1.4. In this concept scheme [13] some power converters are used to connect sources and loads to MVDC bus: conversion stages AC/DC (or eventually double stages AC/DC diode converter + DC/DC buck converter) interface power sources (e.g. turbine generator set) to the bus, while storage systems (e.g. fuel cell, battery, flywheel) are connected to MVDC bus by power converters (AC/DC converter or DC/DC converter) endowed with compact high frequency transformers. AC loads are supplied by inverters + HF transformers, whereas the high power pulse loads in military vessels should be fed by DC/DC intermittent converters. Electric motors (e.g. propulsion, thruster, pump) are finally supplied by variable speed drives.

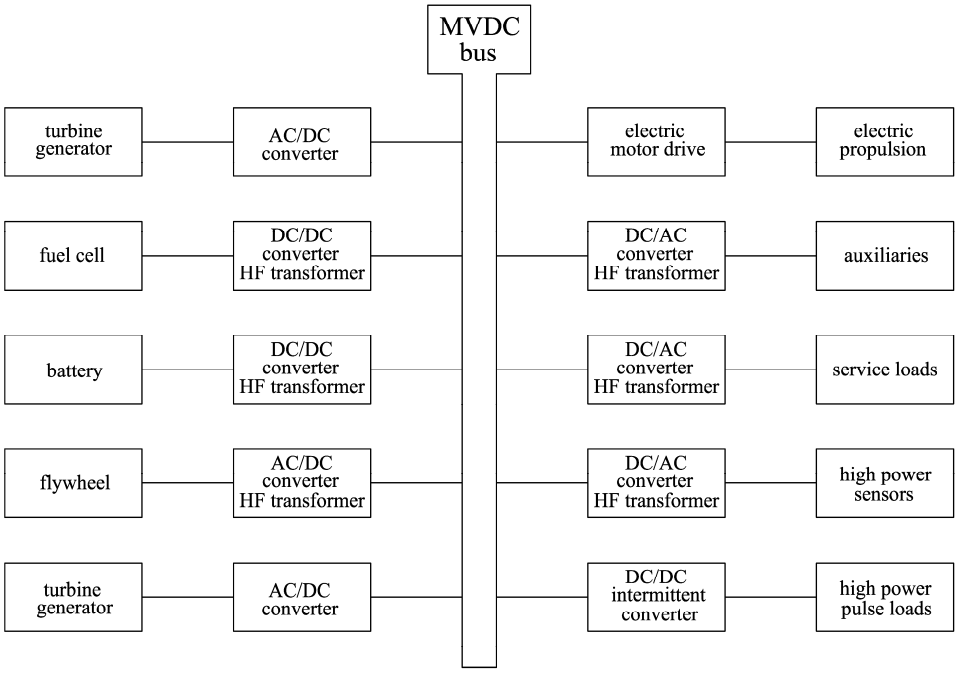

Figure 1.4 Functional block diagram of MVDC radial distribution [13].

Figure 1.5 illustrates how this functional diagram maps into a specific design.

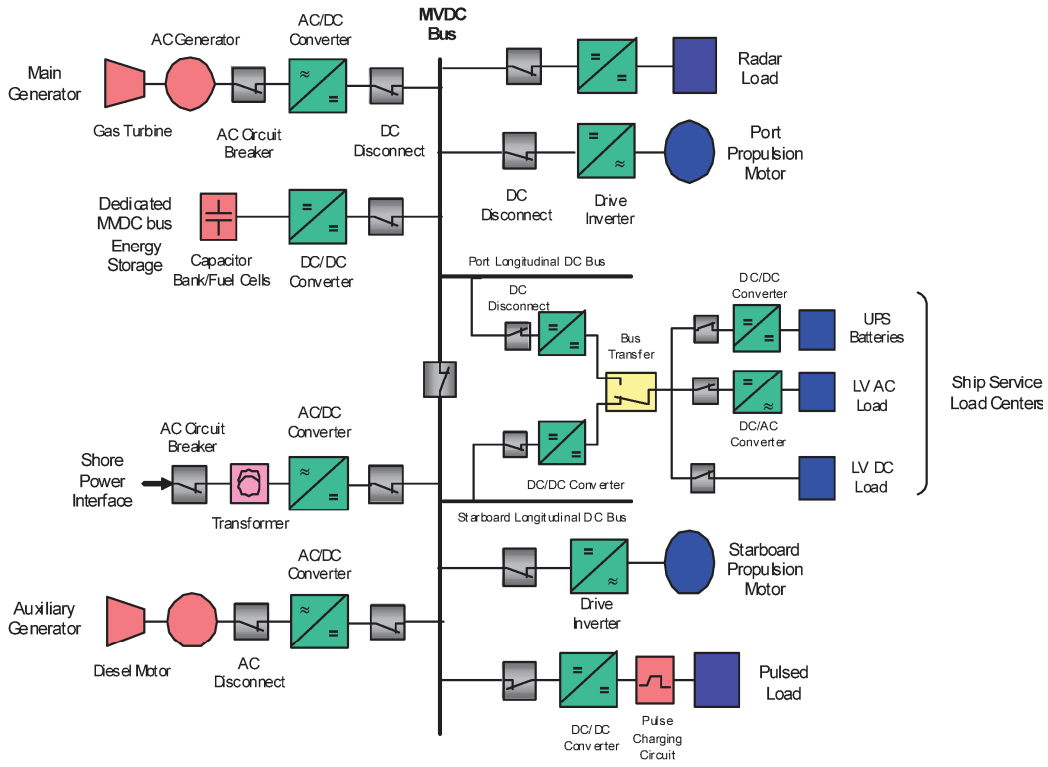

Figure 1.5 MVDC radial distribution [13].

1.4.4 Zonal distribution

In military vessels continuity of power to vital loads is essential: for this type of ships, the concept of zonal regions [18] along the vessel may be capable to assure power supply in every ship's conditions, even under extremely adverse situations. Continuity of power within each zonal load center can be enhanced automatically switching input power between port and starboard buses with automatic bus transfer switches.

Maximize operational capability is the aim of the high-performance MVDC zonal distribution highlighted in Figure 1.6. In such an architecture [13], ship service loads are distributed in four zones from bow (or fore) to stern (or aft) along the ship, fed by both port and starboard DC buses, longitudinally arranged along the ship.

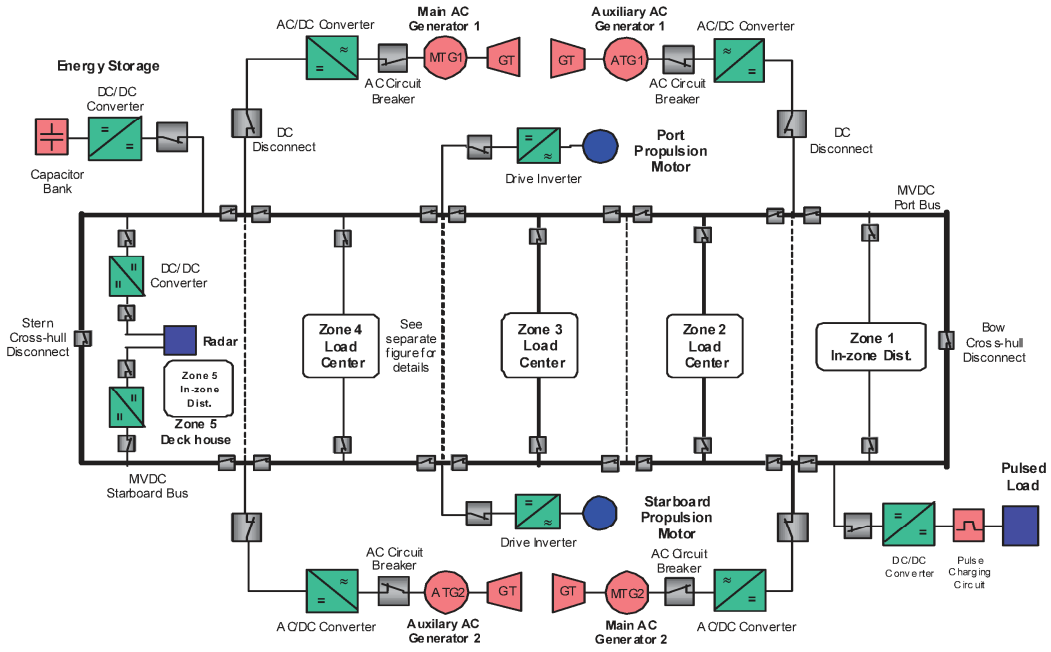

Figure 1.6 MVDC zonal distribution [13].

Bow and stern cross-hull links are provided between the port and starboard DC buses in order to provide the capability of configuring a ring-bus. Thanks to this kind of distribution, power system survivability can be enhanced by opening the bow and stern cross-hull disconnect switches to create a "split-plant" configuration, being main and auxiliary generator set connected to each longitudinal bus.

In an MVDC zonal distribution [13], vital loads (e.g. radar) are continuously fed from either port or starboard buses by operating on automatic bus transfer switches. On the other hand, ship service loads (e.g. variable speed drives, pulse loads) are directly connected to the MVDC bus by AC/DC and DC/DC power converters. Zonal load centers may present DC or AC loads: in the first case, MVDC power from the port and starboard longitudinal buses is stepped down to low-voltage DC (e.g., 800 V) by buck converters, whereas low-voltage AC (e.g. 450 V) is supplied by means of inverters.

1.5 MVDC power systems requirements

To realize an efficient and safe MVDC power system, it is necessary to respect some requirements, briefly listed in this Section. In particular, common ratings related to voltage control issue (e.g. rated voltages or stability) will be presented, whereas other aspects independent from voltage regulation (such as withstand voltages or short circuit requisites) are deeply discussed in [13,21].

1.5.1 Rated voltages

The system DC voltage is determined by desired generator voltage, propulsion motor voltage, converter design, load considerations, standard cable ratings, efficiency and arc fault energy: thus MVDC bus voltage is to be chosen to satisfy components requirements. The preferred rated voltages [13] are

1.5 kV, 3 kV, 6 kV, 12 kV, 18 kV, 24 kV or 30 kV,

obtainable with the following levels:

± 0.75 kV, ± 1.5 kV, ± 3 kV, ± 6 kV, ± 9 kV, ± 12 kV or ± 15kV

On the other hand, insulation levels depend on grounding and control/protection.

The voltage capability of MVDC power system components is classified by means of recommended voltage classes, as visible in Table 1.2. For a chosen rated voltage, the only equipment available is that categorized for a voltage class equal to or greater than the rated voltage.

	MVDC Class kV	Nominal MVDC Class Rated Voltage (kV)	Maximum MVDC Class Rated Voltage (kV)
Already established Classes	1.5	1.5 or ± 0.75	2 or ± 1
	3	3 or ± 1.5	5 or ± 2.5
Future Design Classes	6	6 or ± 3	10 or ± 5
	12	12 or ± 6	16 or ± 8
	18	18 or ± 9	22 or ± 11
	24	24 or ± 12	28 or ± 14
	30	30 or ± 15	34 or ± 17

Table 1.2 Recommended MVDC voltage classes [13].

1.5.2 Voltage tolerance

The voltage control design is strictly dependent on voltage tolerance (i.e. steady state and transient limits), therefore it is paramount to focus on this topic [13]. Design considerations (e.g. voltage loads, insulation breakdown, etc.) support the continuous (steady state) DC voltage tolerance limit, which is established equal to ± 10%, although

tighter tolerances are achievable when the sources are actively controlled through power converters.

Transient limits are highlighted in Figure 1.7, where required bus performance is stated. The time associated with zero voltage of the low voltage line is determined by how long it takes to clear a fault on the DC bus or a fault in the power source and restore the voltage to the required level.

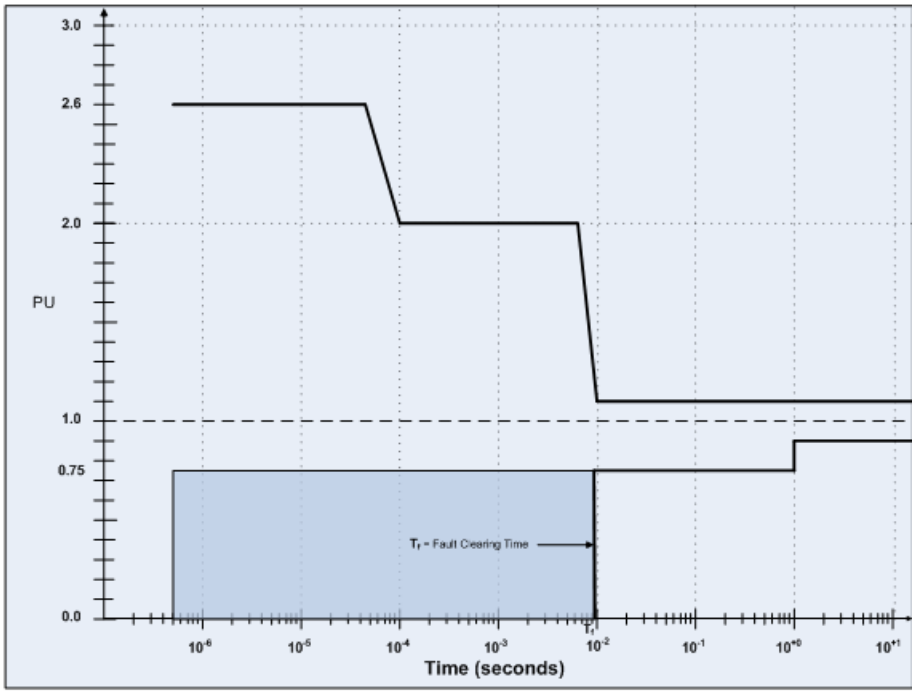

Figure 1.7 MVDC voltage tolerances worst case envelope [13].

Evidently, voltage control systems designed and tested in this thesis are in accordance with this worst case envelope.

1.5.3 Efficiency

Medium Voltage DC power systems are expected to be efficient to meet economic constraints: in such a way, it is important to achieve high efficiency under a wide range of operating situations, representative of ship mission and service conditions [13]. To provide a valiant evaluation of the overall MVDC power system, efficiency calculations has to consider every ship components, i.e. generators, motors, converters, storage devices, transformers, cables, etc. In particular, special attention should be paid to reducing the converters losses, being a dominant part of the entire MVDC system's losses. Also system voltage has to be chosen to decrease losses at most.

A range of operating conditions should be defined to calculate system efficiency, starting from the efficiency of each component typically calculated in some load points. Load conditions may be 10%, 25%, 50%, 75%, 90% and 100% respect to the rated

power, assuming 1.0 per unit voltage in each case. It is important to notice that the use of power electronics would assure high efficiency also at partial loads.

Talking about efficiency it is important to highlight the double effect of power electronics [13]: on one hand power converters are featured by additional losses, on the other hand the system losses may be decreased because there is no reactive power flow in the cables and the majority of transformers can be removed. Therefore, additional losses due to converters may be offset by an increase in overall energy efficiency.

1.5.4 Quality of service

A valuable metric of how reliably the power system provides power to the loads is given by Quality of service (QoS) [13,17]. It takes into account equipment failures and normal system operation transients, whereas survivability events (e.g. battle damage, collisions, fires, or flooding) are not considered by this metric.

Depending on service interruption time, QoS [13] may be used to classify loads by four categories: un-interruptible, short-term interrupt, long-term interrupt and exempt.

- Un-interruptible loads, which cannot tolerate service interruptions less than the reconfiguration time t_1, where t_1 is defined as the maximum time to reconfigure the distribution system without bringing on additional generation capacity (generally on the order of two seconds for conventional circuit breakers).
- Short-term interrupt loads, which can tolerate service interruptions of time t_1 but cannot tolerate interruptions longer than time t_2, that is the maximum time to bring the slowest power generation set online (usually on the order of one to five minutes).
- Long-term interrupt loads, which can tolerate service interruptions greater than t_2.
- Exempt loads, which are only used in sizing the installed generation capacity of the ship and do not need to be restored within time t_2.

To provide the QoS specified by previous load categories, proper studies are to be developed to design MVDC power system. In such an analysis, following points are evaluated:

- load shedding strategies,
- rapid-response offered by energy storage,
- propulsion motor regenerative power.

1.5.5 Quality of power

As well known, the fundamental frequency is zero in a DC power system, therefore the usual concept of harmonic distortion is not feasible to determine the DC power quality. Conversely, the quality of power on the MVDC bus is defined as a compliance with specified voltage tolerances and voltage ripple [13,15].

DC may be produced from different converters (e.g. AC/DC un-controlled rectifiers, AC/DC controlled PWM rectifiers, DC/DC buck converters) varying the output voltage

around the desired DC level. Each conversion is therefore characterized by a ripple, a superimposed component on the DC side, which depends on the operating frequency of the interfaced power converter. To ensure the optimal loads operation, filtering stage (e.g. second order RLC filters) are usually employed in order to limit this unwanted component, thus guaranteeing an rms value of ripple not higher than 5% per unit.

1.5.6 Power management

Three functions are fulfilled by the power management system [13]:

- management of power under normal conditions,
- guarantee of QoS,
- maximization of survivability.

Power management system has the important task to provide the average balance of the energy absorbed by loads and the energy produced by generation. Configuring the power system, the power management must be able to supply sufficient power to all loads under normal conditions, ensuring a sufficient spinning reserve to face possible load changes (e.g. pulse loads, large motors, large radars) and the dynamic load sharing among generators. To realize the power sharing, several approaches are possible exploiting one source converter to control the DC bus voltage while all the others regulate the DC current, or using the droop method.

The power system must be properly designed to prevent generators over-speed eventuality, caused by expected system dynamics, uncontrolled cross dynamics between generators (or prime movers) and energy storage malfunctioning. For the crash-back maneuver of propulsion motors, an energy disposal (e.g. a resistor) could be necessary in order to control the MVDC bus voltage by dissipating regenerative energy. Certainly, the energy rate (power) and the total energy dissipated are to be controlled to avoid system damage caused by heating. Instead energy storage systems (e.g. flywheels, batteries) are an efficient technology to satisfy short time imbalances between generation and loads, achieving system functionalities and performance requirements.

As well known, an MVDC power system is based on a large employment of power converters to interface sources and loads. These electronics devices should be based on the concept of PEBBs [22,23], Power Electronics Building Blocks which are commercially available. The intelligence of each PEBB is programmable and self-protecting, making possible an automatic control for smooth insertion and removal of power sources and sharing of loads. Therefore some quality of service issues are solved down-stream at the loads, eventually utilizing local energy storage. Electrical distribution reconfiguration ordered by power management system may be instead necessary to restore the power of short-term interrupt loads, whereas long-term interrupt loads rely on additional power generation commanded by power management.

Shedding strategies in priority order could be applied by power management system in critical conditions (e.g. damage or equipment failure), when a survivability response is required to supply vital loads. Survivability also involves restoring power to shed loads, in case of sufficient capacity, connectivity and minimal safety risk of reenergize.

1.5.7 Stability

Assuming a given initial operational condition, power system's stability can be defined [24] as the capacity of an electric power system to recover the equilibrium point after being subjected to a perturbation: practically a stable system is described by system variables which remain bounded after a small or large physical disturbance. The fundamental stability requirement has to be carefully evaluated in MVDC power systems, being characterized by remarkable differences in respect to terrestrial AC power systems. Anyway, being sufficient similarities in equipment, specifications, and functionality between MVAC and MVDC systems, definitions and methods treated in [24] can be useful to establish terminology, modeling and analysis approaches also in MVDC case.

Comparing future MVDC shipboard power system and the MVAC terrestrial one [13], the main difference is inherent to the islanded feature of MVDC systems, where load changes may represent a large percentage of available energy than in terrestrial systems: therefore in many cases, physical disturbances (e.g. step-loads, pulse loads) are to be considered as large perturbation in MVDC distribution systems.

The second important different aspect regards the widespread availability of power converters [13,20]: in effect in a terrestrial power grid only few lines are equipped by power electronics, whereas an MVDC system utilizes high-speed switching converters in a majority of its power transmission paths. The switching behavior of power converters leads to states whose derivatives vary continuously, thus determining a substantial change in the dynamic nature of the power system.

In addition, there are some differences in the physical nature of the instabilities [13]. For instance, MVAC power systems are characterized by the typical problem of rotor angle and frequency instability: on the other hand, this issue is naturally solved in MVDC systems, being the generators frequencies well decoupled from the MVDC bus. Conversely the high bandwidth control of MVDC loads may cause negative interactions between subsystems, even dangerous voltage instability.

The differences explained in this Subsection have the aim to make aware about MVDC stability concept, deeply different from the common idea of AC stability. Therefore analytical studies and simulations have to carefully analyze critical situations in order to guarantee the stability of the MVDC power system, by verifying one or both following stability criteria [13]:

a. Time domain criteria
   - Transient recovery time (e.g. 2 s)
   - Bounded transients (e.g. 16% – 20% maximum)
   - Absence of limit cycle behavior

b. Frequency domain criteria
   - e.g. 6 dB per 30 degrees margins
   - Frequency domain techniques using a time domain model

Stability evaluated as explained in Subsection 1.6.2 has to be ensured also in presence of Constant Power Loads (CPLs), whose destabilizing effect is focused in Chapter 2.

1.6 MVDC recommended studies and analyses

Some studies are necessary to assess MVDC system performance over the entire range of operations: in this way, next recommendations [13] may help the system designer in realizing a safe and effective DC power system. In particular, following information is mandatory in the design procedure:

- Detailed knowledge of the whole system.
- All relevant system conditions (e.g. steady state, fault, black-start).
- Required system performance in order to verify and refine the design.
- Suitable tools, methods and techniques to support the design.

In despite of AC systems, two aspects play a key role throughout all aspects of MVDC power system design: modeling and simulation, which are implemented to assist and to conduct design steps up to final realization. Thus, studies and analysis methods described herein are to be considered as an integral part of the system design.

1.6.1 Time domain system analysis

Time domain analysis is the method recommended for design MVDC power systems [13], being capable of capturing all the relevant aspects of the power system, such as non-linearity and power electronic switching. Therefore, initial conditions, input parameters, control techniques and so on are to be evaluated through a set of arranged simulations. Considering the wide number of possible power systems, design and simulations should be combined with statistical methods to obtain a fair system response over a wide range of initial conditions, inputs and system parameters.

To simulate the phenomena of interest, designers should select from several software packages, which are able to simulate MVDC power systems. The availability of proper models to suitably represent the system components (e.g. electric machines, power converters, control systems) is the main criteria in the choice of an efficient software. In any cases, the capability of the software to simulate the phenomena of interest must be verified and validated, particularizing generic models to represent the actual equipment of the system designed. Other criteria can regard the simulation time or the time to realize the entire model.

An average value model (AVM) of the entire MVDC power system can be conveniently used [13] to provide a first dynamic analysis, in order to verify control systems. The realization of this simplified model is based on an assumption about the dynamics of interest, neglecting the fast action of power converters. In effect, it is possible to implement continuous time model of the system, assuming that the slow system dynamics (given by the actions of turbine, exciter, electric machines, controllers, etc.) could be separated from the fast switching dynamics of the converters. Obviously AVM is not able to represent system dynamics around the switching frequencies, therefore averaged model has only to be considered as a quick tester to verify the interactions between power system and control. Detailed analysis by using complete model has to follow the AVM analysis, in order to take into account the switching of power converters, thus determining dynamics rather similar to reality.

1.6.2 Stability studies

As explained in Subsection 2.2, MVDC power systems are to be designed to supply high-bandwidth controlled loads. The latter constitute the so-called Constant Power Loads, which are non-linear loads responsible of the voltage's stability problem. Being the stability a key issue in an MVDC design [13,15,25], great efforts have to be paid to guarantee this requirement: in other words, system designer must ensure that the resultant non-linear system regains an equilibrium point after being subjected to perturbations. The stability of an MVDC system may be studied by several approaches, exploiting mathematical tools or analyzing the system in the frequency/time domain.

Mathematical analysis can be very useful to conclude about the small-signal stability of linearized system (e.g. Routh-Hurwitz criterion, eigenvalues study) [26,27] or about the large-signal stability of non-linear system (Lyapunov method) [27,28]. Although the potentiality of these methods is demonstrated, the stability in presence of important perturbation is hardly estimable due to the complexity of non-linear system's study.

The stability may be also verified in the frequency domain, thanks to analyses based on the developments of Nyquist stability criterion. One possibility is represented by the several stability criteria [29,30,31,32], that are useful to predict the small-signal stability of an MVDC power system: in general, the stability is verified if the product of the source impedance (S) and the load admittance (L) does not encircle the –1 point in the complex plane. In order to apply the stability criterion, input and output impedances of MVDC system (e.g. sources, loads, and cabling) are to be calculated from time-domain models (switching or average) [29] or measured by equipment commercially available. The Middelbrook criterion is common in such an analysis: being rather conservative, its utilization typically determines system designs with larger filter capacitors and slower dynamic responses. Being the MVDC power system composed by a lot of sources and loads, generalized admittance and impedance approach [32] may be valuable to assist the design of a stable MVDC system. Another effective methodology to study the stability is that offered by Passivity-Based Stability Criterion (PBSC) [33].

Finally, the stability may be investigated by the time domain analysis: the respect of stability requirements can be verified simulating the dynamic response of the modeled MVDC system, by applying suitable perturbations around the equilibrium points. In the thesis, this kind of analyses will be utilized to evaluate the stability, previously examined by mathematical tools.

1.6.3 Steps to design a stable MVDC system

The procedure [13] to guarantee small and large-signal stability for a given MVDC power system is summarized in the following:

1) Designate the stable operating (equilibrium) points.
2) Determine a stability criteria and metrics (e.g linearized system inequalities, Lyapunov conditions, damping factor, phase margin).
3) Develop the shipboard MVDC model, including switching power converters, controllers, initial conditions, system parameters and inputs.
4) Take into account non-linear behaviors (e.g iron saturation, controller limits).

5) Identify relevant steady-state operating conditions and transients between operating points, together with some “worst case” scenarios.
6) Evaluate the small-signal stability for each of the chosen operating conditions.
7) Perform enough simulations in order to confidently assess about small and large-signal stability.
8) Review the dynamic response, verifying the respect of stability criteria and metrics.

It is remarkable to notice that stability requirement can be reached thanks to the stabilizing action of control systems [27]. In these cases, as proposed in the thesis, the design of specific control techniques has to be put between points six and seven.

1.7 Conclusions

An innovative MVDC distribution for large electric propelled ships has been presented in the first Chapter. Initial considerations about the developments in AESs cruise liners have been necessary to foresee a technological transfer to military vessels. In such a sector, high power density and enhanced quality of services are of paramount importance: an evolution towards MVDC power systems has appeared as the best solution to fulfill these strategic requirements.

Therefore, a possible MVDC distribution system has been described by means of two schemes (i.e. radial and zonal) to highlight its winning advantages and challenges to face. The power system characteristics have been defined by a complete list of system requirements, e.g. rated voltages, quality of power, stability. To provide suitable tools for designing MVDC power systems, recommended studies and analysis have been proposed in the end of this Chapter.

2. Constant Power Load issue: problem definition and stability analysis

2.1 Introduction

Chapter 2 is useful to explain the causes of stability problem, one of the most critical aspects of Medium Voltage Direct Current power systems on ships. After an introduction about the CPL feature, a large dissertation will be offered to illustrate the stability studies. These analyses will provide valuable tools to conclude about the voltage stability of a given MVDC shipboard power system that employs Constant Power Loads.

2.2 CPL stability issue

The Constant Power Load behavior is characteristic of MVDC power systems [13,27]. As explained in the following, this feature may cause DC voltage instability, so the system collapse in case of perturbation. Starting from the physical cause, the Section will treat the non-linear load characteristic. Then a single converter reference case will be established together with the equivalent circuit model and the equilibrium points evaluation.

2.2.1 Cause

Future MVDC power systems are to be based on a large diffusion of power converters, in order to interface generating systems and loads to MVDC bus [13]. From the stability point of view, the most important characteristic of these power converters is the expected high-bandwidth control.

The tight control, although desirable, tends to keep the load power constant even under fast current/voltage variation: such an aspect reflects at the converter input terminal as a Constant Power Load (CPL) behavior [28,34,35,36].

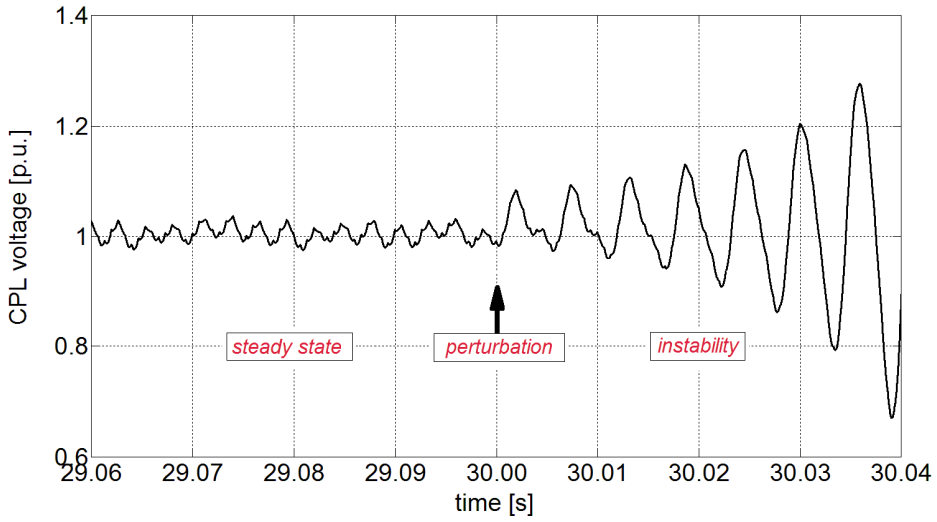

Figure 2.1 Constant Power Load stability issue.

The instability problem arises because of two elements [28]: the above-mentioned CPL and the DC filtering stage, indispensable to guarantee acceptable ripples in DC voltage and current. After a perturbation (small or large) the CPL combined with the DC filter determines negatively damped oscillations, thus the voltage instability shown in Figure 2.1.

2.2.2 Load characteristic

A possible CPL [35] is represented by a motor drive, therefore an electric motor fed by a high-bandwidth controlled DC/AC power converter (i.e. an inverter).

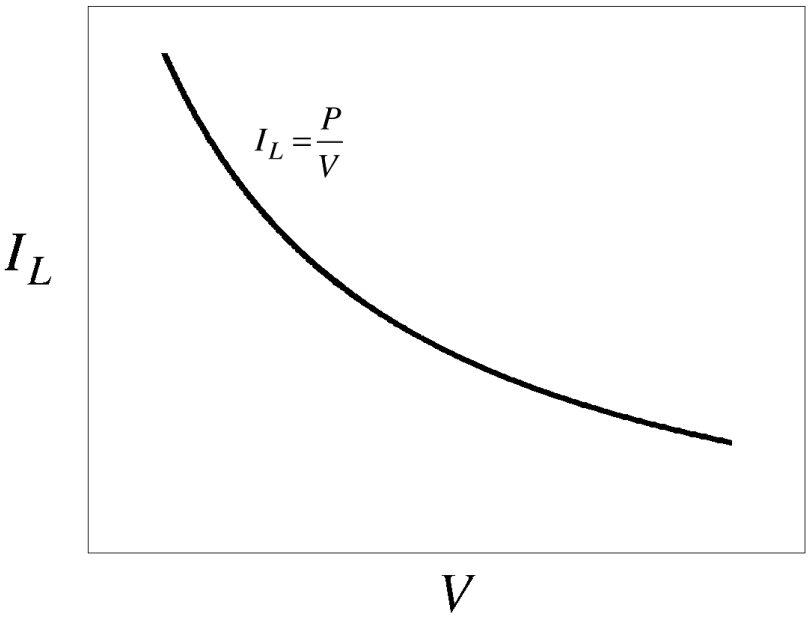

Figure 2.2 Constant Power Load non-linear characteristic.

Hypothesizing a linear relation between torque τ and speed ω and assuming a tight control capable for maintaining ω almost constant, it is possible to conclude about the torque constancy. As well known, the motor drive output power is given by the multiplication of speed and torque: therefore the constancy of the input power *P* is verified, being constant the output power and drive system efficiency.

Thus the motor drive can be modeled by a non-linear load ($I_L=P/V$), so that an increase of the load voltage *V* imposes a decrease of the load current I_L (Figure 2.2). In presence of a perturbation, this non-linear characteristic triggers the instable phenomenon depicted in Figure 2.1.

2.2.3 Case of study

For further analysis, the following figure (Figure 2.3) provides a simple reference scheme to model a single converter case. Knowing the complexity of stability study, it is important to start with this very basic case, whereas the extension to multi-converter MVDC power systems will be developed in Chapters 5 and 6.

In particular the proposed power system exploits a single DC/DC interface converter (Subsection 4.2.2) to supply a generic Constant Power Load (CPL) through the filtering stage. All the elements responsible for DC stability issue are therefore considered in this scheme.

In order to provide a slim mathematical symbolism, the whole thesis presents the same index simplification: variable quantities (e.g. *V*) are to be considered function of time, so *V(t)* in the example.

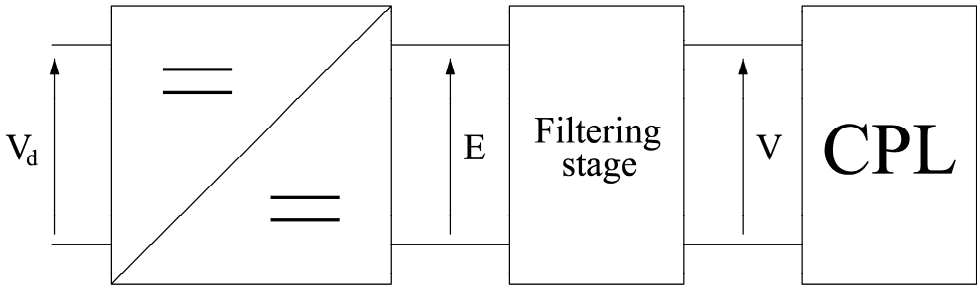

Figure 2.3 Reference scheme.

2.2.4 Equivalent circuit model

For the stability analysis, the case of study can be modeled by the DC-link equivalent circuit of Figure 2.4. Although such a model may appear very simplified, its effectiveness for modeling the CPL voltage instability is universally recognized [15,26,27,28].

The next mathematical developments are based on some assumptions: first of all the input voltage *E* is the mean value of the output DC/DC converter voltage (average value model AVM adoption), therefore the interface converter switching is neglected; secondly, *P* is the power of the CPL, modeled by the non-linear load.

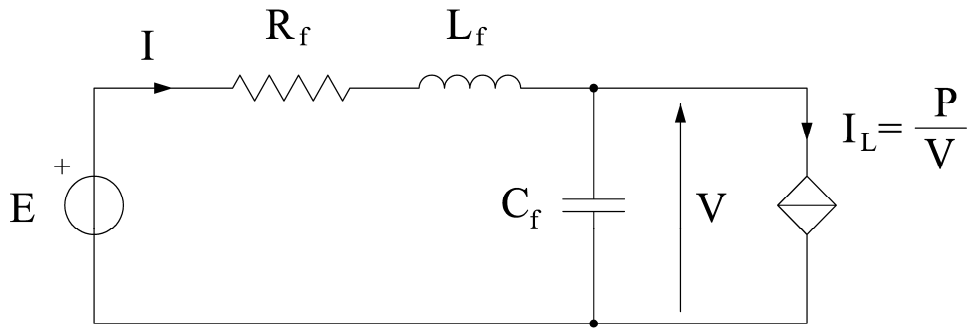

Figure 2.4 DC-link equivalent circuit.

The MVDC power system is completed by a low-pass 2nd order filter (parameters are R_f, L_f and C_f), in order to suitably filter the square-wave voltage of the interface converter. Consequently the following non-linear 2nd order system of equations (non-linearity appears in the term $I_L=P/V$) may be used to represent the interested dynamics:

$$\begin{cases} L_f \dfrac{\mathrm{d}I}{\mathrm{d}t} = E - R_f I - V & (2.1) \\ C_f \dfrac{\mathrm{d}V}{\mathrm{d}t} = I - I_L = I - \dfrac{P}{V} & (2.2) \end{cases}$$

2.2.5 Equilibrium points

It is possible to obtain the two equilibrium points for the system starting from (2.1)-(2.2). By annulling the derivative terms, next equations are defined

$$\begin{cases} 0 = E - R_f I - V & (2.3) \\ 0 = I - I_L = I - \dfrac{P}{V} & (2.4) \end{cases}$$

whereas following formula is determined after a substitution

$$V = E - R_f I = E - R_f \frac{P}{V} \qquad (2.5)$$

The second degree equation is found multiplying the previous one by the CPL voltage V,

$$V^2 - EV + R_f P = 0 \tag{2.6}$$

thus the equilibrium points are finally defined

$$\begin{cases} {}_1V_2 = \dfrac{E}{2} \pm \sqrt{\left(\dfrac{E}{2}\right)^2 - R_f P} & (2.7) \\ {}_1I_2 = \dfrac{P}{{}_1V_2} & (2.8) \end{cases}$$

Equilibrium points [28] could be graphically deduced (Figure 2.5) intersecting the source equation (2.3) and the load equation (2.4). By observing (2.7)-(2.8), $R_f P$ results critical in the complex solution: if this term is small, the equilibrium points are real and positive, otherwise the equilibrium points become complex if $R_f P$ becomes larger than half the source voltage E squared. Obviously equilibrium points values cannot be complex, being representative of physical current and voltage.

The points of intersection on the (V,I_L) plane may be either two, one, or none: the two intersections merge into one point as the slope (-1/R_f) of the source line is decreased. The equilibrium points (intersections) disappear if the slope is decreased further: the intersection point absence between source and load lines states a no physically realizable operating point.

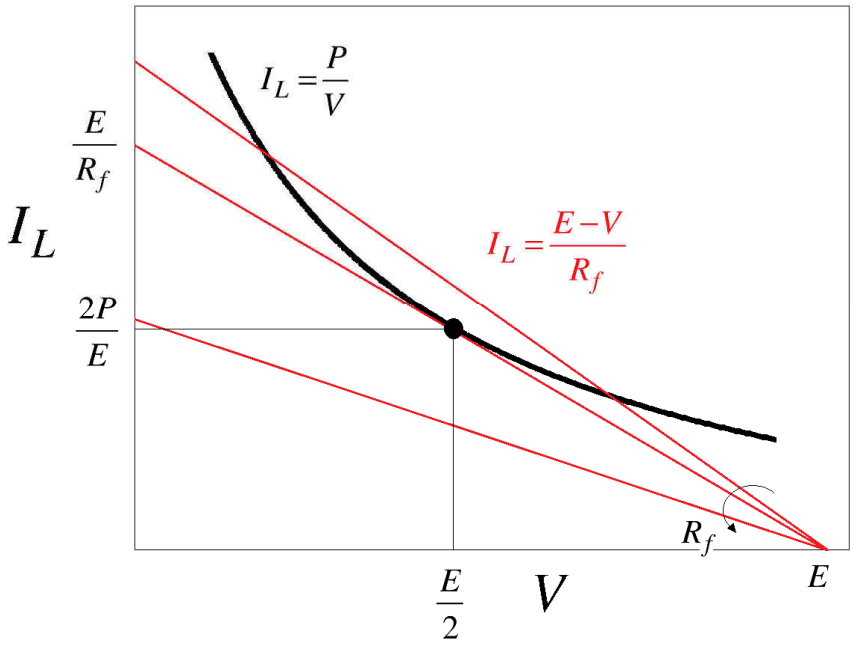

Figure 2.5 Equilibrium points graphical determination.

To avoid unfeasible equilibrium points, resistor R_f should satisfy

$$R_f P \leq \left(\frac{E}{2}\right)^2 \quad \Rightarrow \quad R_f \leq \frac{E^2}{4P} \tag{2.9}$$

This condition on R_f is the first stability criterion: a voltage instability is certainly shown up in case of condition violation.

The general considerations given are now applied to a particular case, where a proper choice of the source voltage E_0 is capable in forcing the desired steady state condition (CPL voltage V_0 and relative current I_0) :

$$E = E_0 = R_f I_0 + V_0 = R_f \frac{P}{V_0} + V_0 \tag{2.10}$$

Thus previous equation (2.7) for equilibrium points determination can be used to verify the chosen steady state equilibrium point (V_0,I_0) and to determine the second one, as shown in Figure 2.6.

$$\begin{aligned} V_{0_{12}} &= \frac{R_f P}{2V_0} + \frac{V_0}{2} \pm \sqrt{\left(\frac{R_f P}{2V_0} + \frac{V_0}{2}\right)^2 - R_f P} = \\ &= \frac{R_f P}{2V_0} + \frac{V_0}{2} \pm \sqrt{\frac{R_f^2 P^2}{4V_0^2} + \frac{V_0^2}{4} + \frac{R_f P}{2} - R_f P} = \\ &= \frac{R_f P}{2V_0} + \frac{V_0}{2} \pm \sqrt{\left(-\frac{R_f P}{2V_0} + \frac{V_0}{2}\right)^2} = \\ &= \frac{R_f P}{2V_0} + \frac{V_0}{2} \pm \left(-\frac{R_f P}{2V_0} + \frac{V_0}{2}\right) \end{aligned} \tag{2.11}$$

The first equilibrium point (V_{01},I_{01}) is the desired steady state point calculated by imposing the plus, whereas the second one (V_{02},I_{02}) corresponds to an instable operating point, as explained in Subsection 2.3.3.

$$\begin{cases} V_{0_1} = V_0 \\ I_{0_1} = \dfrac{P}{V_0} \end{cases} \tag{2.12}$$

$$\begin{cases} V_{0_2} = \dfrac{R_f P}{V_0} \\ I_{0_2} = \dfrac{V_0}{R_f} \end{cases} \tag{2.13}$$

The equilibrium points 1 and 2 may be moved by varying the source voltage E_0, tending to merge into one singular point t as E_0 is reduced. When the left term in (2.11) is null,

$$-\frac{R_f P}{2V_0} + \frac{V_0}{2} = 0 \qquad \Rightarrow \qquad V_0 = \sqrt{R_f P} \tag{2.14}$$

the source characteristic is tangent to the hyperbole and the two intersections coincide into one point t, whose voltage and current are defined by substituting equation (2.14) in (2.12) or in (2.13):

$$\begin{cases} V_{0_t} = \sqrt{R_f P} \\ I_{0_t} = \sqrt{\dfrac{P}{R_f}} \end{cases} \tag{2.15}$$

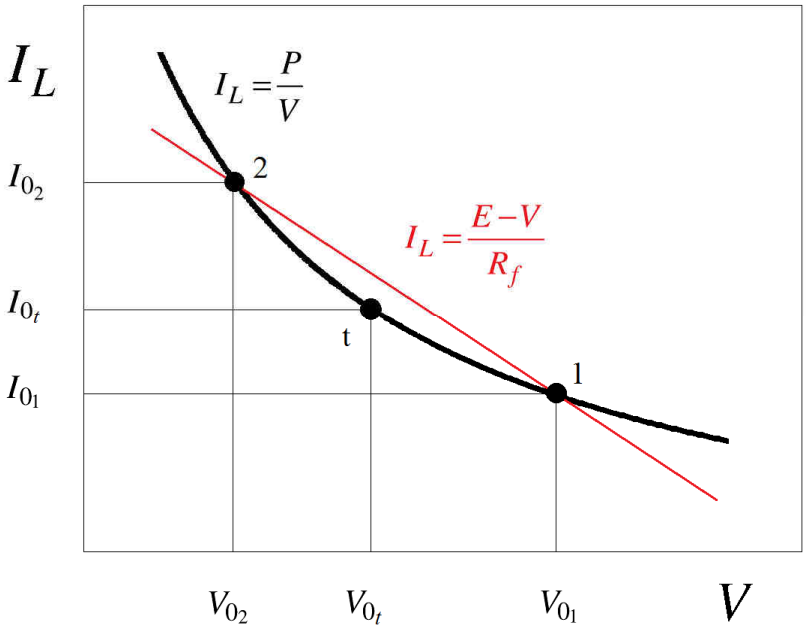

Figure 2.6 Equilibrium points.

Figure 2.6 clearly shows the behavior of equilibrium points: as voltage E_0 is dropping, point 2 tends to move to the right whereas point 1 is shifting to the left. These movements are bound by point t, whose related voltage represents the upper value for V_{02} and the lower one for V_{01}.

2.3 Small-signal stability

It is possible to obtain a small-signal model [27] by linearizing the system (2.1)-(2.2) in the equilibrium point 1, characterized by voltage $V_{01}=V_0$ and current $I_{01}=I_0$. The stability of this point is now hypothesized a priori, whereas a complete analysis of equilibrium points stability will be provided in Subsection 2.3.3.

2.3.1 Linearization method

The linearization procedure is utilized to define the equivalent circuit reported in Figure 2.7, useful in small-signal stability study. The well-known method of linearization [37,38] proposes to develop the non-linear function in an equilibrium point 0 by means of the Taylor series: the final linear function is obtained by cutting the series at the first term.

$$\begin{cases} L_f \dfrac{\mathrm{d}(\Delta I)}{\mathrm{d}t} = \Delta E - R_f \Delta I - \Delta V & (2.16) \\ C_f \dfrac{\mathrm{d}(\Delta V)}{\mathrm{d}t} = \Delta I - \left(\dfrac{\partial I_L}{\partial V}\right)_0 = \Delta I - \left(-\dfrac{P}{V^2}\right)_0 \Delta V = \Delta I - \dfrac{\Delta V}{-R^0} & (2.17) \end{cases}$$

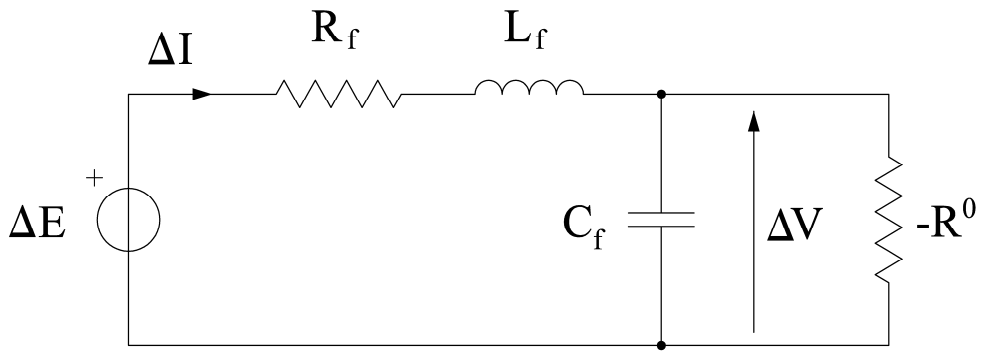

Figure 2.7 DC-link small-signal equivalent circuit.

In the scheme of Figure 2.7, a negative resistance $-R^0=(-V^2/P)_0$ appears, capable for modeling the CPL behavior in the neighborhood of the equilibrium point [35]. The linearization method is explained by Figure 2.8, where the non-linear behavior of hyperbole is conveniently approximated by its tangent (green line) in the equilibrium point 0: the slope of the green line is given by $(-1/R^0)$.

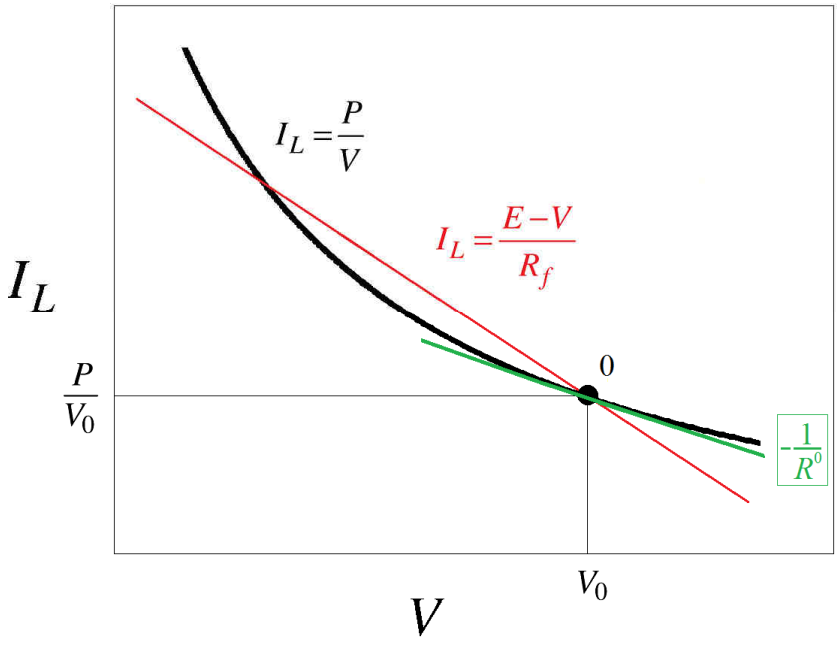

Figure 2.8 Small-signal equivalent circuit explanation.

2.3.2 Stability analysis

The characteristic equation related to the linearized system (2.16)-(2.17) is needed to evaluate the small-signal stability [27]. Therefore, a second order differential equation is deduced by deriving (2.17) and substituting in it the current derivative:

$$\begin{aligned}\frac{\mathrm{d}^2(\Delta V)}{\mathrm{d}t^2} &= \frac{1}{C_f}\frac{\mathrm{d}(\Delta I)}{\mathrm{d}t} + \frac{1}{R^0 C_f}\frac{\mathrm{d}(\Delta V)}{\mathrm{d}t} = \\ &= \frac{1}{L_f C_f}\left[\Delta E - R_f \Delta I - \Delta V\right] + \frac{1}{R^0 C_f}\frac{\mathrm{d}(\Delta V)}{\mathrm{d}t} \\ &= \frac{1}{L_f C_f}\left[\Delta E - C_f R_f \frac{\mathrm{d}(\Delta V)}{\mathrm{d}t} + R_f \frac{\Delta V}{R^0} - \Delta V\right] + \frac{1}{R^0 C_f}\frac{\mathrm{d}(\Delta V)}{\mathrm{d}t}\end{aligned} \tag{2.18}$$

Annulling the voltage input,

$$\frac{\mathrm{d}^2(\Delta V)}{\mathrm{d}t^2} + \frac{1}{L_f C_f}\left(C_f R_f - \frac{L_f}{R^0}\right)\frac{\mathrm{d}(\Delta V)}{\mathrm{d}t} + \frac{1}{L_f C_f}\left(1 - \frac{R_f}{R^0}\right) = 0 \tag{2.19}$$

the characteristic equation is clearly identified (2.20),

$$s^2+\frac{1}{L_fC_f}\left(C_fR_f-\frac{L_f}{R^0}\right)s+\frac{1}{L_fC_f}\left(1-\frac{R_f}{R^0}\right)=0 \tag{2.20}$$

as well as the stability conditions

$$\begin{cases}1-\dfrac{R_f}{R^0}>0\\ C_fR_f-\dfrac{L_f}{R^0}>0\end{cases}\Rightarrow\begin{cases}R^0>R_f & (2.21)\\ R^0>\dfrac{L_f}{R_fC_f} & (2.22)\end{cases}$$

In presence of a perturbation, the validity of the two conditions assures a stable damped voltage behavior, oscillatory (complex poles, blue line in Figure 2.9) or aperiodic (real poles, green line) depending on parameters values [27].

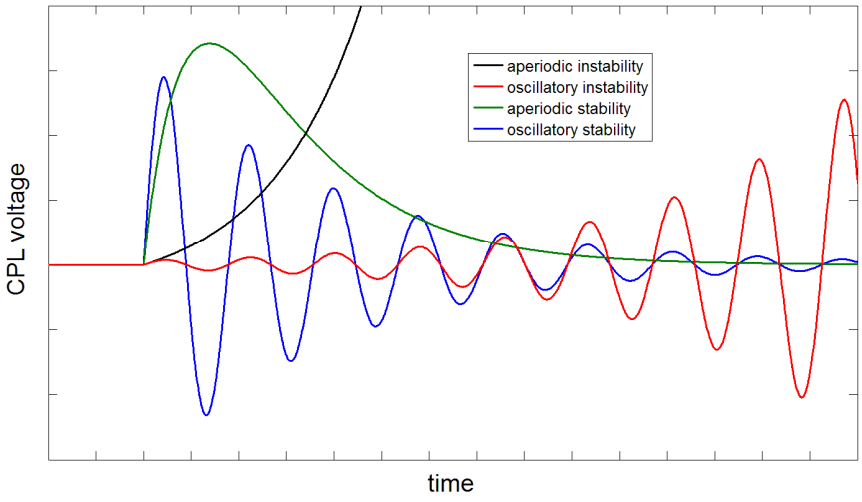

Figure 2.9 Stability conditions analysis by impulse response.

If (2.21) is the only verified condition, the consequent instability can be oscillatory (red line) or even aperiodic (black line) due to two poles with positive real part. Instead, if condition (2.21) does not hold, an aperiodic instability arises (black line), independently from the (2.22) validity, being one real pole positive.

In conditions (2.21)-(2.22), the three parameters R_f, L_f, C_f are related to the filtering stage whereas only R^0 is function of the CPL power. It is evident the role of the filtering stage in the stability issue: only a dedicated design (i.e. a high current ripple and a low voltage ripple, that is a small L_f and a large C_f) is capable for assuring the voltage stability in presence of a small negative resistance R^0 (i.e. a large non-linear power P).

2.3.3 Equilibrium points stability

The stability of an equilibrium point may be evaluated thanks to the previous linearization method, thus linerizing the non-linear system in that point and determining the eigenvalues [37,38]: an equilibrium point behaves as an asymptotically stable point if the eigenvalues have negative real part, whereas the equilibrium point is instable if there is at least one eigenvalue characterized by positive real part.

As specified in [37], an alternative procedure can follow the theory stated avoiding the eigenvalues determination: the equilibrium points stability may be evaluated by using the characteristic equation obtained in (2.20),

$$s^2 + \frac{1}{L_f C_f}\left(C_f R_f - \frac{L_f}{R^{0x}}\right)s + \frac{1}{L_f C_f}\left(1 - \frac{R_f}{R^{0x}}\right) = 0 \tag{2.23}$$

imposing the stability conditions derived from (2.21)-(2.22),

$$\begin{cases} 1 - \dfrac{R_f}{R^{0x}} > 0 \\ C_f R_f - \dfrac{L_f}{R^{0x}} > 0 \end{cases} \Rightarrow \quad \begin{cases} R^{0x} > R_f & (2.24) \\ R^{0x} > \dfrac{L_f}{R_f C_f} & (2.25) \end{cases}$$

and considering a generic negative resistance R^{0x} to model a generic equilibrium point. Defining R^{0x} as follows,

$$R^{0x} = -\left(-\frac{V^2}{P}\right)_{0x} = \frac{V_{0x}^2}{P} \tag{2.26}$$

conditions (2.27)-(2.28) can be rewritten in terms of equilibrium point voltage:

$$\begin{cases} V_{0x} > \sqrt{R_f P} & (2.27) \\ V_{0x} > \sqrt{\dfrac{L_f P}{C_f R_f}} & (2.28) \end{cases}$$

Voltage limits of equations (2.27)-(2.28) express stability conditions for every generic equilibrium point x.

As observed in 2.2.5, the voltage of equilibrium point 2 has a maximum defined by the point t voltage (Figure 2.6), which results equal to the limit (2.27): it is therefore clear that voltage V_{02} can never respect the first stability condition, thus point 2 is definitely always instable.

On the other hand, being the limit (2.27) a minimum for voltage V_{01}, previous conditions may be utilized to study the stability of equilibrium point 1, which corresponds (2.12) to the desired steady state point. Therefore the operating point (V_0,I_0) imposed by a proper source voltage E_0 is asymptotically stable if and only if

$$\begin{cases} V_0 > \sqrt{R_f P} & (2.29) \\ V_0 > \sqrt{\dfrac{L_f P}{C_f R_f}} & (2.30) \end{cases}$$

2.4 Large-signal stability

Analysis on linearized system considers a so called small range of perturbations, therefore it may only ensure the small-signal stability. Such an analysis is very useful in AC land system (perturbations are usually limited), but it can appear insufficient in case of islanded MVDC shipboard power systems, where large disturbances are expected to arise being the loads power comparable to the generators one. This is the reason why both small and large-signals stability investigations are considered necessary in MVDC voltage control design.

2.4.1 Lyapunov method

The large-signal stability can be studied by the Lyapunov theory [38,39], proving the asymptotic stability of the equilibrium point previously established by (2.29)-(2.30) and then estimating the attraction region for the non-linear system. This corresponds to determine how far the state can be perturbed and still (asymptotically) return to the equilibrium point. The main difficulty in applying this non-linear method is the analytical definition of a valid Lyapunov function candidate [32,40], making numerical approach the prevalent resolution. Anyway, in this Subsection a Lyapunov method will be utilized to define the region of attraction around the equilibrium point 0.

For the single converter case presented in this Chapter, the Lyapunov condition (2.31) may be found in [27]. This paper has offered a methodology to study the stability of a controlled non-linear system, but its equations may be also used to study the no-controlled case by annulling control gains:

$$V \geq \sqrt{\frac{L_f P}{R_f C_f}} = V_{\lim} \qquad (2.31)$$

This simple condition is useful to confirm the equilibrium point stability and to define a region of attraction around a stable equilibrium point, which acts as an attracting point. It means that the free evolution of the system having initial states

(characterized by $V(t_0)$ initial capacitor voltage and $I(t_0)$ initial inductor current) belonging to this region do have trajectories that end into the equilibrium point. Any perturbation (small or large) that moves the states of the system from the initial equilibrium point (V_0,I_0) to another point which belongs to the region of attraction will provoke a stable system response, that will eventually bring the states back to the initial equilibrium point. For larger perturbations, for which voltage V drops below the previous limit, instability is not guaranteed, considering that Lyapunov theory provides only a sufficient condition (2.31): initial states for which conditions are not verified may be in any case stable.

Last general voltage equation may be particularized in two different ways. By substituting V_0 to V, equation (2.31) may ensure equilibrium point stability, providing the same condition discussed in (2.30). Instead the stability of the initial state $V(t_0)$ can be studied by rewriting (2.31) as follows:

$$V(t_0) \geq \sqrt{\frac{L_f P}{R_f C_f}} = V_{\lim} \tag{2.32}$$

As said in the small-signal stability study (Subsection 2.3.2), it is possible to conclude about the influence of system parameters by observing the large-signal inequality (2.32): the region of attraction tends to decline (thus $V_{\lim}$ grows) as R_f and C_f decrease or L_f and P increase. This matter suggests the particular importance of the filter design in guaranteeing the large-signal DC stability in case of a given power P.

2.5 Conclusions

The Chapter 2 has treated the stability related to CPLs, a key issue in MVDC power systems. Starting from some considerations about the causes of such non-linear behavior, a case of study has been proposed in order to set up proper methods to study stability.

Firstly, the linearization method has demonstrated to be a valuable approach to ensure equilibrium point stability. Secondly, this method is useful to evaluate the small-signal stability, therefore to study the system behavior in presence of small perturbations, by observing the eigenvalues of linearized system.

Being islanded shipboard power systems characterized by loads power comparable to the generators one, the small-signal analysis has resulted insufficient in the MVDC system design: indeed, it is important to guarantee stability in presence of large perturbations, as those caused by the connections/disconnections of high power loads. To this aim, a Lypaunov method has been taken from literature in order to provide a sufficient stability condition.

3. Voltage control solutions to face the CPL instability

3.1 Introduction

In the last Chapter, the stability issue related to CPLs has been studied and some methods have been proposed to verify the system behavior in presence of small or large perturbations. The destabilizing effect of a CPL may be solved by different approaches, introduced in the present Chapter. After a brief summary about voltage control system requirements, the voltage actuators approach will be utilized to solve instability in a single converter case by exploiting different techniques (i.e State Feedback, Active Damping and Linearization via State Feedback). Numerical simulations will be performed to analyze techniques operation, highlighting related pros and cons. Best solutions will be applied in the multi-converter case of Chapters 5 and 6.

3.2 Approaches to achieve voltage stability

Many contributions can be found in literature concerning the CPL instability and several approaches [36] have been proposed for solving this problem. They can be summarized in plant solutions (addition of dedicated filters, addition of energy storage devices) and control solutions. Being system feasibility and reliability key issues in MVDC power system design, plant solutions are not considered in this thesis, which prefers to develop control solutions. By reference to the latter, two different approaches may be employed: the load approach and the voltage actuator approach.

The former focuses on destabilizing loads by proposing converter's design procedures [29,30,31,32] to avoid the MVDC power system instability: load converters themselves can be designed to prevent the voltage instability, either by the operation of proper control algorithms or by the application of automatic shut-down procedures, if the voltage tends to exit from stable operative ranges [41,42]. However, the load approach makes it necessary to specify dedicated requirements for load converters [27], thus preventing the employment of Commercial-Off-The-Shelf (COTS) equipment.

The voltage actuator approach [27] may be an alternative to stabilize the MVDC bus, by utilizing the generating systems as sources of stabilizing power, thus avoiding the addition of dedicated devices to solve the CPL instability problem. Such an approach

foresees to employ fast controlled converters to interface generators to the MVDC bus, in order to control it in a stable way. Stabilizing power is provided by interface converters, which are properly controlled by additional stabilizing functions. This approach appears very interesting for MVDC power systems, being suitable to affect system parameters in order to satisfy stability conditions. Therefore stability may be achieved without imposing a dedicated control to the CPL and without manipulating filter stages. Finally, the stabilizing power solution allows a free utilization of COTS components on the load side, which can be developed within the Power Electronic Building Blocks (PEBBs) concept, as recommended in Subsection 1.5.6.

For the important reasons specified, the voltage actuator approach will be followed in the thesis: particular attention will be spent in the development of stabilizing functions, which will be able to realize the voltage control and the stabilization, obeying the requirements exposed in the next Section.

3.3 Control system requirements

The design of any feedback control system has to take into account some important aspects. Therefore, also voltage control systems presented in this Chapter are to be designed in order to meet as much as possible the specific requirements [37] summarized in the following.

3.3.1 Stability

As discussed in Subsection 1.5.7, the stability is a fundamental requirement of each feedback controlled system [37] and it depends from both system and regulator. The controller has to be properly design in order to guarantee a stable behavior. Nevertheless, the stability requirement is not actually achievable in case of very critical system.

For the case analyzed, voltage stability may be defined [24] as the power system ability in re-establishing the rated voltage, after a small or large perturbation. In case of asymptotical stability, voltage returns to the equilibrium point V_0, whereas a simple stability requirement only ensures voltage's bounded evolution.

As it known, control system design and simulations are based on models, which are generally different from real systems: several motivations (e.g. parameters uncertainty, poles neglecting, operation outside the linearization point, modeling errors) are responsible of this behavior dissimilarity. It is important to guarantee the stability requirement (i.e. the robust stability) also in these perturbed conditions.

3.3.2 Steady state performance

Once assured the stability requirement, the voltage control system has to be capable in provide given performance [37]. In this way, the steady state performance is related to the system behavior for $t \to \infty$, when the initial transient is finished. It is requested a null error e in presence of specified (limited) signals w, d and n (respectively voltage reference, disturbance on the regulator and disturbance on the system).

3.3.3 Dynamic performance

Ideally, the voltage control system should be able to ensure a perfect coincidence between signal y (system output, controlled voltage) and signal w (voltage reference) in each time instant. In reality this is an unfeasible requirement being impossible to completely compensate the system dynamics by the regulator: the dynamic performance requirement [37] is therefore aimed to limit the step response into a specified region, defined by some parameters. For instance the steady state value y_∞, the maximum overshoot percentage $S_{\%}$, the rise time T_r, the settling time T_s are some values usually utilized to characterize the desired output response.

Talking about disturbances (*d* and *n*) consequence, it would be desirable a null effect on *y* output: again, the voltage control requirement limits this ideal circumstance, requesting limited (in magnitude and time) *y* variations.

Finally, another dynamic requirement regards the limitation of control variable (regulator output), which acts on the controlled system. This requisite is usually demanded to avoid actuator saturation (i.e. loss of control capability) and to limit the actuator stress.

3.3.4 Robustness

The stated performance is to be assured also in presence of critical perturbation, such as model errors or system parameters uncertainty. Obviously, the desired performance cannot be guaranteed for each possible perturbation. At most it is possible to conclude about the robust performance of the voltage control system [37], if the performance is respected even in presence of a limited perturbation range.

3.4 Single converter system modeling

Voltage control techniques developed in this Chapter have the fundamental target to prevent CPL instability. In order to make easier the comprehension of these techniques, a single converter case is chosen, whereas the integration of several generating systems and related multi-converter control will be discussed in Chapters 4, 5 and 6.

The single converter system [27] of Figure 3.1 is composed by an AC generating system (prime mover + alternator) and a DC conversion stage (AC/DC converter + DC/DC interface converter) in order to supply the CPL.

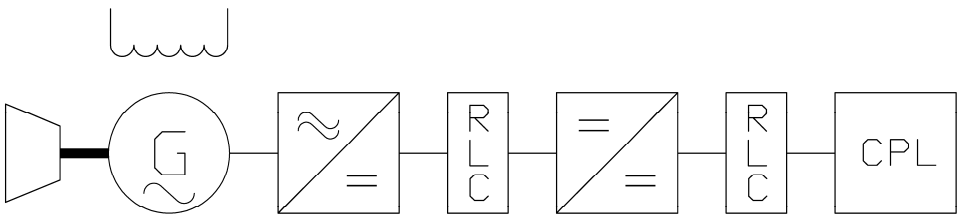

Figure 3.1 Single converter case.

3.4.1 Per unit notation

In order to facilitate the study of the interface converter, a common notation is used expressing system parameters and variables as p.u. quantities. To realize this procedure, a basis set (subscript n) is chosen ($P_n=P$, $V_n=V_0$, $I_n=I_0$, $R_n=V_n/I_n$), assuming the desired equilibrium point (V_0,I_0) and the given CPL power $P=V_0I_0$. Therefore the new p.u. notation defines system variables and parameters as follows

	Absolute values	Per unit
CPL power	P	$p=P/P_n$
CPL voltage	V	$v=V/V_n$
CPL current	I_L	$i_L=I_L/I_n$
Equilibrium point voltage	V_0	$v_0=V_0/V_n$
Equilibrium point current	I_0	$i_0=I_0/I_n$
Converter voltage	E	$e=E/V_n$
Inductance current	I	$i=I/I_n$
Filter resistance	R_f	$r_f=R_f/R_n$
Filter inductance	L_f	$l_f=L_f/R_n$
Filter capacitance	C_f	$c_f=C_fR_n$

Table 3.1 Per unit notation.

Thanks to the above definitions, previous equations expressed in absolute values (2.1)-(2.2) could be taken back to p.u. notation (3.1)-(3.2) by maintaining the same mathematical structure and utilizing minuscule symbols.

$$\begin{cases} l_f \dfrac{\mathrm{d}i}{\mathrm{d}t} = e - r_f i - v & (3.1) \\ c_f \dfrac{\mathrm{d}v}{\mathrm{d}t} = i - \dfrac{p}{v} & (3.2) \end{cases}$$

Regarding p.u. quantities, a simplification will be introduced: numbers are not followed by *p.u.* symbol in order to unburden the discussion.

3.4.2 Averaged model

Last equations describe the physical behavior of a filtered DC/DC interface converter. Starting from (3.1)-(3.2) and neglecting the interface converter switching (e, i, v, i_L are therefore mean values), it is possible to sketch (Figure 3.2) an averaged model circuit (formerly known as AVM, Subsection 1.6.1) capable in approximating the actual dynamics of the single converter case [27].

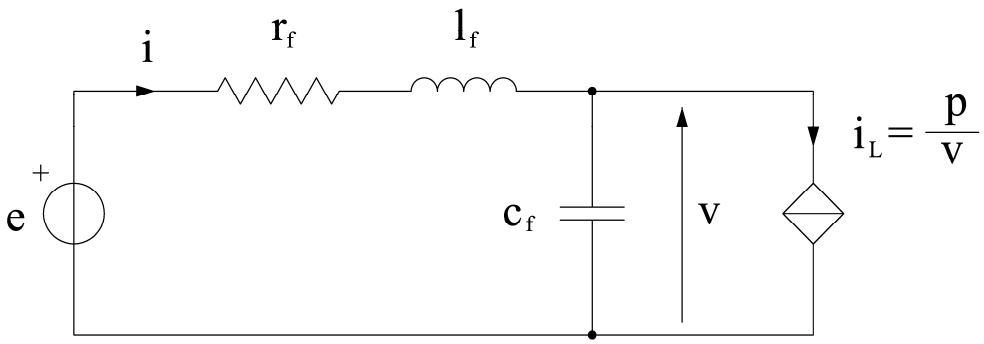

Figure 3.2 Averaged model (p.u. notation).

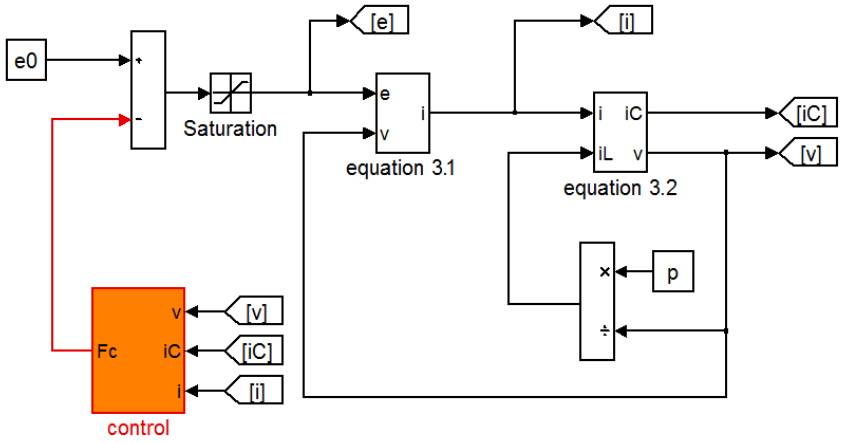

Figure 3.3 Simulink scheme of the averaged model.

The Simulink implementation (Figure 3.3) based on equations (3.1)-(3.2) offers a very simple system to represent the averaged model dynamics. Besides differential equations blocks, it is possible to notice a generic interface converter control (orange block deeply treated in Section 3.6), which provides the control function F_c to contribute in CPL instability solving. In this scheme the interface converter voltage output e is therefore given by the subtraction between constant voltage e_0 and F_c, where a saturation block takes into account real converter saturation. The CPL behaves as an infinite-bandwidth component, therefore the non-linear current i_L is given by the ratio p/v. This represents a worst case scenario [27] considering that constant power behavior will be in any case band-limited.

By observing Figure 3.3, it is possible to notice the limit of this representation: the averaged model studies only the interactions between DC/DC interface converter output and filtering stage. In fact, the dynamics imposed by converter duty cycle D and also linked to converter supply v_d time-evolution (synchronous generator + diode converter) is not considered in such an analysis. This is the reason why system input voltage is assumed as a constant e_0 capable in forcing the desired equilibrium point (v_0,i_0). Such a

value is supposedly given by steady state values D_0 and v_{d0}, being subjected to long time constants compared to quick dynamics of interest. Thus the constant voltage e_0 is clearly identified:

$$e_0 = v_{d0} \cdot D_0 \tag{3.3}$$

Although the effectiveness of this basic circuit in modeling the negative incremental resistance instability has been proven by a large literature [26,27,41,42], a time-domain comparison between the averaged model results and the detailed ones will be provided in Subsection 3.4.4 in order to demonstrate the simplified model potentiality and to confirm previous assumptions.

3.4.3 Detailed model

The complete single converter case (Figure 3.1) has additional elements respect to the averaged model (Figure 3.3), i.e. the interface converter supply. Clearly the detailed model has to represent these elements in a proper way, in order to ensure an effective reference model exploitable in results comparison.

A Simulink detailed simulator (Figure 3.4) of the single converter case has been developed at the Electric Power Generation & Control (EPGC) Laboratory of the University of Trieste. With reference to Figure 3.1, this detailed model [27] has to be composed by four functional blocks, briefly described in the following:

1. Diesel-Alternator (green box)
   This block experimentally verified by some results validations [5] is constituted by the prime mover (proportional torque actuator, first-order model for equivalent fuel delay), the Speed Governor (PID type), the Alternator (eighth-order model, three-phase stator, one field, one d-axis additional, two q-axis additional circuits, magnetic saturation [43]) and the excitation control system (IEEE type AC8B rotating rectifier model, PID Automatic Voltage Regulator, first-order model representing rotating exciter [44]). In particular the eight Alternator state variables result two from d-axis operator functions, two from q-axis operator functions, two from d and q fluxes calculations and two from mechanical equations. Talking about control tuning, the SG is set considering the equivalent time constant of about 10 s, whereas the AVR is tuned with an equivalent time constant of the voltage control closed loop (at no-load) of about 1 s.
2. AC/DC diode converter (magenta box)
   The diode rectifier is based on Matlab code selecting the maximum phase-to-phase AC voltage (as a time varying value) between the three input voltages (v_{ab}, v_{bc} and v_{ca}) in order to reproduce the rectified time varying voltage [45]. The first RLC filter stage of Figure 3.1 is embedded in the diode converter Simulink block.

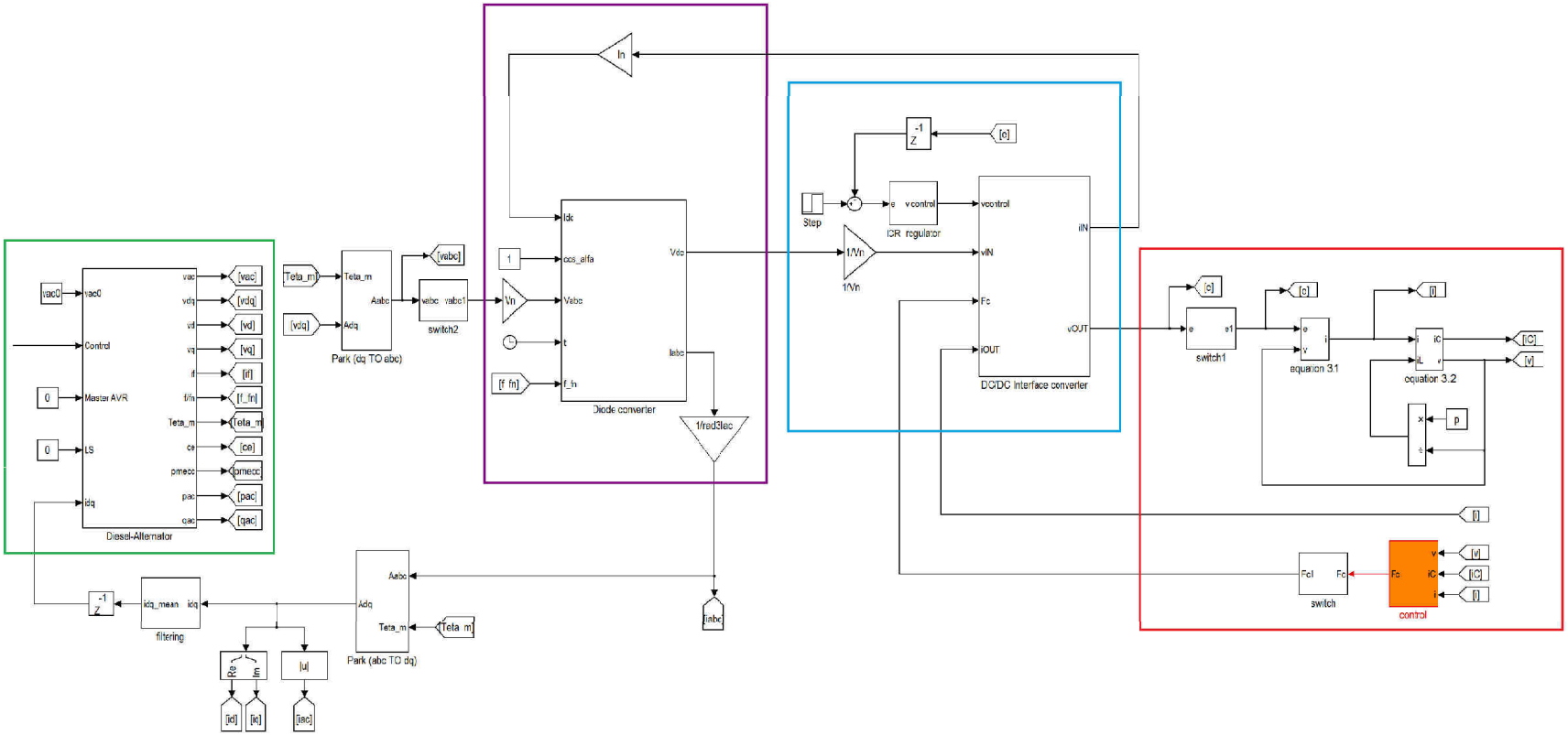

Figure 3.4 Simulink scheme of the detailed model.

3. DC/DC interface converter (cyano box)
   The buck converter has been chosen for the voltage actuator functionality, thus a switching Simulink block implements the well-known buck converter partialization [45] operated at the frequency of 1500 Hz. The Interface Converter Regulator (PI type) establishes the regime value of DC voltage source forcing a proper duty cycle. The ICR is tuned assuming the no-load condition and an equivalent closed loop time constant of about 0.1 s.
4. DC-link (red box)
   The interactions between RLC filtering stage and Constant Power Load are modeled by the DC-link. This model is developed in the same way as in Figure 3.2, except for the *e* source voltage obtained as the output of the interface converter. As the averaged model, the signal F_c is given by the orange block, designed by choosing a time constant τ_{FC}. Adding this control function to the ICR output (which fixed the interface converter steady state), a signal is determined to properly command the voltage actuator. The latter is therefore capable in imposing a suitable DC-link voltage input *e* to compensate for the voltage instability.

To complete the scheme it is necessary to list the Park transform blocks [46] (algebraic blocks performing the transformation) and the filtering block to smooth alternator's current during diodes switching, thus simulating the inductance commutation effect [45].

Regarding control bandwidths, a one decade separation margin is advisable in order to avoid possible coupling among different control loops: this is the reason why time constants are set in such a separated way (τ_{SG}=10 s, τ_{AVR}=1 s, τ_{ICR}=0.1 s).

In particular the latter poses an upper limit for time constant τ_{FC} which has to be lower than (0.01 s), in order to guarantee fair bandwidth separation. In presence of this separation ($\tau_{ICR} >> \tau_{FC}$), the validity of averaged model in approximating detailed results is confirmed being effective the ICR output quasi-constancy hypothesis.

3.4.4 Model cross-validation

A simulation test has been performed to verify the averaged model reliability [27], comparing the voltage and current averaged transients with those obtainable by detailed model. The design example explained in Section 3.5 and a well-performing LSF control technique (Section 3.8) are chosen in order to set-up a proper simulating test.

The main target of this Subsection is to validate averaged model in transient behavior, therefore an hypothetic disturbance has to be defined. In particular, interesting state variable (*v*,*i*) transients may be forced by a voltage impulse disturbance, such as the one applied at the instant t_0=30 s to move instantly the voltage to the desired initial state $v(t_0)$=0.75 per unit. Therefore following figures would propose a visual test to determine how the interface converter supply actually weighs in simulating transients.

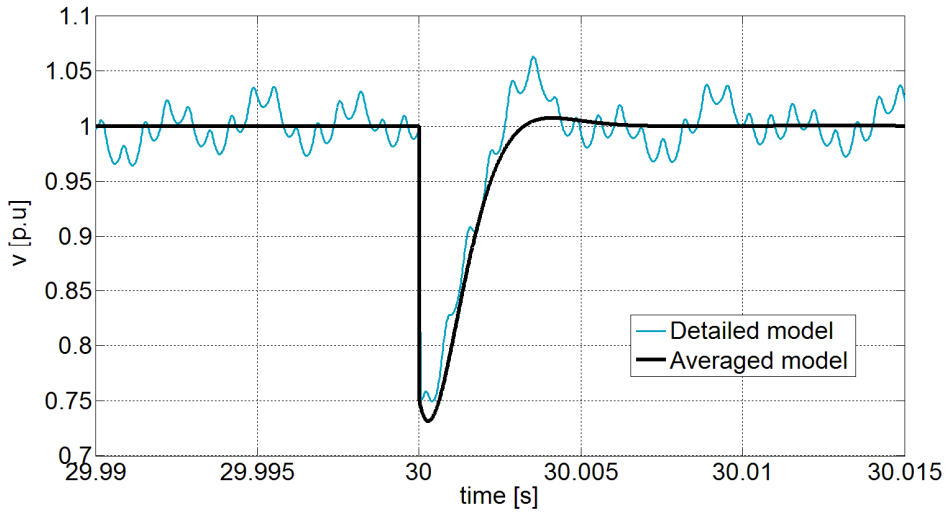

Figure 3.5 Results comparison: voltage transient.

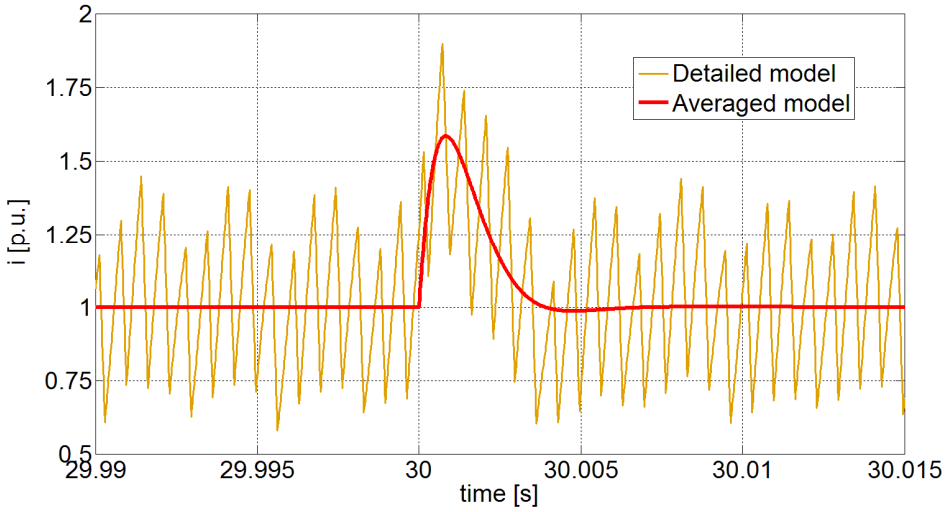

Figure 3.6 Results comparison: current transient.

Excluding stability considerations widely discussed in the following Subsections, the most important aspect to notice is the perfect correspondence in time domain. In effect the voltage (black) and current (red) transients provided by the averaged model are very close to detailed transients (cyano and orange) mean values. This aspect confirms the potentiality of simplified model [27] in studying the system dynamics, verifying its hypothesis:

- Power converter ripples highlighted in voltage and current transients does not influence the DC-link dynamics being the switching frequency quite high (1500 Hz): thus ripples can be neglected from a control point of view.

- Considering the given perturbation, the ICR inactivity is demonstrated by results equivalence. In particular ICR does not contribute to reestablish the voltage equilibrium point, being its equivalent time constant (0.1 s) very much greater than the τ_{FC} (about 0.003 s): approximating ICR action by a constant voltage e_0 does not degrade averaged model results.

By observing previous points, it is possible to conclude about averaged model reliability. This model may be considered enough accurate to develop different control techniques, studied in single converter case (this Chapter) and applied in complex multi-converter power systems (Chapter 5 and 6).

3.5 Case of study

In this Section a DC-link example is proposed along with considerations about stability. These analysis are very important to demonstrate the actual criticality of this case of study. To study stability in p.u. notation it is possible to simply use the equations reported in Chapter 2, as seen in Subsection 3.4.1.

Theoretical concepts related to stability and voltage control are applied on a simulating test, whose averaged equivalent circuit is reported in Figure 3.2. As known the CPL stability strictly depends on filtering stage, therefore the importance of this element is noticed: for the case studied, the filter parameters (R_f =4.58 Ω, L_f =13.9 mH and C_f =51.4 μF) are derived from an experimental arrangement discussed in [41,42].

Choosing the basis quantities in accordance to the experimental test (V_n=400 V, P_n=3.7 kW, I_n=9.25 A, R_n=43.2 Ω), 2nd order filter parameters can be expressed in p.u. notation as specified in Table 3.1 (r_f =0.106, l_f =3.22·10 $^{-4}$ and c_f =2.22· 10 $^{-3}$), while the CPL is supposed at rated condition (p=1). In a no-controlled DC-link characterized by these parameters, the first evaluation regards the equilibrium points stability.

As explained in Subsections 2.2.5, equilibrium points are given by the intersections between CPL equation and source equation. In this context, equation (2.10) may be used to calculate the voltage source e_0 able to impose the desired steady state condition (v_0,i_0)=(1,1):

$$e_0 = r_f i_0 + v_0 = 1.106 \tag{3.4}$$

By applying this voltage expressed in absolute value notation (Subsection 3.4.1), two equilibrium points V_{01} and V_{02} can be determined by means of equations (2.12) and (2.13). However the proposed model is based on p.u. variables: therefore previous equilibrium points are to be rewritten in p.u. notation, obtaining equations (3.5)-(3.6).

The first equilibrium point (v_{01},i_{01}) corresponds to the desired steady state point (v_0,i_0), whereas the second one (v_{02},i_{02}) is an instable point as previously discussed in Subsection 2.3.3.

$$\begin{cases} v_{0_1} = v_0 = 1 \\ i_{0_1} = \dfrac{p}{v_0} = 1 \end{cases} \tag{3.5}$$

$$\begin{cases} v_{0_2} = \dfrac{r_f\, p}{v_0} = 0.106 \\ i_{0_2} = \dfrac{v_0}{r_f} \cong 9.434 \end{cases} \tag{3.6}$$

So only the stability of the point (v_0,i_0) is studied thanks to small-signal stability approach: as seen before, an equilibrium point is stable if the initial non-linear system linearized in that equilibrium point respects stability conditions. By calculating the negative resistance in the desired steady state point $r^0=(v^2/p)_0=1$, conditions (2.21)-(2.22) may be used to verify stability:

$$\begin{cases} r^0 > r_f \\ \dfrac{r_f}{l_f} > \dfrac{1}{c_f r^0} \end{cases} \quad \Rightarrow \quad \begin{cases} 1 > 0.106 & (3.7) \\ 329.19 < 450.45 & (3.8) \end{cases}$$

Stability condition (3.8) is not verified, so the equilibrium point (v_0,i_0) is clearly instable. The no-controlled system (subscript n) linearized in this operating point (Section 2.3) is characterized by the following natural frequency and damping factor, obtained by comparing (2.20) and the common notation for 2nd order systems (3.9)

$$s^2 + 2\xi\omega_0 s + \omega_0^2 = 0 \tag{3.9}$$

$$\begin{cases} \omega_{0n} = \sqrt{\dfrac{1}{l_f c_f}\left(1 - \dfrac{r_f}{r^0}\right)} \cong 1118 \text{ rad/s} & (3.10) \\ \xi_n = \dfrac{1}{2 l_f c_f \omega_{0n}}\left(c_f r_f - \dfrac{l_f}{r^0}\right) \cong -0.05 & (3.11) \end{cases}$$

As foreseen by condition (3.8), the damping factor is slightly negative, therefore the no-controlled system presents an oscillatory instability.

By observing (3.11), it is noteworthy the positive damping effect introduced by filter resistance. To evaluate this damping contribution, following approximated values are calculated by annulling r_f [27]:

$$\begin{cases} \hat{\omega}_0 = \sqrt{\dfrac{1}{l_f c_f}} \cong 1183 \text{ rad/s} & (3.12) \\ \hat{\xi} = -\dfrac{1}{2r^0}\sqrt{\dfrac{l_f}{c_f}} \cong -0.19 & (3.13) \end{cases}$$

Comparing (3.11) and (3.13), the filter resistance damping effect is quantified in +0.136, conforming the remarkable importance of this dissipative element. Theoretically this element [36] may be capable in solving instability, dissipating the energy which resonates among energy storage elements (l_f and c_f). Actually, the filter resistance is usually not enough to dissipate sufficient energy for damping the oscillations.

From (3.11), a power index can be defined (3.14) by annulling the subtraction in the brackets. This value is a CPL power limit for which the no-controlled system presents a null damping factor.

$$c_f r_f - \frac{l_f}{r^0} = 0 \quad \Rightarrow \; p_{\text{lim}} = \frac{c_f r_f}{l_f} = 0.73 \qquad (3.14)$$

Thus if $p>p_{\text{lim}}$ the instability is exhibited, being positive the real part of the poles as explained in Section 2.3. For lower loads ($p<p_{\text{lim}}$), equation shows that the damping factor could become positive, therefore stability gained. Thus, the full load condition ($p=1>p_{\text{lim}}$) is certainly the worst case, being over-loaded eventuality ($p>1$) not considered in this thesis.

The importance of filter parameters in determining equilibrium point stability has been demonstrated in previous analysis, by observing conditions (3.7) and (3.8). The latter is normally not verified in real no-controlled systems, where induction reduction and capacitance increase could be hypothetical solutions for CPL instability. Actually, the first measure is not feasible due to current ripple target, whereas the second one is considered expensive in terms of cost, weight, space and reliability [42]. Therefore given example represents an interesting case for CPL issue, making essential the exploitation of proper voltage control techniques to solve the voltage instability.

3.6 Control techniques

Being the no-controlled system characterized by voltage instability, it is necessary to design proper techniques in order to guarantee a stable operation in the chosen equilibrium point. To this aim, three control techniques are presented along with a description of pros and cons.

3.6.1 State Feedback

The State Feedback (SF) control technique [27] is implemented to solve the above-mentioned CPL issue and to control the load voltage by regulating the output converter voltage: thus the technique is exploited in the so-called voltage actuators approach.

To realize this function, the interface converter is feedback governed by a suitable control signal proportional to the state variables i and v. The control function F_c is therefore easily defined, named k_i and k_v the proportional gains of the two feedback signals:

$$F_c = k_i i + k_v v \tag{3.15}$$

By applying the control function F_c, the SF controlled system may be described by the differential equations (3.16)-(3.17). These are derived from (3.1)-(3.2), considering the presence of the control signal as seen in Figure 3.3:

$$\begin{cases} l_f \dfrac{\mathrm{d}i}{\mathrm{d}t} = (e_0 - k_i i - k_v v) - r_f i - v & (3.16) \\ c_f \dfrac{\mathrm{d}v}{\mathrm{d}t} = i - \dfrac{p}{v} & (3.17) \end{cases}$$

In the averaged model adoption (Subsection 3.4.2), e_0 is assumed as a constant voltage, able to impose the expected equilibrium point (v_0,i_0)=(1,1) and to cancel the steady state droop effect, related to control signals action:

$$e_0 = r_f i_0 + v_0 + k_i i_0 + k_v v_0 \tag{3.18}$$

The method introduced in Subsection 2.3.1 is now useful to determine the differential equations (3.19)-(3.20), which describe the system linearized in the equilibrium point (v_0,i_0):

$$\begin{cases} l_f \dfrac{\mathrm{d}(\Delta i)}{\mathrm{d}t} = (\Delta e - k_i \Delta i - k_v \Delta v) - r_f \Delta i - \Delta v & (3.19) \\ c_f \dfrac{\mathrm{d}(\Delta v)}{\mathrm{d}t} = \Delta i - \dfrac{\Delta v}{-r^0} & (3.20) \end{cases}$$

Following the line of reasoning specified in Subsection 2.3.2, the 2nd order system characteristic equation (3.21) can be determined:

$$s^2+\frac{1}{l_f c_f}\left(c_f(r_f+k_i)-\frac{l_f}{r^0}\right)s+\frac{1}{l_f c_f}\left(1+k_v-\frac{r_f+k_i}{r^0}\right)=0 \tag{3.21}$$

as well as the stability conditions (3.22)-(3.23) to evaluate the small-signal stability

$$\begin{cases} r^0(1+k_v)>r_f+k_i & (3.22)\\ \dfrac{r_f+k_i}{l_f}>\dfrac{1}{c_f r^0} & (3.23)\end{cases}$$

Only a suitable choice of gains k_i and k_v may comply with stability conditions, guaranteeing stability in a neighborhood of the equilibrium point. Otherwise equilibrium point instability appears, as discussed in Section 3.5 for the no-controlled system. Although control gains k_i and k_v are designed on the averaged model by linearizing the non-linear system in (v_0,i_0) and considering small disturbances, the effect of proportional gains will be examined by hypothesizing large disturbances in the following Section 3.7.

Comparing equation (3.21) with the common notation for 2nd order systems (3.9), it is possible to study the gains impact on filter dynamics (3.24)-(3.25), where ω_0 is the natural angular frequency and ξ the damping factor of the SF controlled system.

$$\begin{cases} \omega_0=\sqrt{\dfrac{1}{l_f c_f}\left(1-\dfrac{r_f+k_i}{r^0}+k_v\right)} & (3.24)\\ \xi=\dfrac{1}{2l_f c_f \omega_0}\left(c_f(r_f+k_i)-\dfrac{l_f}{r^0}\right) & (3.25)\end{cases}$$

Besides ensuring small-signal stability (3.22)-(3.23), state feedback gains k_i and k_v can be calculated by imposing a proper dynamics, represented by the desired values for ω_0 and ξ.

$$\begin{cases} k_i=\dfrac{l}{r^0 c_f}-r_f+2\xi\omega_0 l_f & (3.26)\\ k_v=\omega_0^2 l_f c_f-1+\dfrac{k_i+r_f}{r^0} & (3.27)\end{cases}$$

Assuming the worst case scenario (r^0=1) and the design target of well-damped transients (ξ= 0.3), a series of gain values k_i and k_v can be obtained (Table II), from the application of equations (3.26)-(3.27) and considering different values of the ratio ω_0/ω_{0n}, where the last natural angular frequency regards the no-controlled system (3.10).

ω_0/ω_{0n}	k_i	k_v	$\sqrt{(k_i^2+k_v^2)}$
0.2	0.0823	-0.7760	0.7803
0.4	0.1255	-0.6255	0.6380
0.6	0.1687	-0.4035	0.4373
0.8	0.2119	-0.1099	0.2387
1.0	0.2551	0.2551	0.3608
1.2	0.2983	0.6917	0.7533
1.4	0.3415	1.1998	1.2474
1.6	0.3847	1.7794	1.8205

Table 3.2 Gain values and energy index for different natural frequency.

It is expedient to complete the table with an additional column, which provides an energetic index of the control action [27] in order to choose a suitable ω_0. In Table II, this energy index shows its minimum (0.2387) around ω_0/ω_{0n}=0.8, correspondent to a pair of optimal control gains (k_i = 0.2119, k_v = -0.1099). Thus the averaged model input voltage e_0 may be determined

$$e_0 = r_f i_0 + v_0 + k_i i_0 + k_v v_0 = 1.208 \tag{3.28}$$

Talking about stability, the choice of optimal gains k_i and k_v complies with stability conditions (3.29)-(3.30), therefore the small-signal stability is guaranteed:

$$\begin{cases} r^0(1+k_v) > r_f + k_i \\ \dfrac{r_f + k_i}{l_f} > \dfrac{1}{c_f r^0} \end{cases} \Rightarrow \begin{cases} 0.89 > 0.32 & (3.29) \\ 987.24 > 450.45 & (3.30) \end{cases}$$

However in a shipboard power system the small-signal stability is insufficient, being loads characterized by a power level similar to the power level of generators, thus plausible the presence of large disturbances able to considerably move the state variables. Therefore the small-signal analysis utilized in control design is not enough to assure the voltage stability: instead it is fundamental to check the large-signal stability, estimating the region of attraction around a stable equilibrium point [47].

Starting from the considerations of Section 2.4 and applying the control function F_c, it is possible to rewrite the Lyapunov theory for the SF controlled system, obtaining the following sufficient condition for large-signal stability [27]:

$$v(t_0) \geq \sqrt{\frac{l_f p}{(k_i + r_f) \cdot c_f}} = v_{sf} = 0.6755 \tag{3.31}$$

As discussed in Subsection 2.4.1, condition (3.31) defines a region of attraction, that is a half plane where the Lyapunov first derivative becomes negative: assuming a large disturbance, the stability is ensured if the system starts to evolve from a voltage value equal or upper than the limit v_{sf}. While the voltage instability is not guaranteed if the inequality (3.31) does not hold, considering that Lyapunov theory provides a sufficient but not necessary stability condition.

3.6.2 Active Damping

As explained before (Section 3.5), the potentiality of the resistive element in solving the CPL instability problem is well-known: in effect a possible way of compensating the negative incremental resistance is increasing the filter resistance r_f, damping the oscillations, but causing high dissipation and therefore lower system efficiency.

In order to overcome this problem, a simple feedback loop control technique [48,49] may be utilized in shipboard power system: the Active Damping (AD). The AD is a non-dissipative method to transiently increase the filter resistance, by measuring the inductor current i and subtracting the relative voltage droop from the control voltage. In this case, the control signal F_c is represented by the following equation:

$$F_c = r(t) \cdot i \tag{3.32}$$

In the last formula, the virtual resistance $r(t)$ is a function of time, obtained by a 1st order high-pass filter as explained hereinafter. This resistance is variable from r_{ad} at the very first instant after a voltage perturbation to 0 at the steady state. This is the reason why the constant voltage e_0 has only to compensate for the voltage droop on the filter resistance at the steady state, thus e_0=1.106 as the no-controlled case (3.4).

Comparing equations (3.15) and (3.32), it is possible to notice the similarity between the function offered by the control gain k_i and that related to virtual resistance $r(t)$: in the instant of perturbation (when $r(t)=r_{ad}$), a proper equation (3.33) may express the damping factor of the AD controlled system, similarly to (3.25). Assuming the same targets of the SF technique (ξ = 0.3 and $\omega_0=0.8 \cdot \omega_{0n}$=895 rad/s), the maximum value of $r(t)$ should be therefore equal to the optimal SF current gain, thus $r_{ad}=k_1$=0.2119.

$$\xi = \frac{1}{2 l_f c_f \omega_0} \left(c_f (r_f + r_{ad}) - \frac{l_f}{r^0} \right) \tag{3.33}$$

Actually, in order to guarantee similar performance among SF and AD techniques, it is advisable to oversize the r_{ad} value of a 20% in order to partially compensate the *r(t)* decreasing in the earliest instants after the perturbation:

$$r_{ad} = 1.2 \cdot k_i = 0.2543 \tag{3.34}$$

The resistance given by (3.34) represents the highest value for *r(t)*, which varies during the transient up to zero at the steady state condition. This transient effect is guaranteed by a 1st order high-pass filter, whose pole is placed between $0.1\omega_{0n}$ and $0.2\omega_{0n}$: being ω_{0n} the natural angular frequency for the no-controlled system (3.10), the AD designed has a pole in about 110 rad/s. The Bode diagram of the virtual resistance is shown in Figure 3.7.

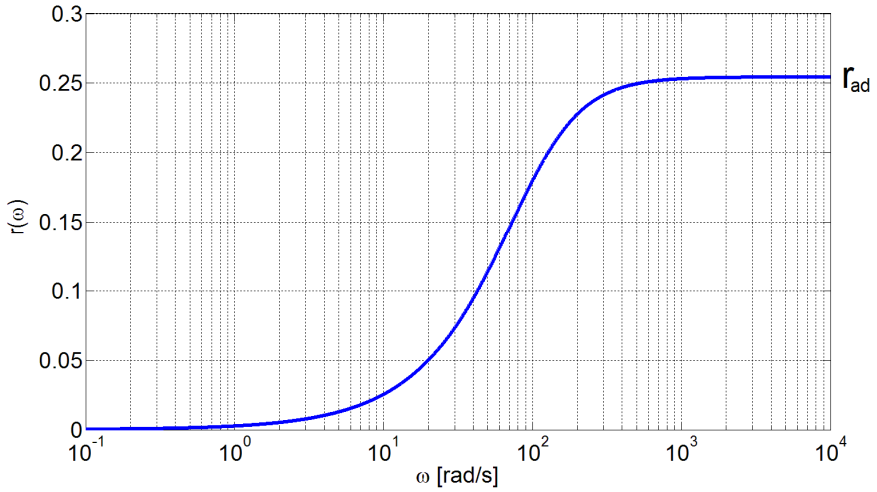

Figure 3.7 Active Damping virtual resistance.

Regarding the small-signal stability in the instant of perturbation (when $r(t)=r_{ad}$), considerations may be similar of those expressed for SF technique,

$$\begin{cases} r^0 > r_f + r_{ad} \\ \dfrac{r_f + r_{ad}}{l_f} > \dfrac{1}{c_f r^0} \end{cases} \Rightarrow \begin{cases} 1 > 0.36 & (3.35) \\ 111894 > 450.45 & (3.36) \end{cases}$$

as well as the sufficient condition v_{ad} for large-signal stability [27]

$$v(t_0) \geq \sqrt{\frac{l_f p}{(r_{ad} + r_f) \cdot c_f}} = v_{ad} = 0.6345 \tag{3.37}$$

3.6.3 Linearization via State Feedback

The Linearization via State Feedback (LSF) is a well-performing technique to solve the CPL instability in MVDC power systems [50,51,52,53,54]. Unlike the AD method which increases the transient damping factor through a inductor current feedback, LSF technique tries to do something more, solving the non-linearity at the beginning.

The LSF method, also called loop-cancellation technique, is generally based on the introduction of a suitable non-linear feedback, applied by the DC/DC interface converter as SF and AD (Subsection 3.4.3). This non-linear feedback is capable for removing the CPL destabilizing effect, basically compensating for the non-linearity: actually the system still behaves as non-linear, but this non-linearity do not compare externally (i.e. in voltage *V* transient), being canceled by the non-linear feedback. Thus the resulting (external) linear system can be controlled utilizing linear control theory.

To properly control a resulting linear system, the loop-cancellation technique has to use a suitable control signal F_c, composed by two different terms f_l and f_d: the first term f_l is needed to cancel the non-linearity, whereas the second one f_d is able to impose the desired 2nd order dynamics:

$$F_c = f_l + f_d \tag{3.38}$$

In order to determine the non-linear term f_l and to fix f_d, it is necessary to consider these feedbacks in equations (3.1)-(3.2):

$$\begin{cases} l_f \dfrac{\mathrm{d}i}{\mathrm{d}t} = (e_0 - f_l - f_d) - r_f i - v & (3.39) \\ c_f \dfrac{\mathrm{d}v}{\mathrm{d}t} = i - \dfrac{p}{v} & (3.40) \end{cases}$$

A first equation is obtained by deriving (3.40),

$$c_f \frac{\mathrm{d}^2 v}{\mathrm{d}t^2} = \frac{\mathrm{d}i}{\mathrm{d}t} + \frac{p}{v^2}\frac{\mathrm{d}v}{\mathrm{d}t} \tag{3.41}$$

then substituting (3.39) in (3.41), a second formula is found

$$c_f \frac{\mathrm{d}^2 v}{\mathrm{d}t^2} + \frac{r_f}{l_f} i + \frac{1}{l_f} v + \frac{1}{l_f}(f_l + f_c) - \frac{p}{v^2}\frac{\mathrm{d}v}{\mathrm{d}t} = \frac{e_0}{l_f} \tag{3.42}$$

Finally the second order differential equation may be obtained from (3.42), considering the current *i* derivable from (3.40)

$$\frac{\mathrm{d}^2 v}{\mathrm{d}t^2}+\frac{r_f}{l_f}\frac{\mathrm{d}v}{\mathrm{d}t}+\frac{1}{c_f l_f}v+\frac{1}{c_f l_f}\left(f_l+f_c\right)+\left(\frac{r_f}{c_f l_f}\frac{p}{v}-\frac{1}{c_f}\frac{p}{v^2}\frac{\mathrm{d}v}{\mathrm{d}t}\right)=\frac{e_0}{c_f l_f} \tag{3.43}$$

By observing (3.43), the task of the F_c terms is clear: on one hand f_l has to compensate the non-linear term in the bracket, on the other hand f_d has to pose the poles of the resulting linear system at appropriate places. Therefore these functions are defined:

$$\begin{cases} f_l = r_f \dfrac{p}{v} - l_f \dfrac{p}{v^2}\dfrac{\mathrm{d}v}{\mathrm{d}t} & (3.44) \\ f_d = k_1 \cdot v + k_2 \cdot i_c & (3.45) \end{cases}$$

It is a matter of fact that a proper f_l (3.44) is able to cancel the non-linearity: in this case, any consideration (small and large analysis) about stability is therefore useless, being the LSF controlled system linear.

By applying F_c, the equation of the closed-loop system is became linear and the dynamics is governed by k_1 and k_2, gains of the feedback voltage v and capacitive current i_c respectively

$$\frac{\mathrm{d}^2 v}{\mathrm{d}t^2}+\frac{1}{l_f}\left(r_f+k_2\right)\frac{\mathrm{d}v}{\mathrm{d}t}+\frac{1}{c_f l_f}\left(1+k_1\right)\cdot v=\frac{e_0}{c_f l_f} \tag{3.46}$$

Thus proportional gains can be tuned (3.48) in order to impose the same dynamics as the SF case (ξ=0.3 and ω_0=0.8·ω_{0n}=895 rad/s), once the characteristic equation is obtained (3.47) and compared to the common notation for 2nd order systems (3.9),

$$s^2+\frac{1}{l_f}\left(r_f+k_2\right)\cdot s+\frac{1}{c_f l_f}\left(1+k_1\right)=0 \tag{3.47}$$

$$\begin{cases} k_1 = -1+\omega_0^2 c_f l_f = \text{-}0.4278 \\ k_2 = -r+2\xi\omega_0 l_f = 0.0668 \end{cases} \tag{3.48}$$

Assuming the steady state condition, the averaged model input voltage e_0 may be evaluated by using (3.39), (3.44)-(3.45).

$$e_0 = r_f i_0 + v_0 + r\frac{p}{v_0} + k_1 v_0 = 0.5722 \tag{3.49}$$

As explained in Subsection 3.4.2, the voltage e_0 is chosen to impose the desired operating point (v_0,i_0), compensating for the steady state droop-effect of the implemented control.

3.6.4 Pros and cons

In previous Subsections some studies has been presented in order to provide a wide overview on actual control strategies capable in solving CPL issue: starting from the simplest SF, the evaluation has considered the transient effect of AD and the loop-cancellation offered by LSF.

Although the potentialities of these three methods are quite different, their aim is the same: to realize the voltage control in MVDC power systems, assuring stability against small and large perturbations. A comparison between control techniques is provided in Table III, where pros and cons are highlighted. SF and AD are similar from a control point of view, thus related pros and cons can be considered in the same row. On the other hand, LSF is discussed separately being based on a totally different theory.

	pros	cons
SF - AD	• basic technique • feedback of standard real-time measurements • simple implementation on digital controllers	• stability ensured in presence of limited CPLs • non-linear damped system • stability guaranteed only for non critical system • stability ensured in presence of limited disturbance • system dynamics set considering stability issue
LSF	• any CPL non-linearity cancelled • standard linear system obtained • stability guaranteed even for critical system • stability ensured in presence of wichever disturbance • system dynamics set indipendently from stability issue	• complex technique • derivative variable calculus • partial non-linearity cancellation in presence of measurements errors • partial non-linearity cancellation in presence of system parameters uncertainty • voltage actuator saturation due to the derivative action of control signal

Table 3.3 Control techniques: pros and cons.

By observing the Table 3.3, it is possible to conclude about the substantial difference between these techniques: basic techniques like SF or AD may improve the system stability by damping the oscillations, but they are not enough in case of particularly negative situation (i.e. very large disturbance, large CPL, small filter capacitance or large filter inductance). In these critical conditions, the only control possibility to guarantee the MVDC stability requirement is given by the Linearization via State Feedback [52].

Evidently LSF disadvantages are also to be considered in a fair evaluation among techniques. In particular three aspects represent the weakest points of loop-cancellation technique: possible partial cancellation of non-linearity, derivative variable calculus in f_l and voltage actuator saturation may invalidate the linearization procedure. In order to solve these problems, some possibilities are presented in the following and examined in the next Subsections.

Talking about the first aspect, an over-linearization technique [52] has demonstrated to be an achievable idea to overcome measurements errors and system parameters uncertainty: an application of this approach is described in Section 6.7. Secondly, the hard calculation of derivative variables in f_l can be overtaken by using standard measurements, as proposed in Subsection 6.5. Finally, the voltage actuator saturation can be taken into account by studying the consequent non-linear system: this analysis will be offered in Section 3.8.

3.7 Controlled single converter: time-domain study

In order to validate control techniques, a numerical simulation implemented in Simulink is proposed. This time-domain analysis is useful to verify:

(i) control performance, by checking if natural frequency ω_0 and damping factor ξ are in compliance with control targets (minimum energy case and damped behavior);
(ii) sufficient conditions for large-signal stability, by observing if the stability of SF and AD is preserved in case a large voltage perturbation moves v over the limit values (v_{sf} and v_{ad});
(iii) LSF potentiality, by showing if this method guarantees stability when SF-AD failure occurs.

3.7.1 Numerical simulations

As explained in Subsection 3.4.4, a series of simulations has been carried out on the averaged model, in which the source voltage e_0 is applied as an ideal constant value (related values are specified in Section 3.6 for each control technique). Figure 3.3 shows the blocks scheme of the averaged model, based on state equations previously defined: this model considers the presence of a CPL, which destabilizing effect is compensated for control techniques (orange block). Being the CPL an infinite-bandwidth component also for large variations, the analyzed case is in effect a worst case scenario [27], considering that the constant power behavior will be in any case band-limited. Note also

that the Simulink schematic keeps into account voltage source saturation conditions, making this simulation already quite realistic.

Assuming an equilibrium point $(v_0,i_0)=(1,1)$, four scenarios of state variables transients have been considered to test the system in presence of small and large-signal variations: voltage perturbations are emulated by setting the initial condition $v(t_0)$ on capacitor, maintaining the initial DC inductor current equal to the steady state value, thus $i(t_0)=1$.

In the first test $v(t_0)$ is put equal to 1.1 to analyze the small-signal stability; similarly the second one starts from an initial value rather near to equilibrium point voltage, i.e. $v(t_0)=0.9$. On the other hand, third and fourth tests want to verify the large-signal stability, by imposing $v(t_0)=0.68$ (third test, over the voltage limits v_{sf} and v_{ad}) and $v(t_0)=0.6$ (fourth test, under those limits).

In the following pages, several transients are shown in order to verify the effectiveness of the techniques (SF, AD and LSF) in the four scenarios: in particular, the transients of state variables (capacitor voltage *v* and inductor current *i*) and voltage input *e* are considered as the most interesting to understand controls action.

3.7.2 Simulation results

The first two scenarios (Figures 3.8, 3.9, 3.10, 3.11, 3.12 and 3.13) consider a small perturbation, indeed the initial voltage is moved in proximity (±10%) of the equilibrium value. In these cases, all designed controllers (SF, AD and LSF) are able to quickly react, re-establishing the nominal conditions and keeping the bus stable. The control systems efficiency is verified, being natural frequency and damping in coherence with the design specifications (ω_0=895 rad/s and ξ=0.3). On the other hand, third and fourth scenarios are necessary to study the large-signal stability (wide perturbations >30%).

In the third scenario (Figures 3.14, 3.15 and 3.16) stability is guaranteed for all control techniques, being $v(t_0)=0.68$ greater than SF-AD stability conditions (v_{sf} =0.6755 and v_{ad} =0.6345) and LSF capable in ensuring a linear system. Although control gains impose the same dynamics for all designed controls, systems controlled by SF and AD are characterized by voltage and current evolutions substantially different from the linear ones (LSF): clearly such aspect depends on perturbation, that is large enough to invalidate the small-signal hypothesis, which are at the base of SF-AD controls design.

The fourth scenario ($v(t_0)=0.6$) is a final test, characterized by the instability of SF-AD cases (Figures 3.17, 3.18 and 3.19) being violated the stability conditions ($v(t_0)<v_{sf}$ and $v(t_0)<v_{ad}$). Conversely, LSF technique is able to provide an efficient voltage control, restoring the rated voltage in accordance with the desired dynamics. Definitely, it is possible to conclude that linearity is ensured by the loop-cancellation, even in presence of large perturbations. In this regard, the system linear behavior is confirmed by observing the absence of saturation (which is chosen equal to e_s =1.52) in the voltage input *e* transient (red line). Actually, the voltage actuator saturation and the consequent linearity loss are strictly related to perturbation entity and dynamics imposed by LSF: to discuss this eventuality, a case of study is proposed in Section 3.8.

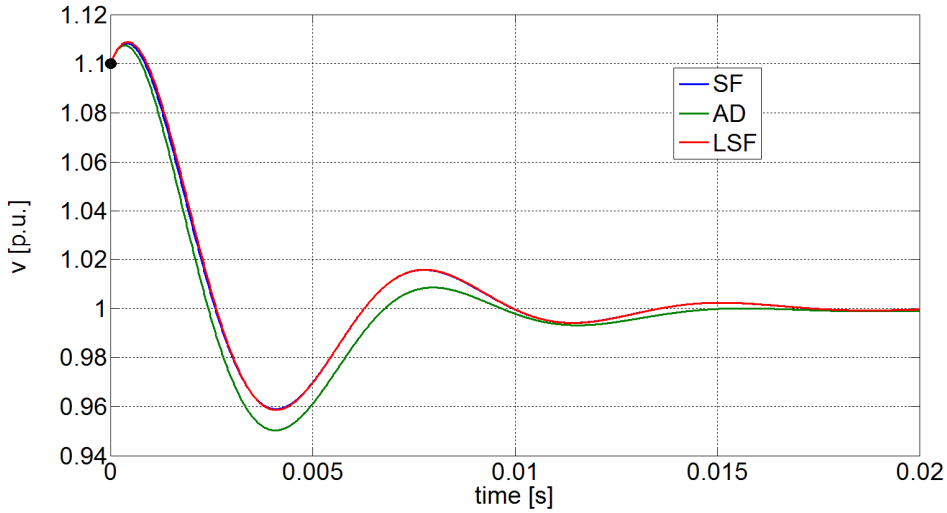

Figure 3.8 Voltage transient: $v(t_0)$=1.1.

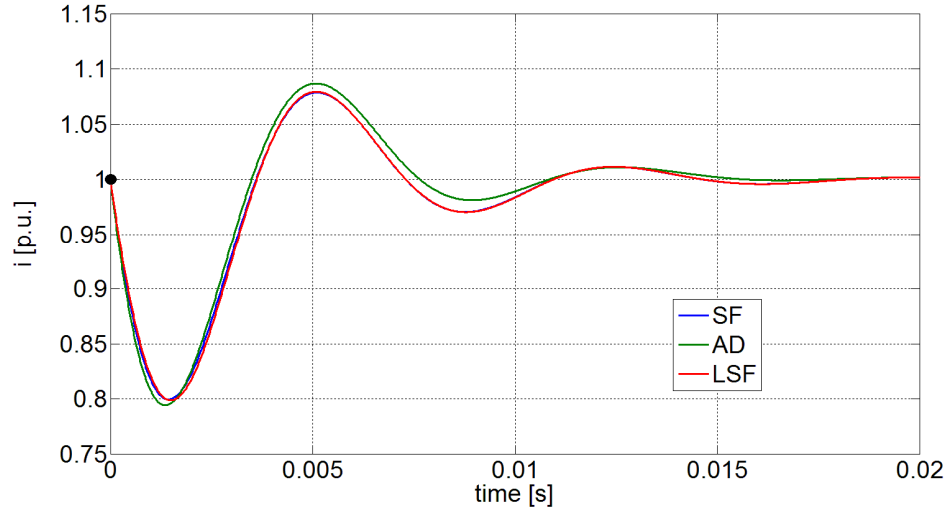

Figure 3.9 Current transient: $v(t_0)$=1.1.

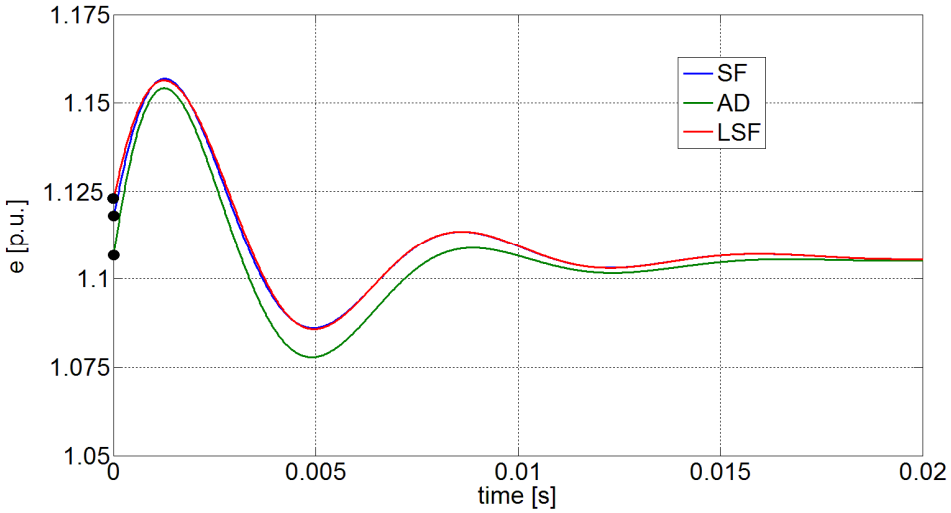

Figure 3.10 Voltage input transient: $v(t_0)$=1.1.

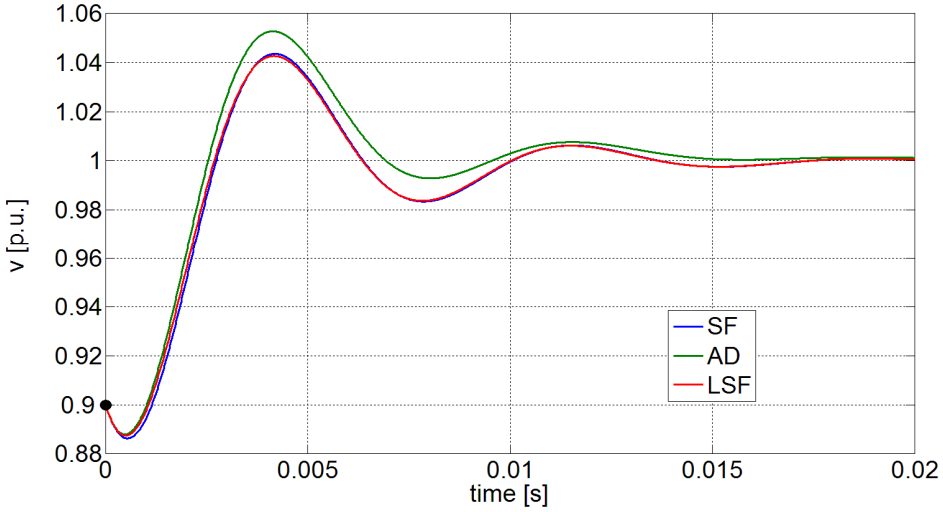

Figure 3.11 Voltage transient: $v(t_0)$=0.9.

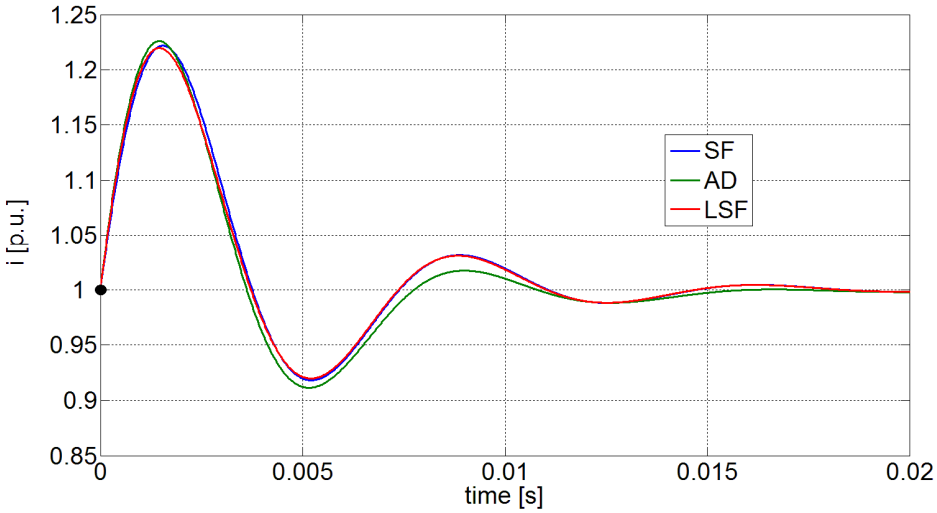

Figure 3.12 Current transient: $v(t_0)$=0.9.

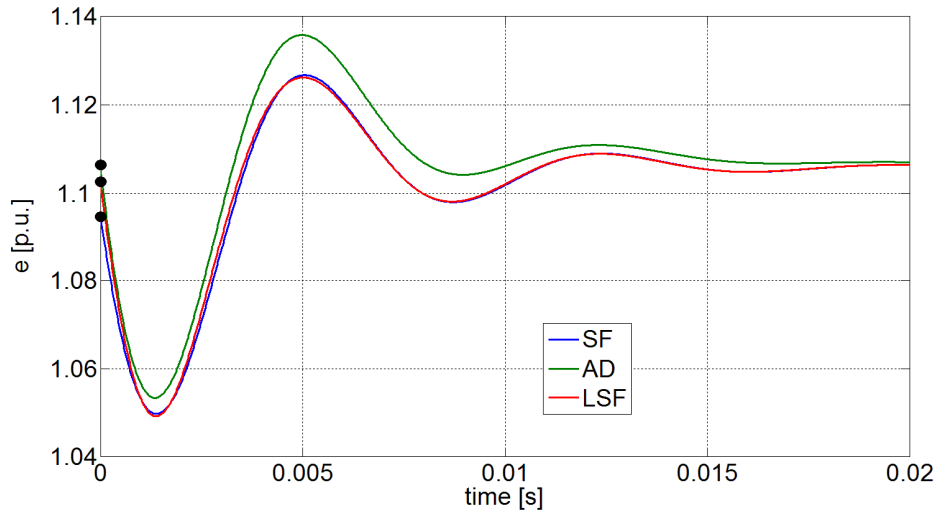

Figure 3.13 Voltage input transient: $v(t_0)$=0.9.

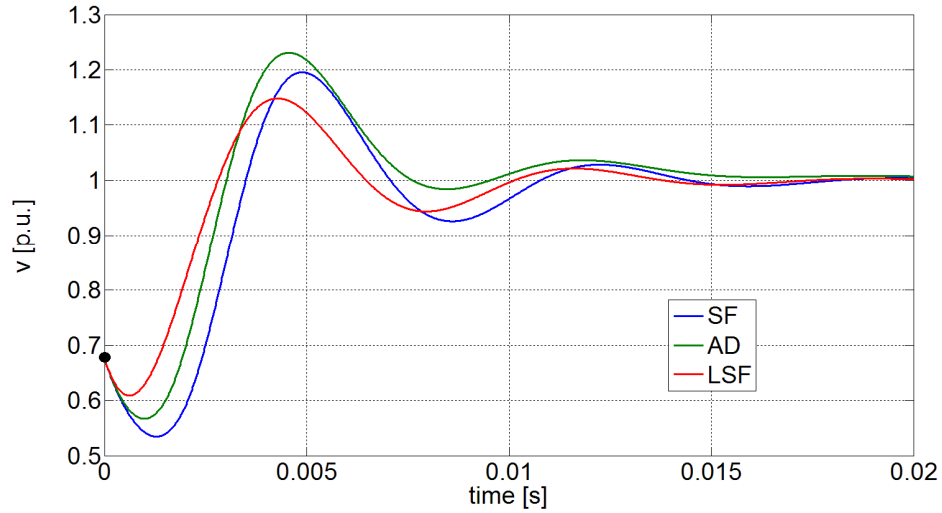

Figure 3.14 Voltage transient: $v(t_0)$=0.68.

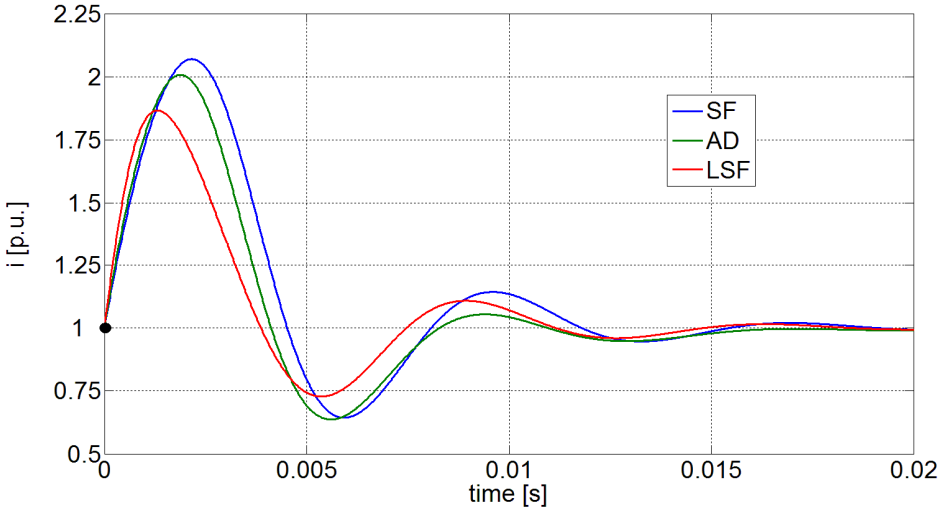

Figure 3.15 Current transient: $v(t_0)$=0.68.

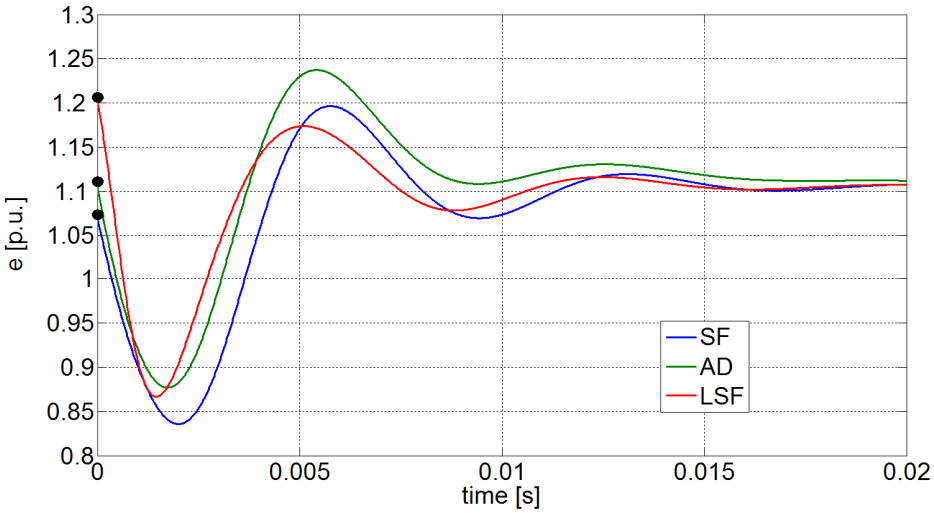

Figure 3.16 Voltage input transient: $v(t_0)$=0.68.

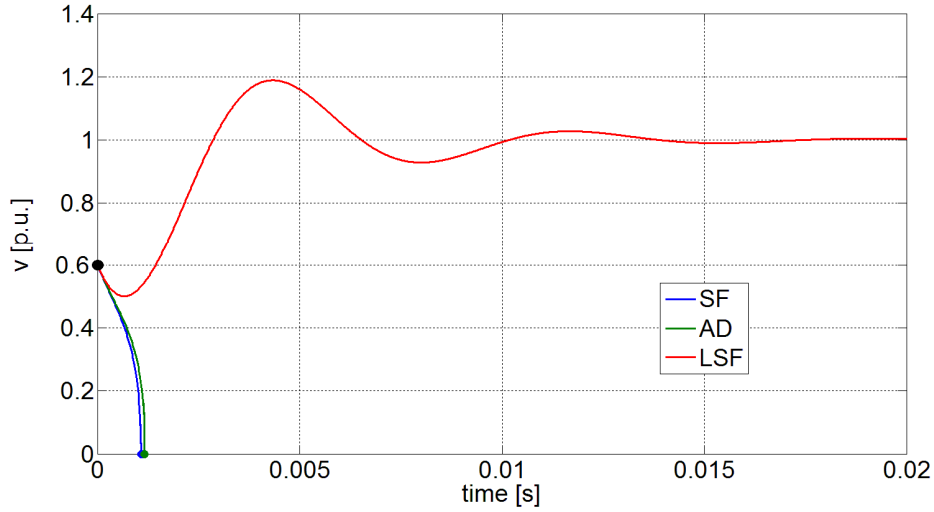

Figure 3.17 Voltage transient: $v(t_0)$=0.6.

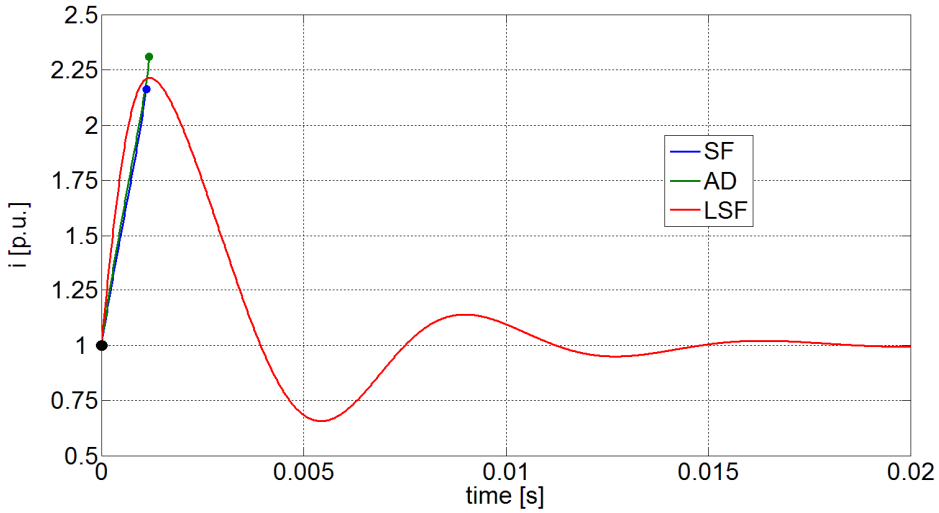

Figure 3.18 Current transient: $v(t_0)$=0.6.

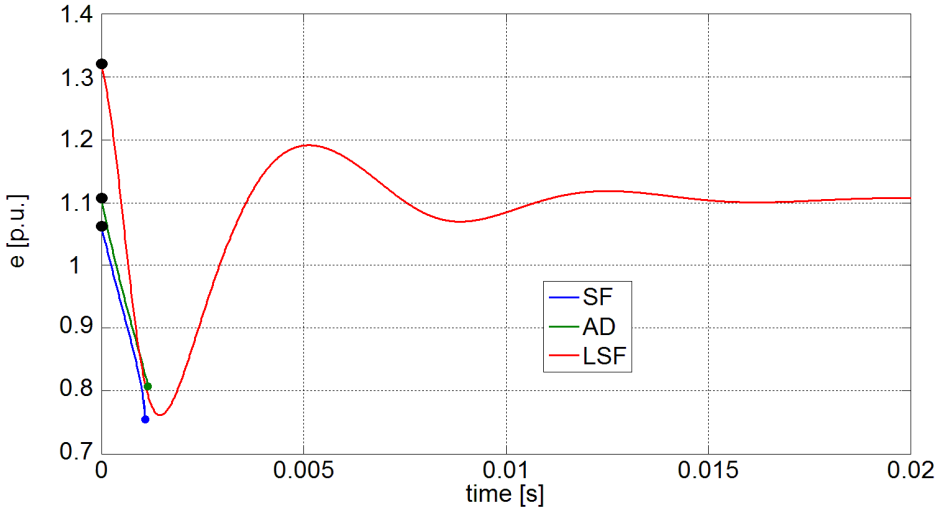

Figure 3.19 Voltage input transient: $v(t_0)$=0.6.

3.8 Saturation of interface converter

Linearization via State Feedback (LSF) has been demonstrated to be an effective technique to maintain system stability even in presence of wide perturbations, making possible a total cancellation of load non-linearity. To realize this compensation, the control signal F_c actuated by the DC/DC interface converter has to perform a derivative action to properly annul the non-linear voltage droop on the inductor and to set the two poles. From a control system point of view, derivative action is critical, being the main reason of interface converter saturation. Therefore such an event cannot be disregarded when LSF controls are employed, as they tend to be very demanding on actuator converters.

In control systems, the actuator saturation is a very common phenomenon [37]. It results particularly negative because it determines control capability loss: indeed the evolution of a saturated system is not controlled by the regulator, but it is forced by the actuator's boundary values. In particular, when the system controlled by LSF enters in saturation, the output voltage of the DC/DC converter remains at a constant value e_s, determining the loss of linearization functionality ($e=e_s$ independently from the control signal) therefore a non-linear system response. Such a response may be stable or instable depending on the saturated value e_s and on system parameters, as explained in Subsections 3.8.2 and 3.8.3.

3.8.1 Worst case scenario

The voltage saturation effect highlighted in this work is mainly due to two causes: perturbation entity and dynamics performance requirements. Talking about the first reason, a specified range of perturbations is defined by Figure 1.7 (voltage tolerances, worst case envelope), which shows the admitted limits for voltage transients. Values 2.00 and 0.75 correspond to recommended limit tolerated values for an MVDC bus voltage under plant normal operation (i.e. in absence of faults).

On the other hand, saturation effect is strongly dependent on dynamics performance: a well-performing control system tends to strongly stress the voltage actuator determining a long time saturation, whereas a standard control preserve the DC/DC interface converter limiting the time of control loss. It is therefore interesting to analyze the system behavior in presence of different couples ω_0 and ξ, in order to demonstrate the correlation between saturation time and controlled system dynamics.

By choosing a large perturbation (in accordance with the previous envelope $v(t_0)$ is put equal to 2), different control systems (namely LSF1, LSF2, LSF3) are tested by simulations in order to weigh the dynamics effect on voltage saturation and to identify a realistic worst case scenario. The first LSF control (LSF1) is set to guarantee ω_0=895 rad/s and ξ=0.3, while LSF2 ensures ω_0=1000 rad/s and ξ=0.5 LSF3. Finally the third (LSF3) provides best performance, defined by ω_0=1240 rad/s and ξ=0.76.

Results obtained by numerical simulations are depicted in the next pages, where Figure 3.20 shows the voltage transients and Figure 3.21 the current ones. Voltage input transients (Figure 3.22) allow to identify saturated behavior, which is characterized by a constant value e_s.

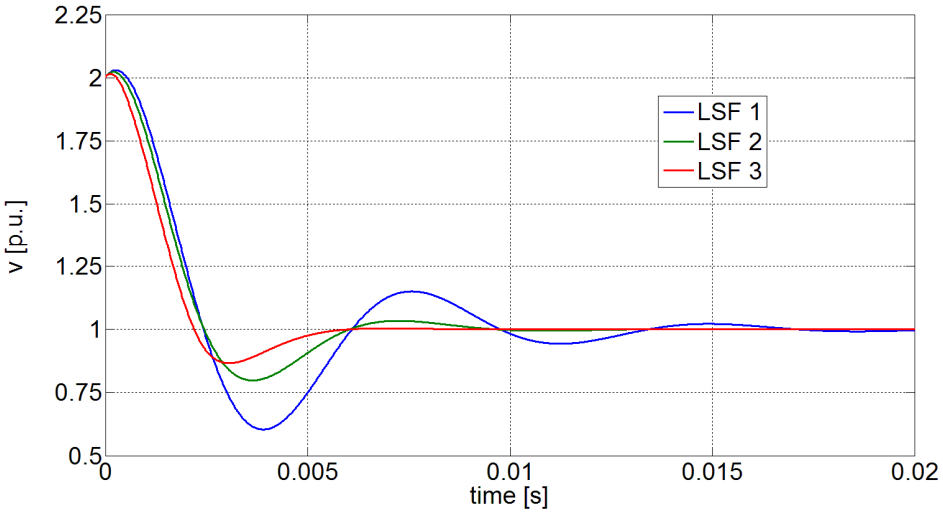

Figure 3.20 Voltage transients: LSF controls comparison.

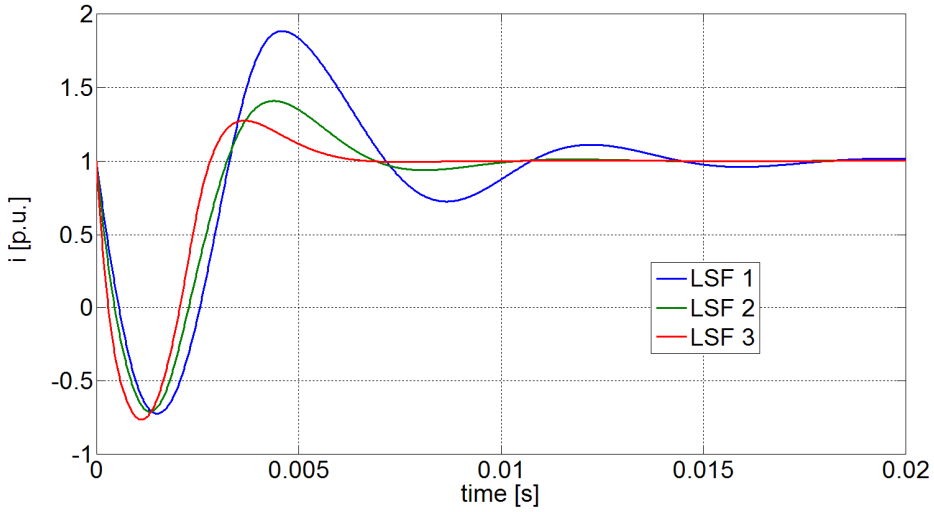

Figure 3.21 Current transients: LSF controls comparison.

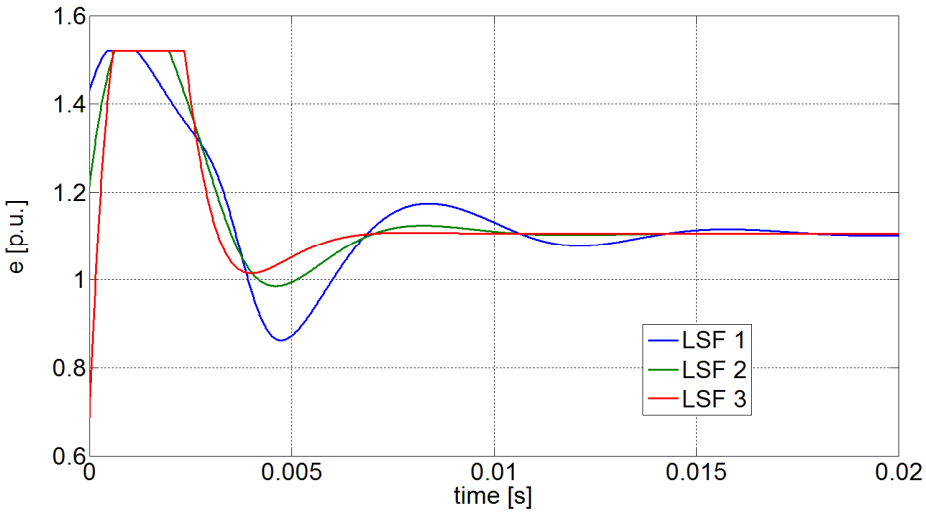

Figure 3.22 Voltage input transients: LSF controls comparison.

The given results demonstrate the stabilizing action provided by each LSF technique: in effect, designed controls are able to suitably restore the steady state voltage with the desired dynamics, solving the instability of CPL. Comparing the evolutions, it is well-rendered the better dynamics offered by LSF3 (red curve), which is characterized by a considerable damping.

In this last case, the price to pay regards the heavy saturation of voltage actuator (Figure 3.22): in presence of control LSF3, the voltage input saturation is long-lasting in respect to others control, about threefold LSF1 scenario. Among the designed dynamics (a control better than LSF3 appears unrealistic), it is evident that control LSF3 constitutes the worst case scenario from a saturation point of view. For this reason, following studies consider control LSF3 to underline stability conditions for the saturated system [55].

3.8.2 Saturated system

Voltage input e is controlled by LSF in order to react in reply to voltage disturbance: as demonstrated in last simulations, interface converter action can be very strong, therefore voltage e may be forced to enter in saturation (when $t = t_s$), remaining at a constant value (e_s) for a variable time interval (for $t \geq t_s$).

In this case, the action of control signal F_c, given by (3.38) and (3.44)-(3.45), is cancelled: the DC-link circuit starts to behave as a non-linear saturated system, supplied by the constant voltage e_s and it could therefore become instable: in this regard, Lyapunov analysis [27] may be useful to provide conditions for system stability under saturation.

Similarly of what presented in Chapter 2, the first step to study system stability is to determine the equilibrium points stability [55]. By substituting the saturated voltage e_s to the difference between constant voltage source e_0 and control function in equation (3.39),

$$e_s = e_0 - f_l - f_d \tag{3.50}$$

the saturated system can be described by equations (3.51)-(3.52):

$$\begin{cases} l_f \dfrac{\mathrm{d}i}{\mathrm{d}t} = e_s - r_f i - v & (3.51) \\ c_f \dfrac{\mathrm{d}v}{\mathrm{d}t} = i - \dfrac{p}{v} & (3.52) \end{cases}$$

Working on differential equations (3.51)-(3.52), the following system equation is obtained:

$$\frac{\mathrm{d}^2 v}{\mathrm{d}t^2} + \frac{1}{c_f l_f}\left(r_f c_f - \frac{l_f p}{v^2}\right)\frac{\mathrm{d}v}{\mathrm{d}t} + \frac{1}{c_f l_f}\left(v + \frac{r_f p}{v}\right) = \frac{e_s}{c_f l_f} \tag{3.53}$$

Putting derivative terms equal to zero in (3.53), two equilibrium points Q_1 and Q_2 are determined, one of which (named Q_1) can be stable. Point Q_1, given by (3.54)-(3.55)

$$\begin{cases} v_1 = \dfrac{e_s + \sqrt{e_s^2 - 4 r_f p}}{2} & (3.54) \\ i_1 = \dfrac{e_s - \sqrt{e_s^2 - 4 r_f p}}{2 r_f} & (3.55) \end{cases}$$

behaves as a stable point if following conditions are verified:

$$\begin{cases} r_1^0 = \dfrac{v_1}{i_1} \geq \dfrac{l_f}{r_f c_f} & (3.56) \\ r_1^0 \geq r_f & (3.57) \end{cases}$$

Conditions (3.56)-(3.57) have been obtained in (2.24)-(2.25) by small-signal system analysis: indeed, the stability of a non-linear system's equilibrium point may be verified by observing the stability of the linearized system in that point [37,38]. On the contrary, Q_2 never becomes a stable point, similarly of what demonstrated in previous Chapters. If the input voltage (i.e. the converter output voltage) remains saturated for $t \to \infty$ and condition detailed in the next paragraph is verified, $v(t)$ tends to v_1, that means the saturated system is stable.

3.8.3 Region of attraction

The region of attraction around the equilibrium point Q_1 can be found using Lyapunov theory. Related analytical developments have been presented in [27], for the system considered feeding a CPL, whose power is equal to the rated value (p=1). When the control action is inactive due to saturation [55], the non-linear system stability can be studied by the sufficient condition (3.58), being $v(t_s)$ the CPL voltage in the instant t_s in which the converter enters in saturation:

$$v(t_s) \geq \sqrt{\frac{l_f}{r_f c_f}} \tag{3.58}$$

As explained in Section 2.4, inequality (3.58) represents a sufficient (but not necessary) condition for the initial state of the non-linear saturated system (3.53) to belong to the region of attraction and to evolve to the stable equilibrium point Q_1.

3.8.4 Analysis in the v-i state plane

In Figure 3.23, a graphic representation of a v-i evolution is presented to understand the system behavior during the saturation [55]. For the studied case, conditions (3.56), (3.57) and (3.58) are verified, therefore the fundamental requirement of stability is ensured. The v-i state plane is divided into two zones: saturated system (green) and unsaturated system (white). The separation line is given by equation (3.50), whereas the limit of condition (3.56) is represented by the oblique dashed line. Considering the system specified in the following (Subsection 3.8.5), two trajectories (bold and narrow) are obtained by simulations.

Firstly, it is necessary to explain the different segments that composed the time evolution (bold trajectory):

- First arc (I-S), which shows the unsaturated system trajectory described by linear equation (3.46).
- Second arc (S-L) described by equation (3.53). This path starts from point S, which corresponds to instant t_s when the system enters in saturation. Corresponding voltage $v(t_s)$ stays in the region of attraction, limited by the horizontal dashed line, i.e. the Lyapunov sufficient condition (3.58).
- Third arc (L-Q_0), which corresponds to the final evolution towards the equilibrium point Q_1. In this trajectory, the system has gone out of the saturation, so evolutions still follows (3.46).

Secondly, the narrow path (L-Q_1) describes the case of a long time saturated system, for $t>t_L$ (where t_L is the instant in which the converter exit from the saturation). This curve represents the trajectory described by non-linear equation (3.53). It is noteworthy that the trajectory is stable and converges to point Q_1 if it behaves as a stable point (i.e. (3.56)-(3.57) satisfied) and if voltage $v(t_s)$ is inside the region of attraction (i.e. equation (3.58) verified).

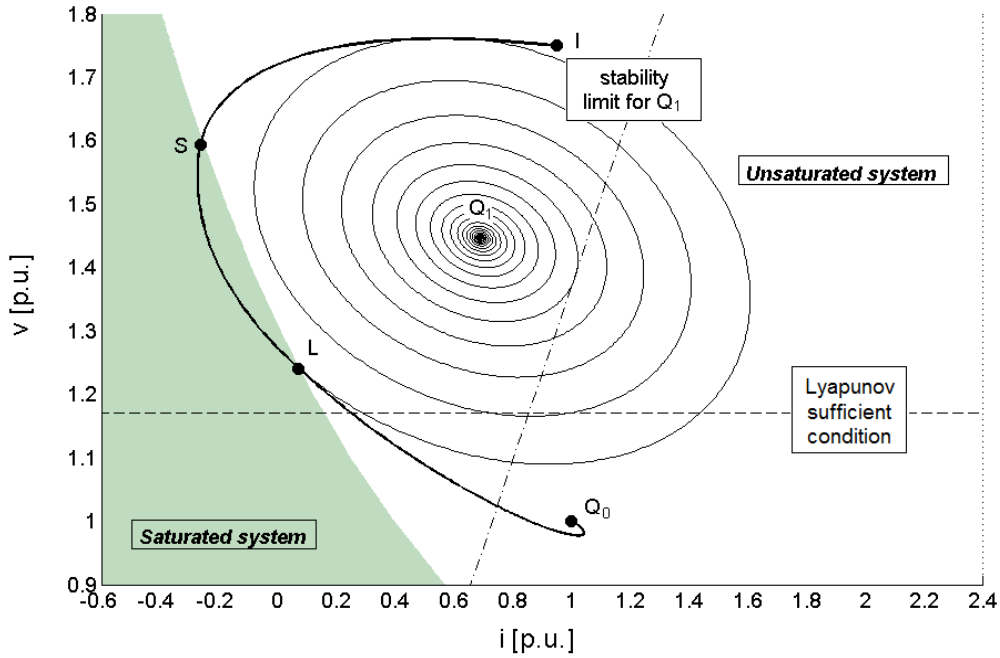

Figure 3.23 Analysis in the v-i state plane.

3.8.5 Numerical simulations

The system behavior in saturated region may be analyzed by developing some simulations [55] on the average value model of Subsection 3.4.2. For what concern system parameters, the case of study of Section 3.5 is assumed as reference. As concluded in Subsection 3.8.1, LSF3 control represents the worst case scenario for saturation issue: therefore related performance indexes are chosen to calculate (3.48) the constants k_1=0.1025 and k_2=0.5018.

In order to simulate the DC/DC interface converter operation, saturation value is fixed at e_s=1.52. This value allows to obtain voltage and current for the equilibrium point Q_1 (v_1,i_1)=(1.45,0.69), by using equations (3.54)-(3.55). By calculating the resistance $r_1^0=v_1/i_1$=2.09, the stability of point Q_1 is guaranteed from inequalities (3.56)-(3.57), being r_1^0 greater than 1.37. For the non-linear saturated system, Lyapunov limit condition (3.58) brings $v(t_s)\geq$1.17.

Designed control is tested observing the system evolution by starting from different initial voltage states, $v(t_0)$. Particularly, four different p.u. values of $v(t_0)$ are chosen: 2, 1.75, 1.5, 1.25 and 0.75. Limit values (2 and 0.75) correspond to recommended limits expressed in [13]. Values 1.75 and 1.25 are instead intermediate values, chosen well within the voltage tolerance range (Figure 1.7). The main purpose of these tests is to proof that, if initial values of voltage are within the tolerance range, than the control system LSF3 is able to recover steady state voltage without violating the limits given by Figure 1.7. The second aim of simulations is to study the converter saturation, highlighting system trajectories for different initial conditions.

3.8.6 Simulations results

Simulation results (CPL voltage and inductor current) are condensed in Figure 3.24, which shows five trajectories in the v-i state plane [55], assuming a steady state point Q_0 of v_0=1, i_0=1. Starting from previous initial values placed in the linear region (white zone), system evolutions are depicted to point out the saturated behavior of two cases, characterized by $v(t_0)$ equal to 2 and 1.75.

By observing Figure 3.24, the relation between voltage disturbance and DC/DC converter action appears clear: after a large voltage perturbation, only a strong converter action may reestablish the CPL voltage, determining at the same time converter saturation. The latter is a very critical situation for MVDC power systems, being the common cause of control capability loss. Therefore, the worst perturbations for the system studied are those which determine the converter saturation, approximately disturbance that move the capacitor voltage over 1.6 (i.e. disconnection of a large CPL) or under 0.7 (i.e. connection of large CPL). Conversely, safe perturbations are those included in the range 0.7-1.6: indeed they are not able to impose a saturated behavior, thus the trajectories remain in the white zone where the LSF control is activated.

Although trajectories traced in the v-i state plane are derived by two time evolution $v(t)$ and $i(t)$, they do not provide dynamics information. Anyway, the dynamics related to larger perturbation ($v(t_0)$=2) can be observed in Figures 3.20, 3.21 and 3.22. In particular the voltage transient of Figure 3.20 demonstrates that the controller is able to quickly reestablish the nominal conditions keeping the bus stable. So it is possible to conclude that LSF3 technique faces properly the worst voltage variation admitted for normal working conditions of the MVDC bus (Figure 1.7).

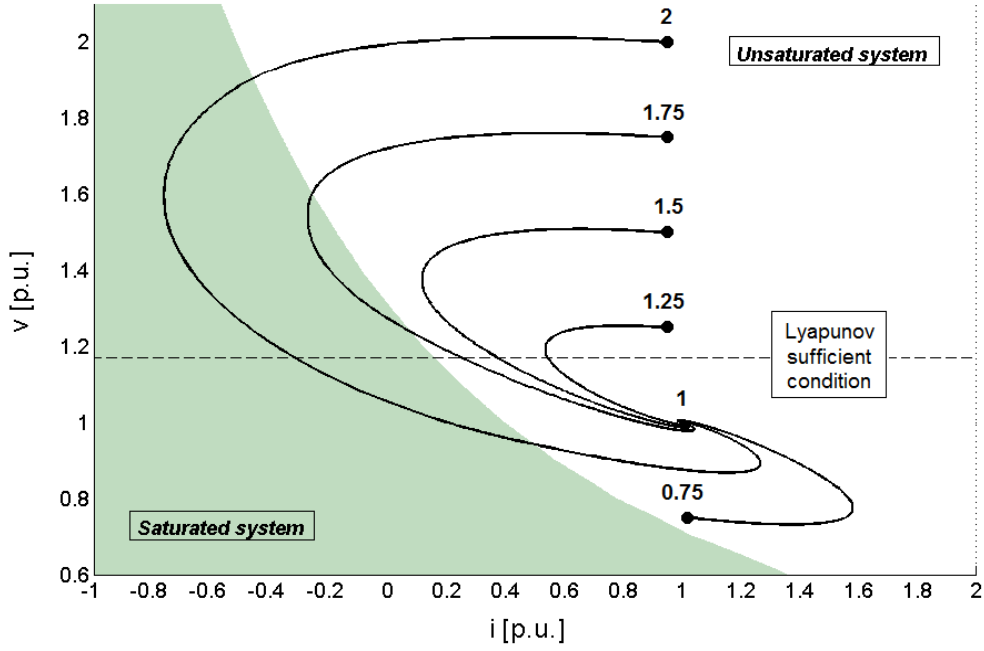

Figure 3.24 Trajectories in the v-i state plane.

3.9 Conclusions

The third Chapter has proposed one feasible approach to solve the voltage instability of Constant Power Loads: in particular, the voltage actuator approach may be a good solution to compensate for the instability effect, by using generating systems as sources of stabilizing power.

After a brief description of common requirements for control systems, the single converter has been modeled to provide a case of study, therefore a basic MVDC power system. Three different techniques (State Feedback, Active Damping, Linearization via State Feedback) have been proposed to control such a power system feeding a CPL: the voltage control techniques have been designed to avoid voltage oscillations and instability after disturbances, ensuring the operation in the stable equilibrium point.

By implementing the case of study by AVM, some simulations have been performed to emphasize pros and cons of each technique. Results obtained by SF and AD controls have shown the simplicity of these techniques, which may be easily implemented also in the power station control of multi-converter arrangement (Chapter 5). On the other hand simulations have also proven intrinsic limits, being basic controls not able to compensate for the CPL destabilizing effect in critical conditions. To complete the evaluation, LSF has demonstrated to be a complex effective control capable for solving instability also in critical scenario, where very large perturbations move state variable v far away the equilibrium value. Also LSF may be usefully implemented in multi-converter power systems (Chapter 6), being the load sharing functionality directly enabled by the linearizing control signal.

The main disadvantage of LSF control technique is the saturation of voltage actuator, due to the presence of derivative terms in the control signal. Such negative aspect has been analyzed by suitable tests on a selected worst case scenario, where the dynamic performance imposed by control LSF3 is remarkable (very high damping factor). The final analysis on the v-i state plane has seemed to be a good tool to study the dangerousness of voltage perturbations, identifying those whose compensation force the converter response in the saturation zone.

4. Multi-converter MVDC power system

4.1 Introduction

A possible multi-converter MVDC power system will be defined in Chapter 4, starting from the IEEE standard, re-designing a common MVAC radial distribution and comparing the suitability of different interface converters. Finally the application described in Section 4.3 will be useful to validate the voltage actuator' choice, whereas the final Section will introduce two strategies to control multi-converter power systems.

4.2 Case of study

The MVDC proposed plant layout is a re-design of an MVAC radial distribution. An example of a possible MVAC Integrated Power System is reported in Figure 4.1.

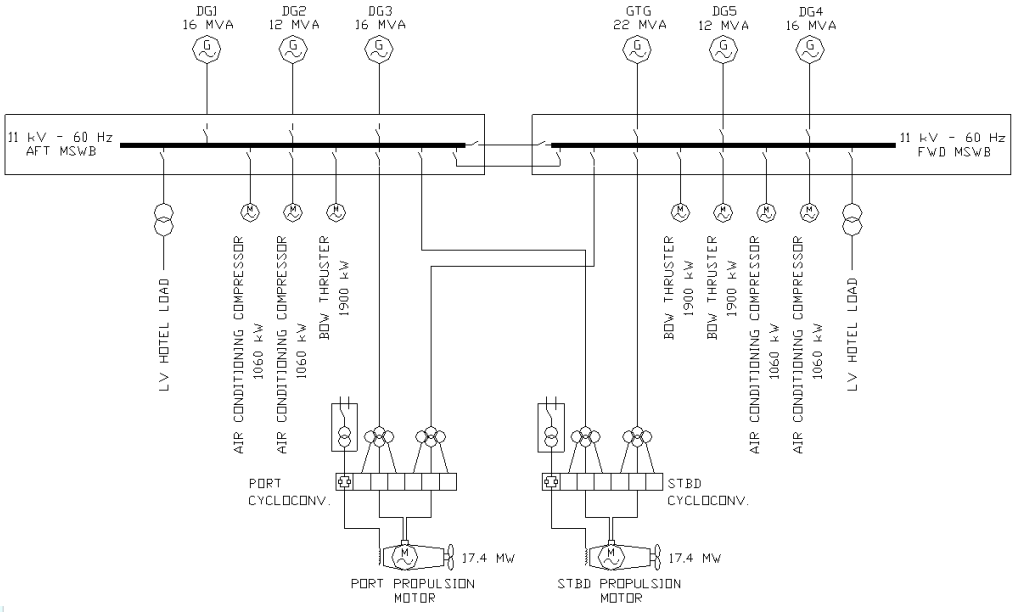

Figure 4.1 Cruise liner MVAC distribution [56].

4.2.1 Basic multi-converter power system

With reference to the MVDC radial concept distribution (Figure 1.5) specified in [13], a feasible project of shipboard MVDC power system is determined in this Subsection. In particular the same AC generators and the same loads of an actual MVAC large all-electric ship are maintained, while MV distribution is realized by the Medium Voltage Direct Current. A basic power system is shown in Figure 4.2, where interface converters are represented by generic AC/DC blocks. The sections are as follows:

- 4 DC generating systems constituted by AC generators (G1-G4) and AC/DC interface converters (C1-C4);
- 6 DC/AC inverters (I1-I3 and I6-I8) directly connected to the MVDC bus feeding propulsion and thrusters (M1-M6);
- 3 load lines, fed by dedicated DC/DC buck converters (B1-B3) supplying loads (L1-L3) which represent the remaining low voltage shipboard users in an equivalent way;
- Converters' output filters (CF1-CF4 and BF1-BF3).

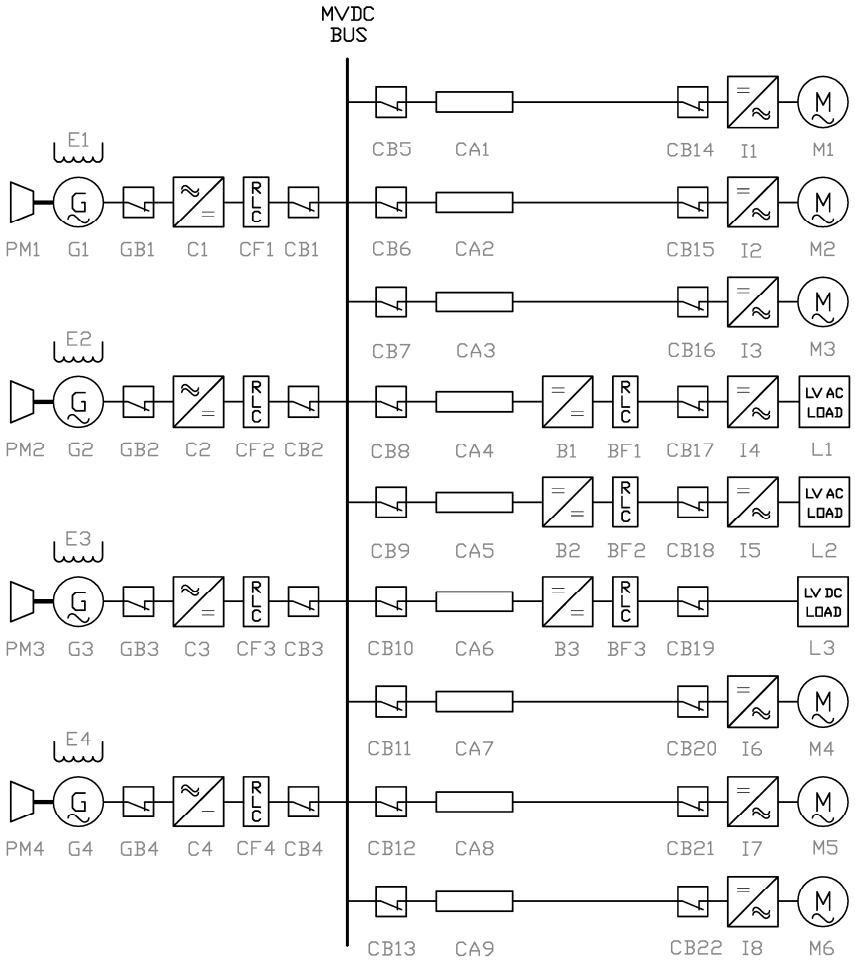

Figure 4.2 Basic multi-converter MVDC power system.

4.2.2 Interface converters

In an MVDC power system the voltage control is realized by means of some dedicated AC/DC power converters (C1-C4 in the previous Figure), acting as “voltage actuators” to interface the AC generating systems and the MVDC bus. The choice of a realistic AC/DC interface converter needs a proper evaluation: then four different options for system arrangement are preliminarily examined [27,57] for determining their performance. The possible options are:

1) diode rectifier;
2) thyristor rectifier;
3) forced commutated rectifier;
4) diode rectifier coupled to a DC/DC buck converter.

Their main characteristics are studied, with particular reference to the rapidity of response and to the maximum deliverable power. Functional aspects (such as switching frequency, transient response, conversion losses, voltage, current and power limits) are also taken into account in this comparison.

Option 1) has been evaluated in some works [58]. From a control point of view, it is not a suitable solution remembering the requirements (Section 3.3): indeed, the diode rectifier’s intrinsic uncontrollability and the insufficient control bandwidth offered by the AVR regulator (acting on AC machine) suggest to consider different types of interface converter.

On the other hand, option 2) appears particularly interesting for its simplicity. Thyristors are available for a wide range of power level making the implementation quite simple. Main limitation of this solution is the switching frequency that coherently limits the maximum control bandwidth. With the 60 Hz AC frequency, the switching frequency of a traditional Graetz bridge is 360 Hz with a maximum bandwidth around 100 Hz (i.e. an angular frequency of about 700 rad/s). Such a bandwidth is considered insufficient for the dynamics of interest. Even if different solutions may be adopted to increase the bandwidth performance (as adopting a multi three-phase generator with a multiple stator to multiply the apparent switching frequency, or using a generator that works at higher frequency), they are not considered for this application, preferring simplicity and feasibility. Also, another drawback of option 2) is the need of reactive power to support the desired steady state firing angle: the more control margin is desired, the more the generator has to be oversized, since generator power factor is basically coincident with the firing angle cosine.

Option 3) is considered less robust, because of its boost behavior. The controllability is actually guaranteed only if the output voltage is kept properly high and this aspect can be seen as a limit in transient but even more in fault conditions.

Instead, option 4) perfectly decouples the generator from the DC bus control, by exploiting a DC/DC converter. This solution allows considerably higher switching frequencies (typically in the order of kHz), which is a mandatory aspect to solve CPL instability, making possible relevant voltage dynamics. Option 4) is only apparently more complicated because of the presence of two stages: in reality, the DC/DC converter can be realized and engineered in the same cabinet that contains the diode rectifier, with no particular disadvantage. Further pro regards the absence of reactive

power impact on the AC source, being diode converters utilized to convert voltage from AC to DC. As a reference, this solution has been actually adopted to build a prototype of an ultra-high-speed generator (Naval Package) for naval MVDC applications [59].

4.2.3 Selected multi-converter power system

For the aims of this thesis, option 4) is chosen and modeled being the better arrangement in terms of dynamics and stabilizing action: therefore it is possible to provide the multi-converter MVDC power system (Figure 4.3) utilized in the following Chapters. The interface converters (e.g. C1) are substituted by diode rectifiers (e.g. D1) and DC/DC buck converters (e.g. B1), conveniently filtered by 2nd order RLC stages (e.g. DF1 and BF1).

To establish the validity of the DC/DC concept, Section 4.3 will treat a possible application, that is an innovative generation system arrangement interfaced by four buck converters [59,60]. Simulations will able to highlight the DC/DC converters dynamics, confirming the effectiveness of the converter choice.

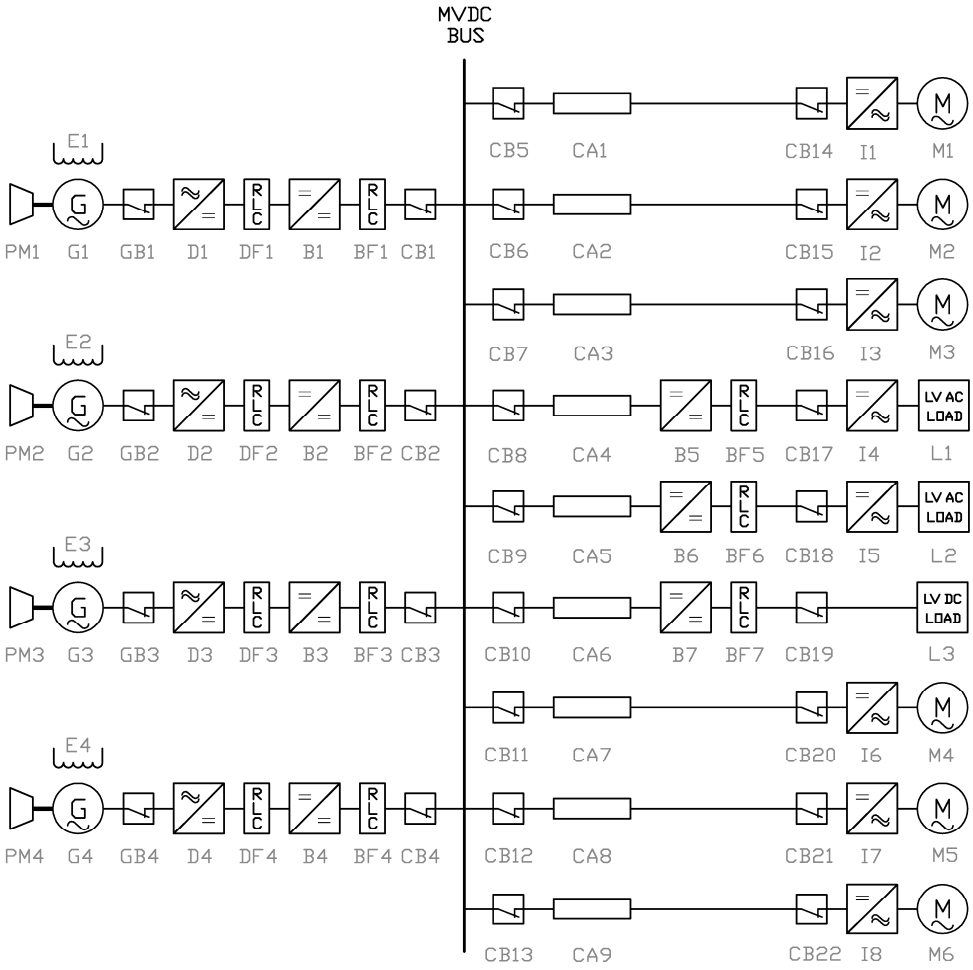

Figure 4.3 Proposed multi-converter MVDC power system.

4.3 Multi-converter resistive case

The study is conveniently focused on a comprehensive linear (resistive) load, omitting the possible presence of non-linear loads (CPL) in order to simplify the comprehension of overall power system behavior. On the other hand, loads non-linearity will be discussed in Chapters 5 and 6, which will propose voltage control techniques to face the CPL stability issue in the multi-converter case.

4.3.1 Naval packages

A promising generation system arrangement is based on a split-phase generator equipped with N stator windings, each connected to an AC/DC converter. Such a topology has been already implemented in two full-scale 2 MW prototype systems [58,59] for future potential use in naval applications (Naval Packages NP1 and NP2). Merging the two Naval Packages, this Subsection would derive a new power system [60] where two actuators are committed to realize the voltage control.

The former (NP1) features a high-speed (6300 rpm) six-phase Wound-Field Synchronous Generator (WFSG) feeding the DC linear load through two diode bridge serial connected. Instead, the latter (NP2) is based on an ultra-high-speed (22500 rpm) 12-phase Permanent Magnet Synchronous Generator (PMSG) supplying the DC resistor through four AC/DC diode converters cascaded by DC/DC buck converters. Talking about the voltage control, Naval Packages of Figure 4.4 utilize different voltage actuators to control the output DC voltage, respectively the generator exciter (NP1) and the buck converters (NP2).

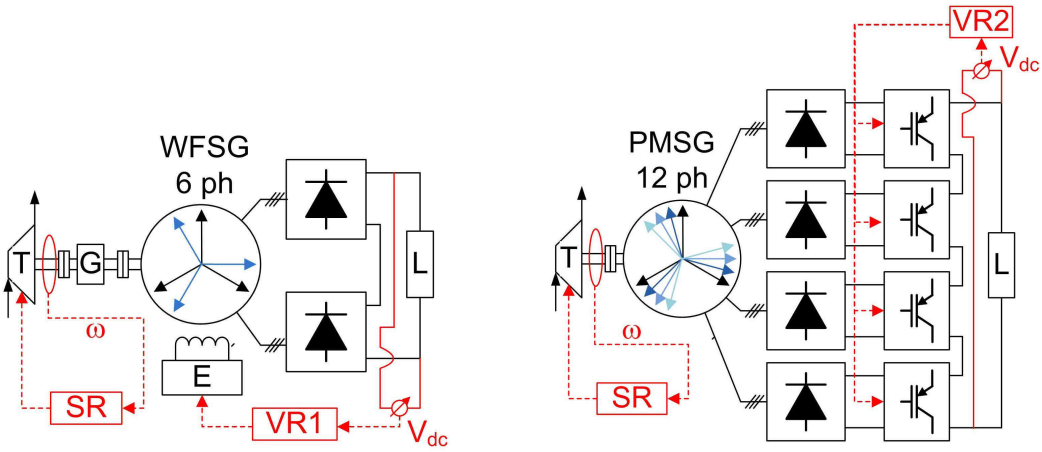

Figure 4.4 Proven Naval Packages: NP1 (left) and NP2 (right).

The “hybrid” power system architecture chosen for this study (Figure 4.5) results from a combination of the configurations NP1 and NP2, being exploited both voltage actuators (Figure 4.4). In particular the system employs a split-phase WFSG (preferred to the PMSG for its better power scalability) along with controlled converters (as usual diode bridges + buck converters) to realize the interface between AC and DC.

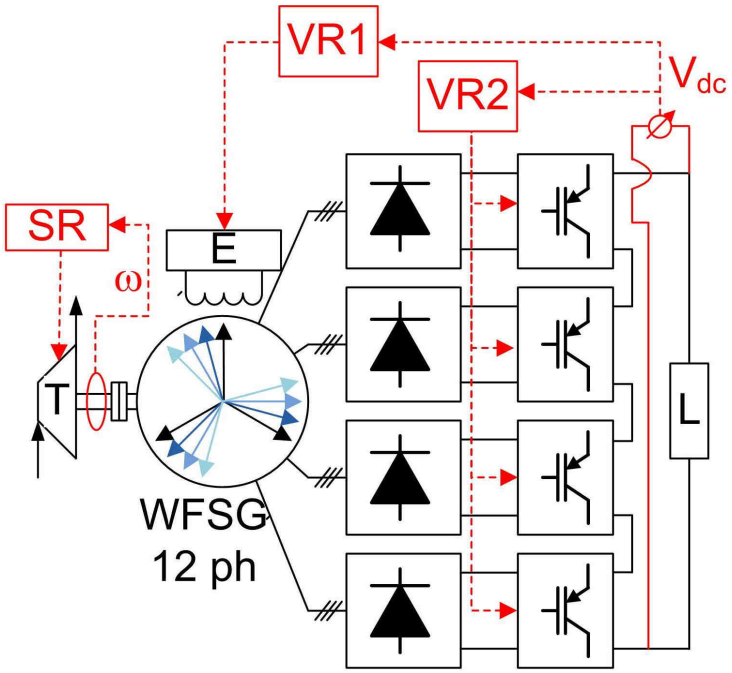

Figure 4.5 New Naval Package.

A 12 phase stator configuration is chosen for the benefits it brings in terms of output voltage and generator air-gap harmonics [61] as well as in terms of winding construction technology for high power implementations [62]. As seen before, from a control viewpoint the main feature of the investigated configuration is the DC bus voltage control, obtained acting on both generator excitation and output buck converters. The two tasks are performed by regulators VR1 and VR2 respectively.

4.3.2 Voltage control design

A standard proportional-integral (PI) structure is assumed [60] for all the regulators, setting a one-decade separation margin between the control loops bandwidths, thus preventing possible instability issue. Normally this separation should be enough to guarantee an almost complete decoupling among loops and to avoid issues due to their possibly detrimental mutual interactions during transients. Neglecting the frequency regulator (the speed control is outer the thesis topic), the time-constants for the two closed-loop control systems are given in Table 4.1: a typical time-constant is selected for the exciter, whereas the one related to DC/DC converter is consequently derived.

Voltage actuator	Closed loop time-constant
Exciter	0.5 s
Buck converter	0.05 s

Table 4.1 Closed-loop time constants.

4.3.3 System modeling

The power system shown (Figure 4.5) is modeled in the Matlab/Simulink environment to test the voltage control [60]. A block scheme representing the whole system is reported in Figure 4.6, which includes all the main components: generator (yellow), power converters (green and gray), filters (red and magenta), voltage controls (cyano and orange) and DC resistive load (blu).

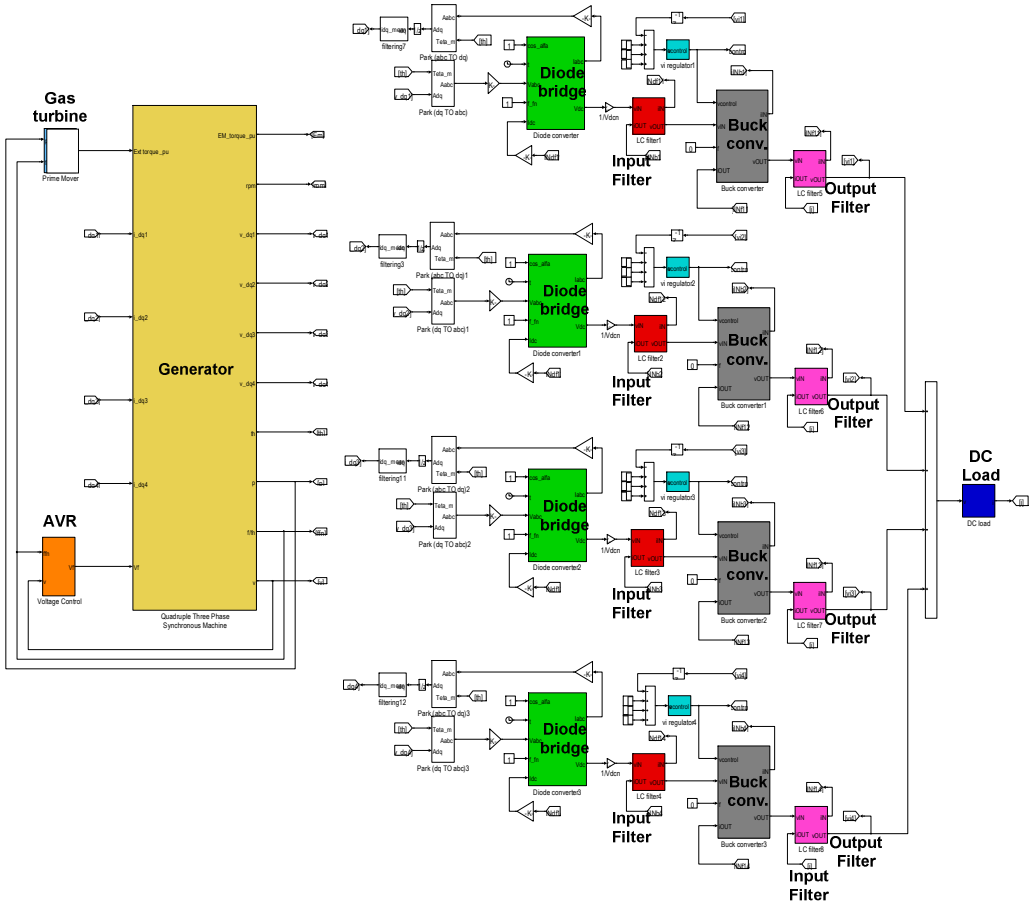

Figure 4.6 Simulink scheme of the new Naval Package.

4.3.4 Simulation results

As seen in Subsection 4.2.3, the selected MVDC power system (Figure 4.3) employs four DC/DC interface converters paralleled on the same bus. Differently from this scheme, the possible future Naval Package here discussed (Figure 4.5) is based on another topology, i.e. DC/DC converters serial connected. Anyway, this difference does not matter because the aim of the simulation only regards the interface converter validation. For this purpose, a simulation is set [60] to understand the tasks realized by the five voltage actuators (i.e. four buck converters and one generator exciter).

Initially the rated speed condition is assumed for the generating system, while the linear load is supposed disconnected. Then next changes are applied in sequence:

1. t=0.05 s, the buck regulator commands the rated voltage (i.e. 1 p.u., 2000 V) on the no-load bus.
2. t=0.25 s, the load is still disconnected, whereas a load voltage reference step is applied to reach the 110% of the rated voltage (i.e. 1.1 p.u., 2200 V).
3. t=0.5 s, the MVDC generating system is connected to the load (related power corresponds to 0.15 p.u., i.e. 0.15 MW), while the reference voltage output is kept equal to 1.1 p.u.
4. t=0.75 s, the resistive load is maintained unchanged, whereas its voltage reference is changed to the rated value, i.e.1.0 p.u.

The following Figures show the response of the MVDC generating system to the previous sequence. Figure 4.7 reports the DC output voltage (i.e. the sum of the four buck voltages) transient, where the reference value is achieved very quickly in both no-load (t<0.5 s) and loaded conditions (t>0.5 s). This waveform is evidently affected by a limited ripple (1.5 kHz is the switching frequency) proving the proper design of filtering stages. Regarding dynamics, the remarkable voltage performance is given by the action of each buck converter, which is controlled by a fast voltage control loop (time-constant of 0.05 s). In this regard, the duty cycle depicted in Figure 4.8 shows the action of one DC voltage actuator.

Instead, talking about the dynamics forced by the AVR regulator, it is possible to observe the slowness of AC voltage control (Figure 4.9). Thus the promptness of the DC voltage regulation is exclusively due to the buck converters action. To complete the overview on transients, Figure 4.10 and Figure 4.11 provide the evolutions of load current and power.

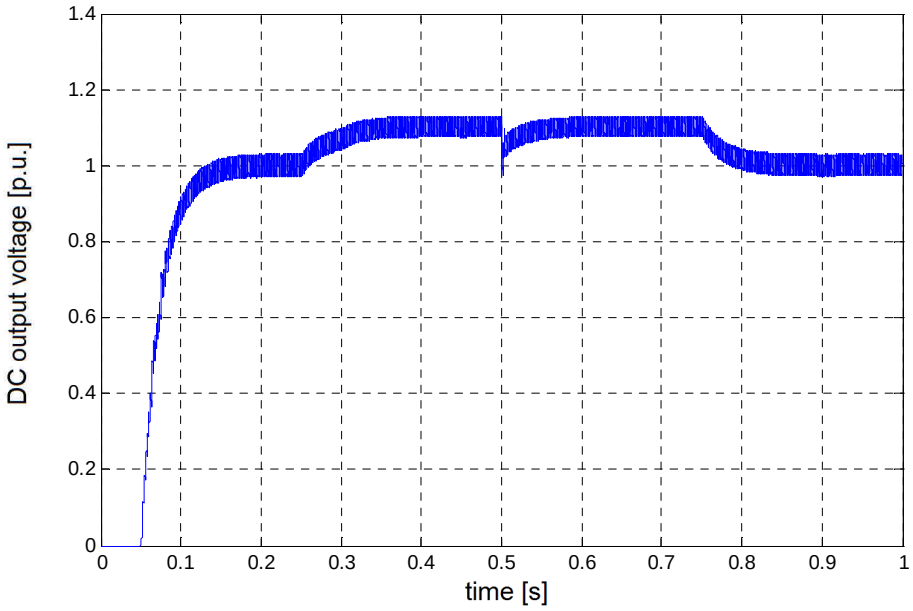

Figure 4.7 DC output voltage transient.

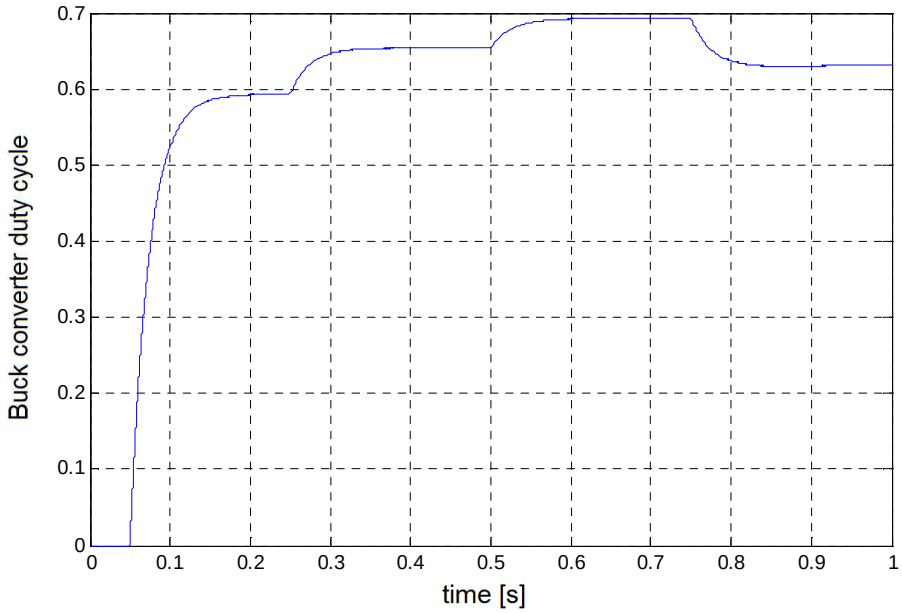

Figure 4.8 Buck converter duty cycle.

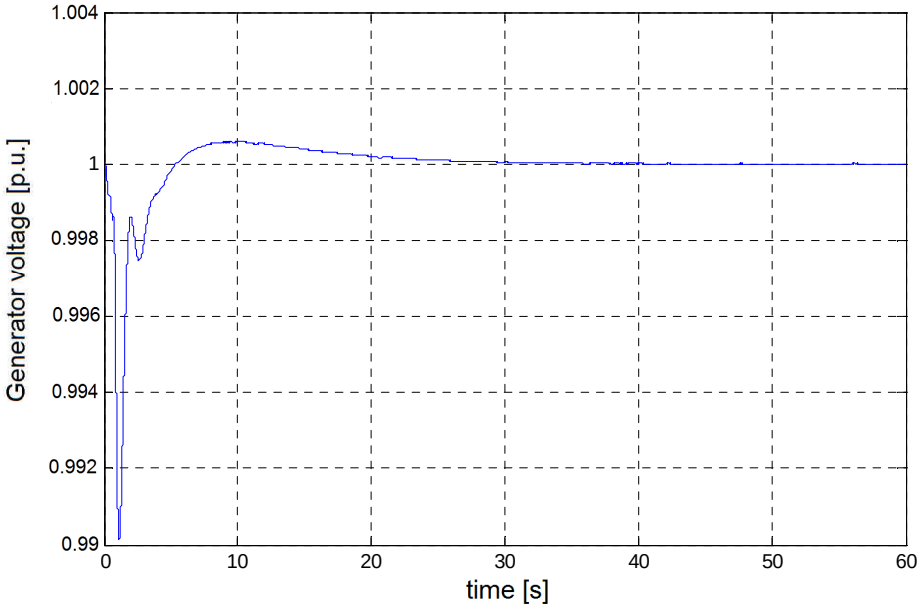

Figure 4.9 Generator voltage transient.

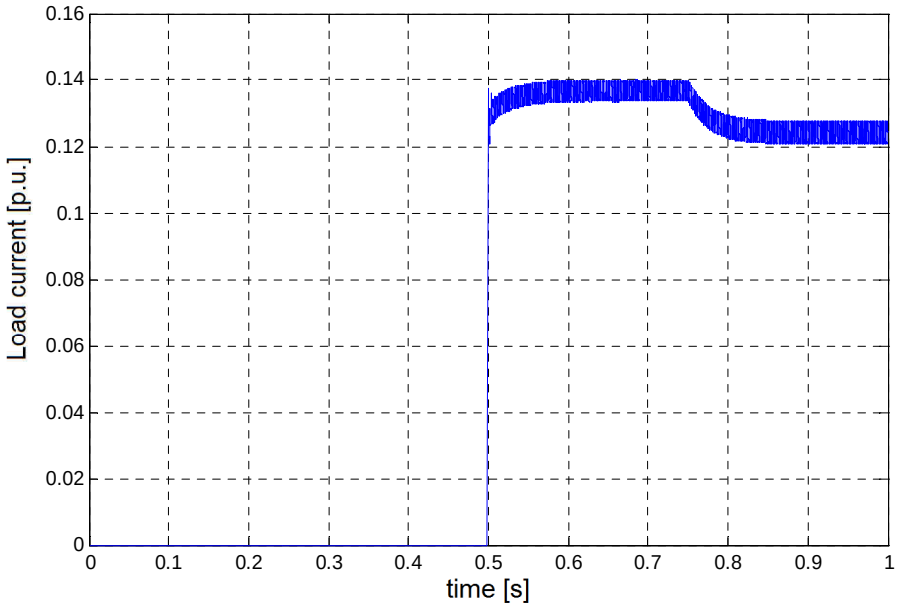

Figure 4.10 Load current transient.

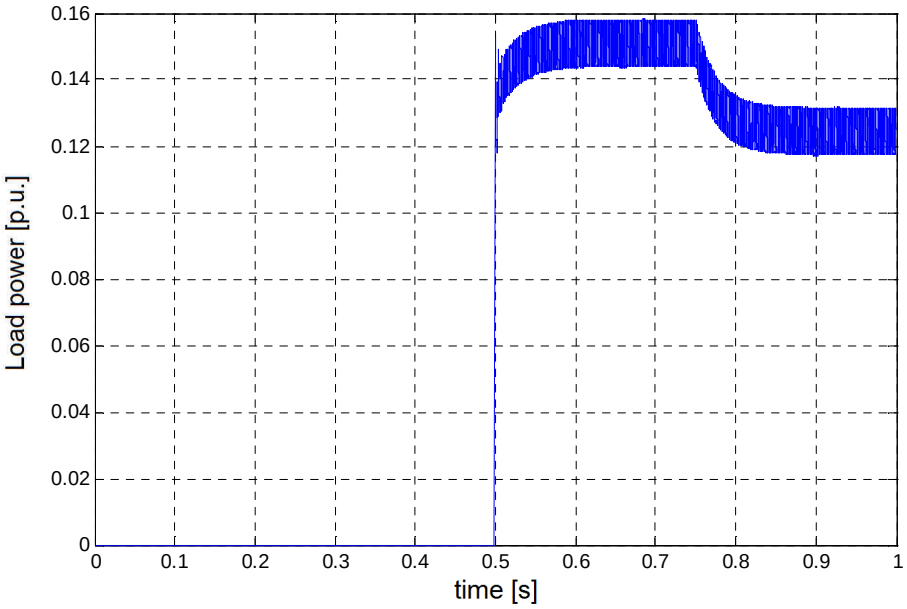

Figure 4.11 Load power transient.

4.4 Voltage control strategies in a multi-converter power system

Results obtained have demonstrated the buck converters ability [60] in controlling the DC voltage with a considerable dynamics. These power converters are widely used in the selected MVDC power system (Figure 4.3), which will be coherently assumed as a reference case for further analysis on multi-converter voltage control. The stability issue, discussed in Chapter 3 for the single machine, is not negligible in case of a real multi-converter power system. In this case the destabilizing CPLs could be very numerous, considering the large employment of controlled load converters to supply propulsion or ship services. Therefore almost each section of the MVDC power system may be cause of voltage instability.

In order to solve this troubling issue in a highly complex system, such as the multi-converter MVDC arrangement, the academia has developed different control approaches, for example the one based on synergetic control theory [63,64]. In this thesis, a different approach will be studied, starting from the definition of two strategies to control all the MVDC power system voltages: the global strategy and the local one. Developed strategies will be based on the employment of voltage actuators (DC/DC interface converters), which are to be controlled to solve CPL instability.

The aim for the global strategy is to guarantee the bus voltage stability, taking advantage of the stabilizing action performed by generating DC/DC converter (e.g. B1-B4 of Figure 4.3). On the other hand, local strategy has the purpose to ensure the voltage stability on loads, by exploiting DC/DC converters like B5-B7. In order to realize these targets, previous techniques analyzed in Chapter 3 will be implemented to properly govern the DC/DC interface converters.

4.5 Conclusions

A possible power system scheme for an MVDC distribution has been proposed and discussed in Chapter 4. In particular, great attention has been paid in evaluating the interface converters, comparing four different typologies. For this aim, a new Naval Package has been utilized to perform simulations, whose dynamics results have recommended to exploit the buck converters as voltage actuators in the on-board MVDC power systems.

The power system behavior shown in this Chapter has represented only a starting point, being supplied a resistive load. Further developments are to be realized to assure voltage stability in presence of CPLs, which may be widely spread on MVDC power systems. In this regard, two control strategies have been introduced (global and local) to regulate the voltage in multi-converter power systems. These strategies will be designed to minimize the CPL destabilizing effect in critical conditions, such as non-linear load connection (treated in Chapter 5) or sudden generator disconnection (Chapter 6).

5. Global AD and local LSF strategies to solve CPLs instability

5.1 Introduction

In this Chapter a complex voltage control based on two strategies (Section 4.4) will be designed in order to solve the CPL stability issue in a multi-converter MVDC power system. Control strategies utilized will apply the stabilizing power approach (Chapter 3), foreseeing to implement additional stabilizing functions into the digital controllers of the DC/DC interface converters. The implemented strategies will have to ensure the stability requirement compliance.

A first strategy (global AD, Active Damping) will stabilize the MVDC bus voltage by controlling the power station. The second one (local LSF, Linearization via State Feedback) will be exploited to solve the instability of highly impacting loads. The AD is a well-known technique (Subsection 3.6.2) based on the introduction of transient virtual resistances into the system. The aim is to improve system's stability using virtual resistances damping effect. Instead, LSF technique (Subsection 3.6.3) is usually utilized in case of high power CPLs, compensating for their non-linearity by means of a non-linear feedback. The resulting linear system can be then controlled utilizing traditional techniques from linear control theory.

5.2 Shipboard MVDC power system

The shipboard MVDC system with radial distribution depicted in Figure 4.3 is chosen for this study [65]. This power system presents a large amount of DC/DC power converters connected to the bus: in particular, 4 converters on the power station side and 3 converters on the load side. Thanks to the presence of many interface converters, the MVDC stability issue may be generally solved in two different ways, by controlling the generating DC/DC converters or the load ones.

Nevertheless, proposed strategies intend to use each converter typology, in order to provide an effective hierarchical control: the stability of highly impacting loads (L1-L3) is guaranteed by the B5-B7 control action (by local LSF), while converters B1-B4 control the MVDC bus (by global AD) facing the instability due to inverters directly connected to the bus (I1-I3, I6-I8).

5.3 Filters design

The aim of this Section is to design [65] the 2nd order output filtering stage (R_{fk}, L_{fk} and C_{fk} are the parameters expressed in absolute values), ignoring the diode converter filtering stage (R_{dk}, L_{dk} and C_{dk}). In effect, the hypothesized control strategies act only on the buck converter stage, therefore AC generator, diode converter and first filtering stage may be neglected in the following studies. Hence a generic DC generating system *k* may appear [49] as the one shown in Figure 5.1.

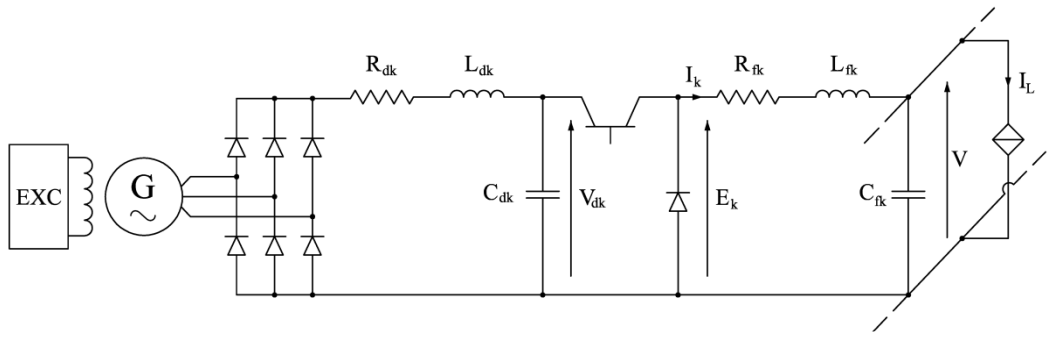

Figure 5.1 DC generating system *k*.

5.3.1 Synthesis

It is well assessed that given combinations of filter parameters with a high CPL power level are responsible for stability issues (Chapter 2). At small-signal level, analytical conditions for stability can be easily determined on filter parameters and on the CPLs power level (Section 2.3). For the case under study, filters parameters R_{fk}, L_{fk} and C_{fk} (being k=1,2,…4) are determined applying well-known design equations [45]. In particular following terms are considered in the synthesis:

- P_{nk} : DC/DC converter rated output power
- V_{dnk} : DC/DC converter rated input voltage
- V_{nk} : filter rated capacitor voltage
- I_{nk} : filter rated inductor current
- f_{sk} : DC/DC converter switching frequency
- $\Delta P_{\%k}$: DC/DC converter + filter losses (percentage)
- $\Delta I_{\%k}$: filter current ripple (peak to peak)
- $\Delta V_{\%k}$: filter voltage ripple (peak to peak)
- R_{fk} : filter resistor
- L_{fk} : filter inductor
- C_{fk} : filter capacitor

Using definitions (5.1)-(5.2), equations (5.3)-(5.4) can be utilized to determine filter parameters basing on ripple specifications:

$$\begin{cases} D_{nk} = \dfrac{V_{nk}}{V_{dnk}} & (5.1) \\ I_{nk} = \dfrac{P_{nk} - \Delta P_{\%k} \cdot P_{nk}}{V_{nk}} & (5.2) \end{cases}$$

$$\begin{cases} L_{fk} = \dfrac{(V_{dnk} - V_n) \cdot D_{nk}}{f_{sk} \cdot I_{nk} \cdot \Delta I_{\%k}} & (5.3) \\ C_{fk} = \dfrac{1 - D_{nk}}{8 \cdot L_{fk} \cdot f_{sk}^2 \cdot \Delta V_{\%k}} & (5.4) \end{cases}$$

Instead, resistor R_{fk} can be expressed as in (5.5),

$$R_{fk} = \frac{\Delta P_{\%k} \cdot P_{nk}}{I_{nk}^2} = \frac{\Delta P_{\%k} \cdot P_{nk}}{(1 - \Delta P_{\%k})^2 \cdot P_{nk}^2} \cdot V_{nk}^2 \quad (5.5)$$

5.3.2 CPL stability analysis

Considering each k filter and linearizing the P_{nk} power load (supposed completely non-linear), it is possible to determine (3.10)-(3.11) the natural angular frequency ω_{0k} (5.6) and the damping factor ξ_k (5.7) of the resulting complex poles:

$$\begin{cases} \omega_{0k} = \sqrt{\dfrac{1}{L_{fk} \cdot C_{fk}} \left(1 - \dfrac{R_{fk}}{R_k^0}\right)} & (5.6) \\ \xi_k = \dfrac{1}{2\omega_{0k} \cdot L_{fk} \cdot C_{fk}} \left(C_{fk} \cdot R_{fk} - \dfrac{L_{fk}}{R_k^0}\right) & (5.7) \end{cases}$$

where $R^0_k = V_{nk}^2 / P_{nk}$ is the absolute value of the negative incremental resistance.

The evaluation (5.7) of the damping factor ξ_k is considered of paramount importance before designing any control system. In particular, the negative value of ξ_k is assumed as an index of system instability, which depends both on the filter parameters and on the loading level P_{nk}, represented by R^0_k.

5.3.3 Design

Table 5.1 encloses the values of damping factor ξ_k calculated for all the output filtering stages present in the system, having assumed each buck converter supplying an infinite-bandwidth CPL whose power is equal to the buck rated power. Starting from specifications about power losses $\Delta P_{\%k}$, current ripple $\Delta I_{\%k}$ and voltage ripple $\Delta V_{\%k}$, previous equations (5.1)-(5.7) are utilized to design filters:

	BF1/BF3	BF2/BF4	BF5	BF6	BF7
P_{nk} [MW]	15.75	10.50	13.50	1.50	2.70
V_{dnk} [V]	8910	8910	6000	6000	6000
V_{nk} [V]	6000	6000	4000	3000	2000
D_{nk}	0.67	0.67	0.67	0.5	0.33
I_{nk} [A]	2494	1662	3206	475	1282
f_{sk} [Hz]	1500	1500	1500	2000	2000
$\Delta P_{\%k}$	5	5	5	5	5
$\Delta V_{\%k}$	1	1	1	1	1
$\Delta I_{\%k}$	35	35	45	40	45
R^0_k [Ω]	2.3	3.4	1.2	6.0	1.5
R_{fk} [mΩ]	126.63	189.95	65.66	332.41	82.08
L_{fk} [mH]	1.50	2.24	0.62	3.95	1.15
C_{fk} [μF]	1212.24	808.16	3005.86	395.83	1803.51
ω_{0k} [rad/s]	721.53	721.53	714.20	777.52	673.35
ξ_k	-0.1915	-0.1915	-0.1219	-0.2166	-0.2252

Table 5.1 Filters design (global AD, local LSF).

For the multi MW, multi-converter DC power system under study, these negative damping factors ξ_k will be considered for practical design of the power station's AD control (Subsection 5.4.1).

5.4 System modeling and control design

The voltage control analysis [65] regards a large All Electric Ship MVDC power system (Figure 4.3), with the realistic presence of many DC/DC interface converters (e.g. B1, on the generating systems, and B5 on the dedicated load lines), to be controlled according to different targets.

5.4.1 Global AD control strategy

It is assumed to control the DC/DC buck converters of the power station (B1-B4) using the AD technique, thus inserting transient virtual resistances serial connected to the physical ones (R_{fk}). AD resistances are introduced into the system by a proper control technique, as explained in Subsection 3.6.2 for a single converter example.

To realize a global AD strategy, three output signals from a Centralized regulator are to be added to the buck voltage references (Figure 5.2). In particular, the Centralized regulator block may be subdivided into three functional blocks (Figure 5.3), because three are the main targets of the global strategy: the Power sharing block (Figure 5.4), the Bus voltage regulator (Figure 5.5) and the Power Signal Stabilizing block (Figure 5.6).

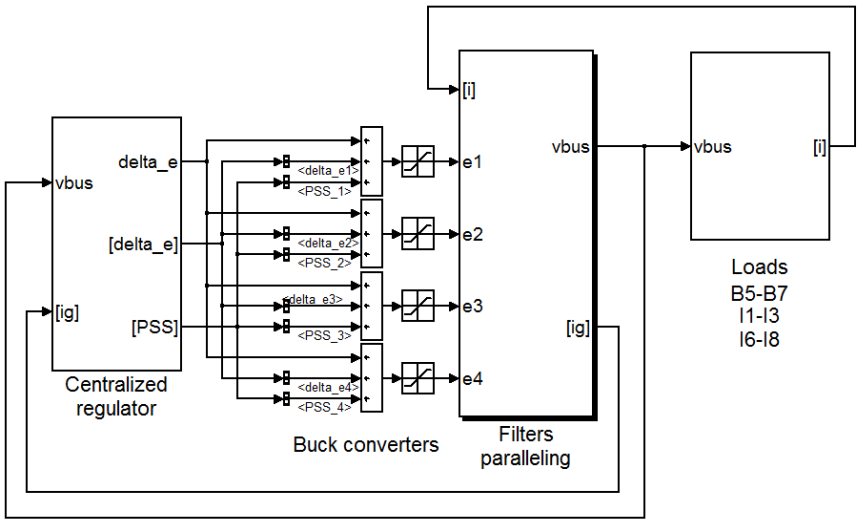

Figure 5.2 Simulink scheme (global AD, local LSF).

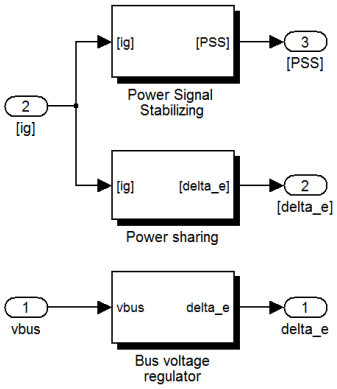

Figure 5.3 Centralized regulator (global AD).

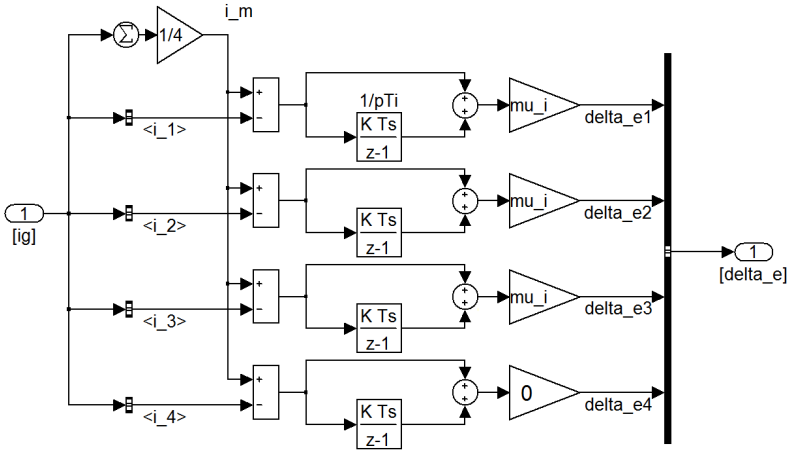

Figure 5.4 Power sharing block.

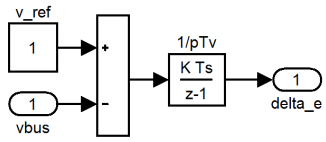

Figure 5.5 Bus voltage regulator.

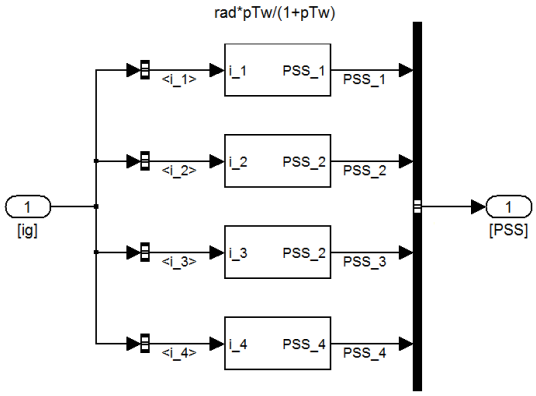

Figure 5.6 Power Signal Stabilizing block.

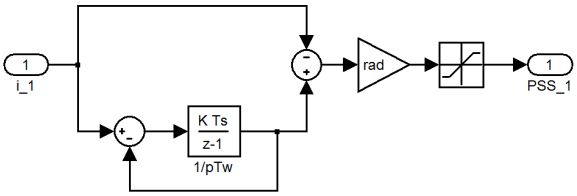

Figure 5.7 Active Damping virtual resistance.

By means of Power sharing block (Figure 5.4), the Centralized regulator is able to implement a steady-state load sharing over the DC generating systems, which result loaded at the same percentage power level (with reference to rated powers). This functionality is obtained by using n-1 integral regulators (being n the generators running), imposing that all the converter' currents equate to their mean value at the steady-state. This equalization is most relevant in the practice of shipboard MVDC power system: otherwise the power system would suffer from huge uncontrolled current exchange between the buck converters themselves, even in case of small differences between buck output voltages. The centralized regulator provides also the elimination of the steady-state bus voltage error by means of the integral regulator shown in Figure 5.5. Talking about CPL destabilizing effect, the block of Figure 5.6 is needed to calculate proper PSS signals to damp the oscillations. This important function is obtained in the voltage control (Figure 5.2), by summing a negative term proportional to the inductor current (PSS signals). The proportional coefficient is given by the desired AD resistance (Figure 5.7), virtually inserted in each filtering stage.

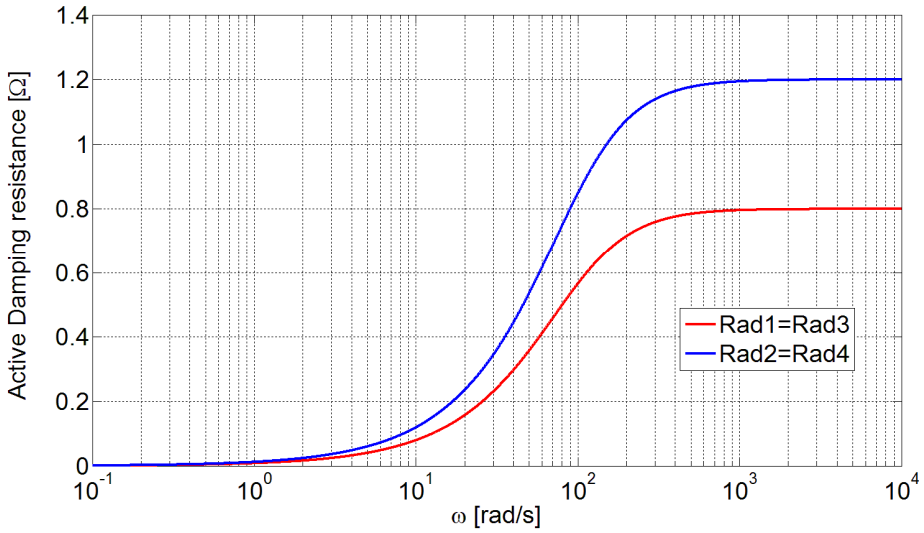

Figure 5.8 Active Damping resistances (global AD).

In order to ensure a desired damping effect (ξ_{ADk}), the AD resistances R_{ADk} are suitably calculated by using the following relationship:

$$\xi_{ADk} = \frac{1}{2\omega_{0k} \cdot L_{fk}} R_{ADk} + \xi_k \tag{5.8}$$

Keeping into account the effect of each physical resistance (ξ_k and ω_{0k}), R_{ADk} values are evaluated considering a damping factor target ξ_{ADk} of 0.18 [66]. The virtual resistances are then "washed-out" by a 1st order high-pass filter, whose pole is placed between $0.1\omega_{0k}$ and $0.2\omega_{0k}$ (about 100 rad/s for the studied case). Figure 5.8 shows the values (as functions of the angular frequency) of the damping resistances. Two values are determined for this case: the red one for generating systems 1=3 and the blue one for generating systems 2=4.

5.4.2 Local LSF control strategy

In the studied power system (Figure 4.3), three lines (i.e. L1-L3) are interfaced to the MVDC bus by means of DC/DC interface converters (i.e. B5-B7) to supply low voltage AC and DC loads. Obviously these load lines could be affected by voltage instability, assuming that supplied loads (I4+L1, I5+L2 and L3) are of the CPL typology. Therefore DC/DC converters (i.e. B5-B7) are to be properly controlled to resolve possible local instabilities.

By observing Table 5.1, the relevant entity of B5 power (13.50 MW) advises to control load line L1 by a LSF well-performing technique, whereas B6 and B7 (low powers) can be regulated by basic techniques not investigated in the thesis (e.g. SF). The linearizing technique has been discussed in Subsection 3.6.3, hence the methodology has

been already developed also for the B5 local LSF control strategy. Therefore, to appropriately place the poles of the system (a natural frequency of 1250 rad/s and a positive damping of 0.3 are chosen as design specifications), control gains k_1 and k_2 may be tuned by using (3.48).

5.5 Numerical simulations

For the proposed MVDC power system, voltage control and stability are studied in the Matlab/Simulink environment depicted in Figure 5.2. Considering the dynamics of interest, the developed power system is modeled basing on the AVM assumption: in effect, the validity of such a simplified model has been demonstrated by the cross-validation of Subsection 3.4.4.

Simulations tests are carried out [65] in order to verify the effectiveness of the comprehensive control, choosing two possible disturbances obtained by load variations and considering the activation/deactivation of the control strategies. For this aim, time evolution of load powers is reported in Table 5.2, where P_n is the total power for each load. Contemporaneous step connection (in t=4 s) of CPLs I1+M1 and I8+M6 is used to check external control loops, therefore the damping introduced by AD method. Later (in t=4.2 s), I4+L1 highly impacting CPL is connected to test the local LSF voltage control.

Bus voltage, I4 load voltage, total load current and generators currents are respectively represented in Figures 5.9-5.16. In order to facilitate the results comprehension, electrical variables are expressed by means of absolute values (kV and kA). Interactions between controls are highlighted and possible cases of instability (leading to interventions of under-voltage fault protections) are pointed out. In voltage transients, the under-voltage fault level is traced by considering the MVDC worst case envelope of Figure 1.7.

	P_n [MW]	Load Power [MW]		
		t<4 s	4 s<t<4.2 s	t>4.2 s
I1+M1	12.0	5.25	11.8125	11.8125
I2+M2	2.2	0	0	0
I3+M3	1.9	0	0	0
I4+L1	13.5	5.25	5.25	13.125
I5+L2	1.5	1.05	1.05	1.05
B7+L3	2.7	2.625	2.625	2.625
I6+M4	3.5	2.625	2.625	2.625
I7+M5	2.2	0	0	0
I8+M6	12.0	5.25	11.8125	11.8125
total	51.5	22.05	35.175	43.05

Table 5.2 Time evolution of load powers (global AD, local LSF).

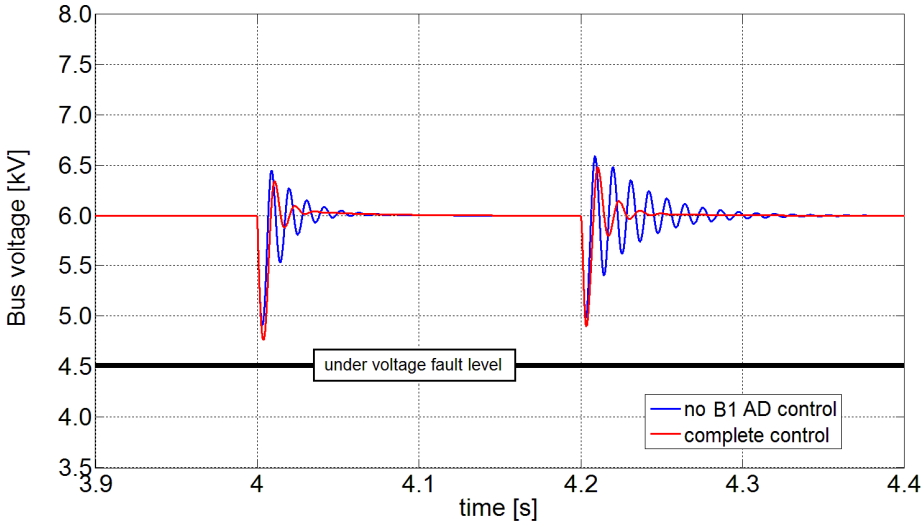

Figure 5.9 Bus voltage transient: loss of AD control.

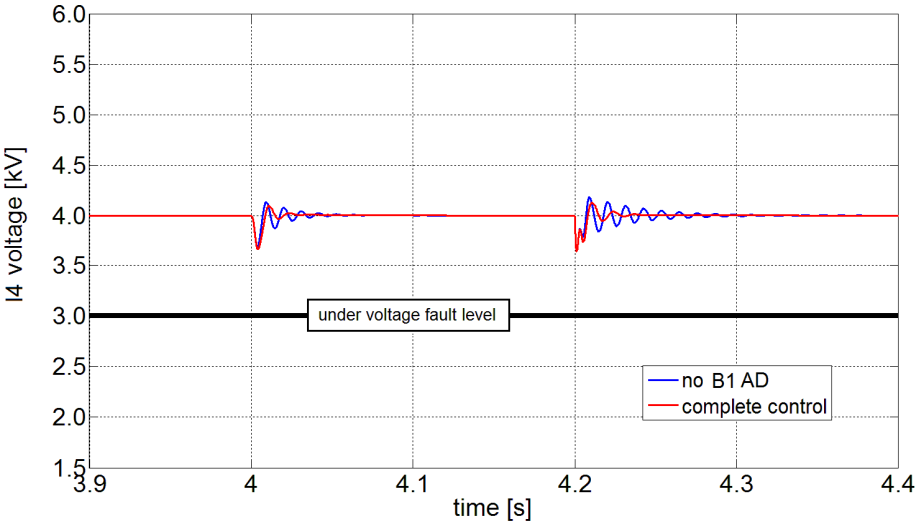

Figure 5.10 Load voltage transient: loss of AD control.

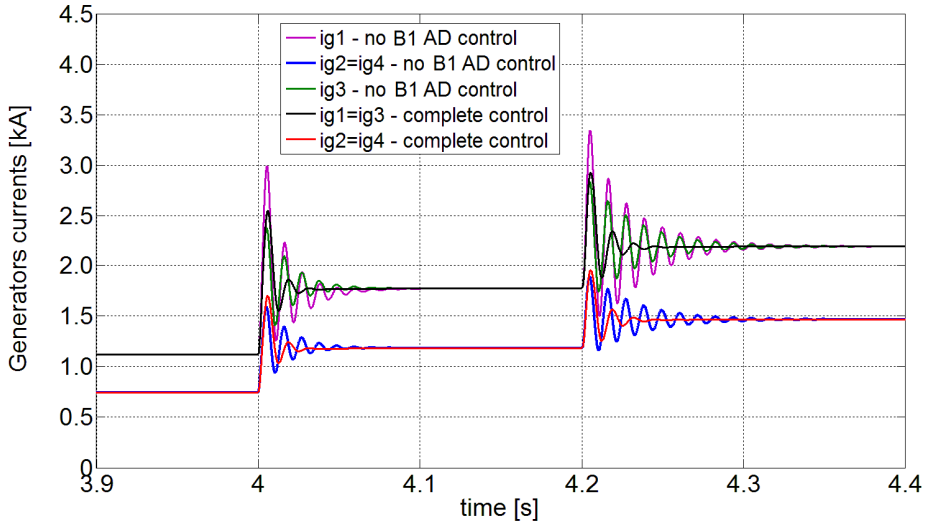

Figure 5.11 Generators currents transient: loss of AD control.

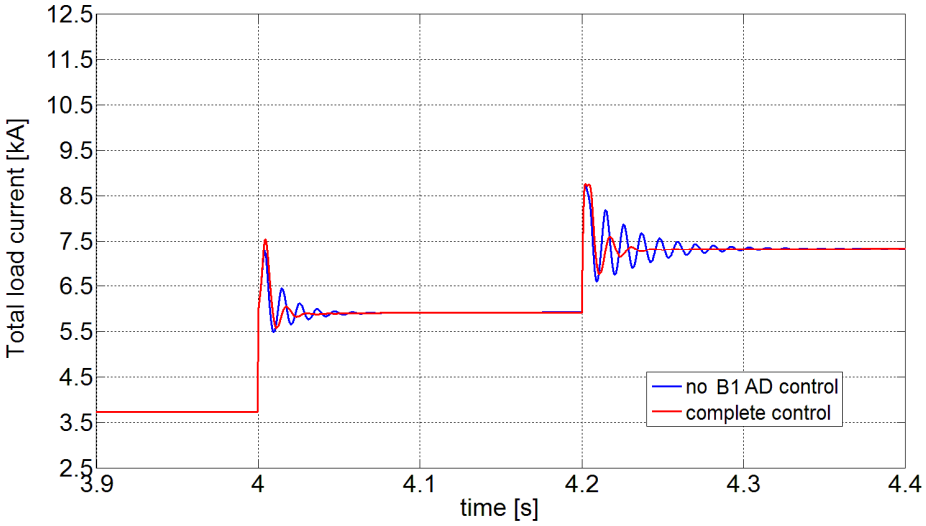

Figure 5.12 Total load current transient: loss of AD control.

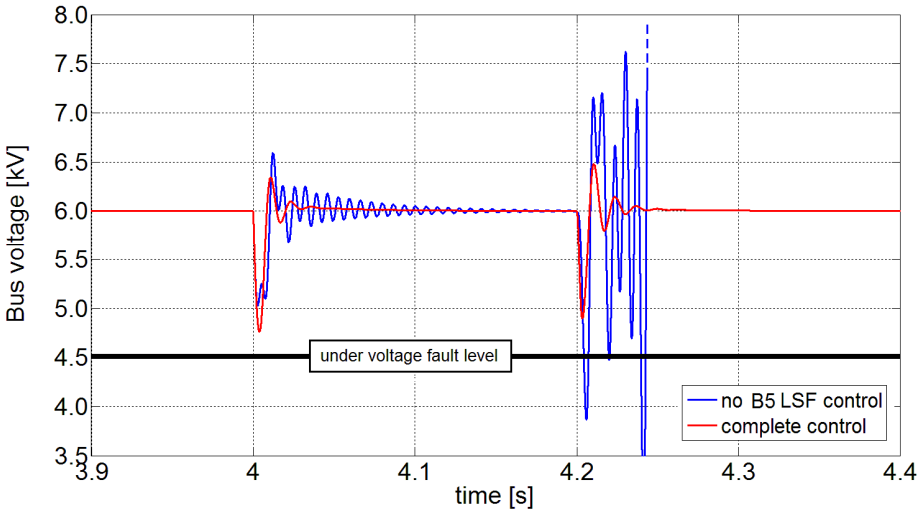

Figure 5.13 Bus voltage transient: loss of LSF control.

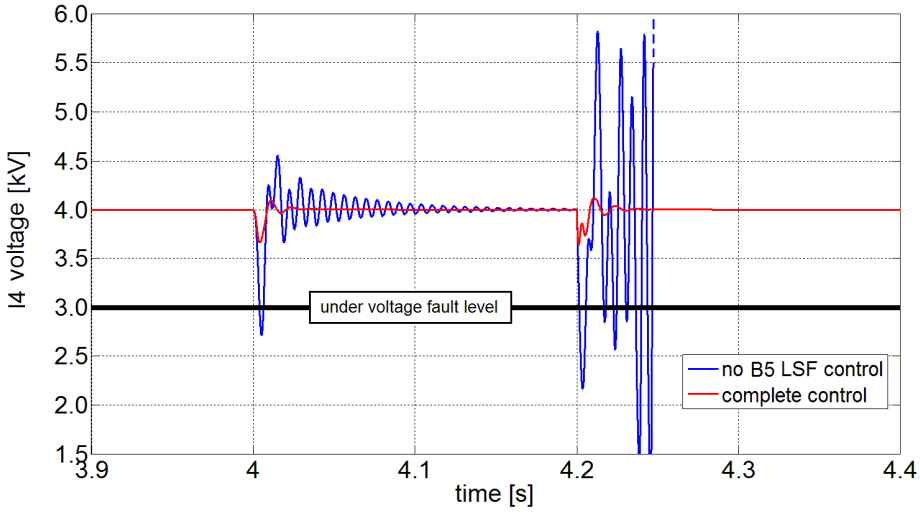

Figure 5.14 Load voltage transient: loss of LSF control.

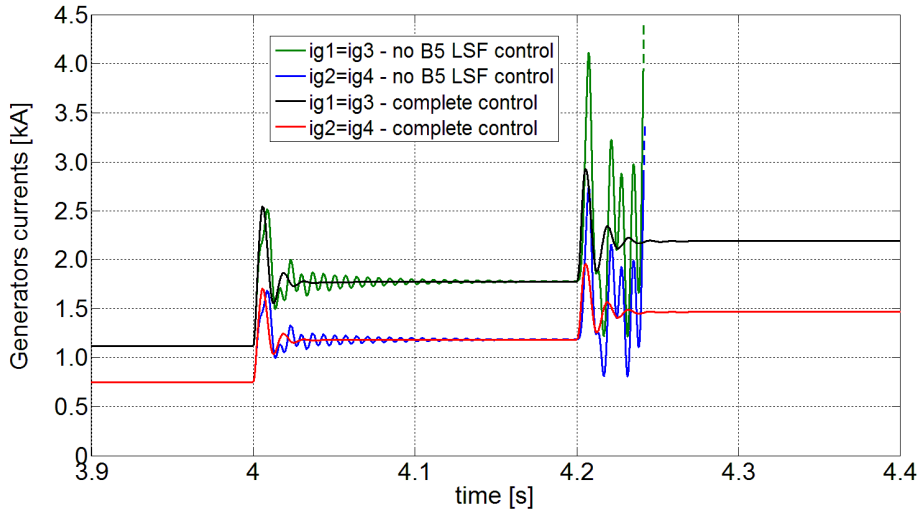

Figure 5.15 Generators currents transient: loss of LSF control.

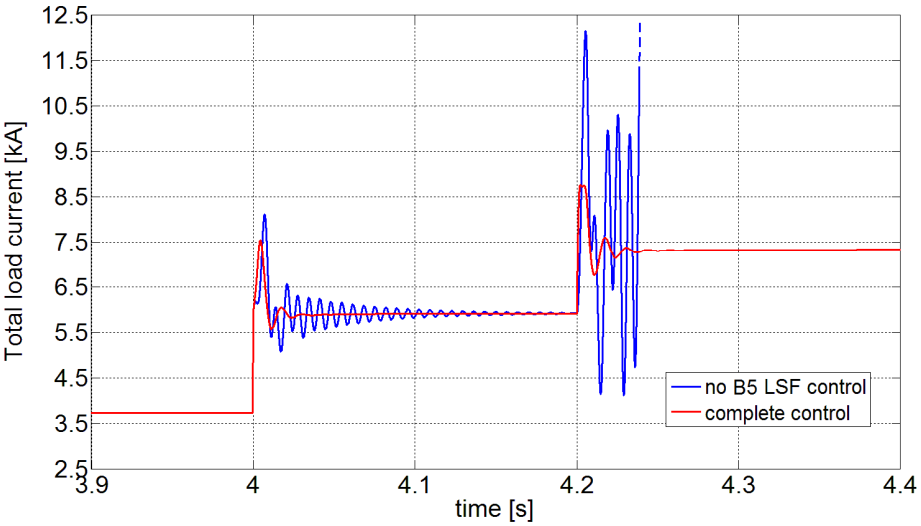

Figure 5.16 Total load current transient: loss of LSF control.

5.6 Simulation results

The positive effect of the designed control strategies is underlined in the numerical results of previous Figures [65]. When disturbances appear, global AD and local LSF are able to guarantee quick and damped voltage responses. In order to deeply understand control interactions between global and local strategies, partial lacks of control are analyzed.

In absence of AD control, chosen disturbances determine a bus voltage under-damped response (Figure 5.9). On the other hand, considering the I4 load voltage (Figure 5.10) the limited action of the AD is highlighted, being I4 load tightly controlled by local LSF. Conversely, in absence of B5 control, the instability (dashed lines) due to the LSF lack is clearly shown in Figure 5.14. By means of B5 operation, this local instability burdens the MVDC bus, leading to ship black-out (Figure 5.13) or under-voltage protection' intervention. The load sharing functionality is verified by Figures 5.11 and 5.15, where shared currents are correctly proportional to the generator' rated powers. Furthermore, Figures 5.12 and 5.16 provide the total load current supplied by the four generating systems.

The different impact of the two disturbances is proven by simulation transients [65]: a bus disturbance (i.e. a variation of the I1, I8 inverters power) bears on the load voltage, by transiently decreasing the input (bus voltage) of the DC/DC load converter (B5); a load disturbance (given by I4 inverter) affects also the bus, which has to engage the current request of B5 converter.

5.7 Conclusions

A methodology to design the voltage control in a multi MW, multi-converter MVDC power system has been discussed in this Chapter. In accordance with the IEEE Standard, the MVDC distribution chosen in Chapter 4 has considered two types of controllable voltage actuators to interface the bus: generating DC/DC buck converters and load DC/DC buck converters. The presence of these actuators has suggested the realization of an integrated voltage control based on two strategies: global Active Damping (AD) and local Linearization via State Feedback (LSF). Each strategy has been devoted to realize a different target, controlling the voltage on the bus (AD) or on impacting loads (LSF).

In order to understand the behavior of proposed control strategies, a series of tests have been set deactivating control section and stimulating the power system by different disturbances. On the power station side, generating DC/DC converters have been utilized to apply AD method, assuring bus voltage stability against disturbances caused by CPL loads directly connected to the bus. On the load side, voltage instability due to a large CPL connection has been locally solved thanks to the non-linear compensation, realized by the LSF controlled load converter.

Simulations have analyzed the action of implemented voltage control strategies, which have been able to face both local and global CPL instability and to realize the power sharing among generators. Results obtained are noteworthy, because they have described the behavior of an entire MVDC power system (subjected to power load variations), pointing out critical interactions between control strategies.

6. Global LSF control strategy to solve CPLs instability

6.1 Introduction

Unlike the previous approach which has exploited two complementary control strategies (global AD and local LSF), this Chapter will treat a control approach only founded on well-performing LSF. Such a control aims to remove the cause of voltage instability, by cancelling the non-linear loads responsible of the destabilizing behavior (Chapter 2). Therefore the last strategy of this thesis is to be intended as a possible solution in relevant cases (e.g. very large CPLs or tiny filter' capacitances), where standard approach (Chapter 5) is doomed to fail.

In this Chapter, the global LSF strategy will be implemented in order to solve the DC instability directly on the generator side, modeling all shipboard CPLs as an equivalent non-linear load. The application of this strategy is based on the prior development of a low order model, which can capture the overall behavior of the multi-converter MVDC system in a second-order non-linear differential equation. This model will be used for defining a non-linear function (Subsection 3.6.3) that controls the generating DC/DC converters in order to accomplish the loop-cancellation. After the employment of LSF technique, the non-linearities still remain into the system, but the controlled multi-converter arrangement may be externally described by a linear differential equation. Once the resulting linear system will be obtained, a traditional pole placement will be realized by means of a conventional state feedback, to guarantee the desired voltage dynamics.

6.2 Design procedure

Considering the complexity of a shipboard MVDC power system, the next procedure [67] is proposed (Figure 6.1) to assist the voltage control design. The stated design method follows some steps, from the definition of power system requirements to the implementation of proper techniques to control the bus voltage. Starting from design data of an actual AES (i.e. generators, loads) and DC plant components (i.e. converters, filters), a simplified circuit model can be derived from the complete one by neglecting the cables. Furthermore, a proper filter' design allows to well-approximate the system

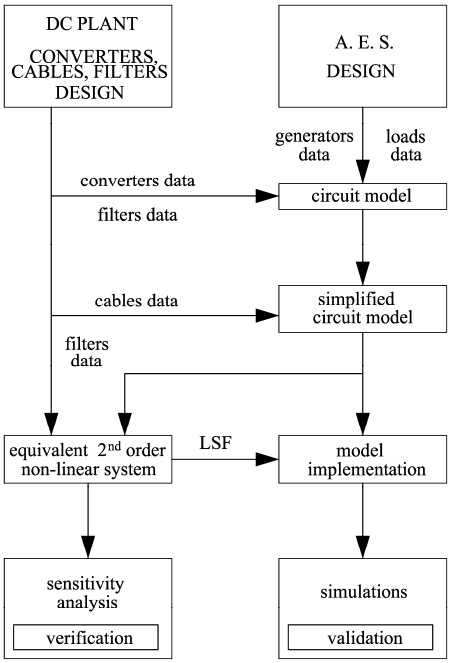

Figure 6.1 Voltage control design procedure.

dynamics by a 2nd order non-linear differential equation: the latter is necessary to define the non-linear function in order to realize the global LSF strategy and to impose the wanted voltage dynamics.

By applying the found LSF function on the simplified model and considering detailed results of [67], it is possible to obtain a validation of the proposed strategy in presence of a critical disturbance (i.e. disconnection of one generator set). The robustness of the LSF technique against relevant system parameters changes or uncertainties is analytically verified on the equivalent 2nd order model. The last evaluation is very important, because it investigates issues related to the main LSF weak point.

6.3 Shipboard MVDC Power System

The circuit of Figure 6.2 (4 DC filtered generating systems in parallel with m=9 CPLs) can conveniently model [53,67] the proposed multi-converter MVDC power system (Figure 4.3). The following assumptions permit to obtain this representation:

- Average Value Model (AVM) adoption. This is well justified for analysis purposes when system dynamics are considered relatively small with respect to the fast switching dynamics of the converters [13];
- a single generating system is modeled by a DC ideal voltage generator E_k. This voltage is the output of a generic DC/DC converter connected to a second order RLC filter (parameters R_{fk}, L_{fk} and C_{fk});
- load lines (B5-L1, B6-L2, B7-L3) and drive lines (I1, I2, I3 and I6, I7, I8) constitute non-linear CPLs [52];

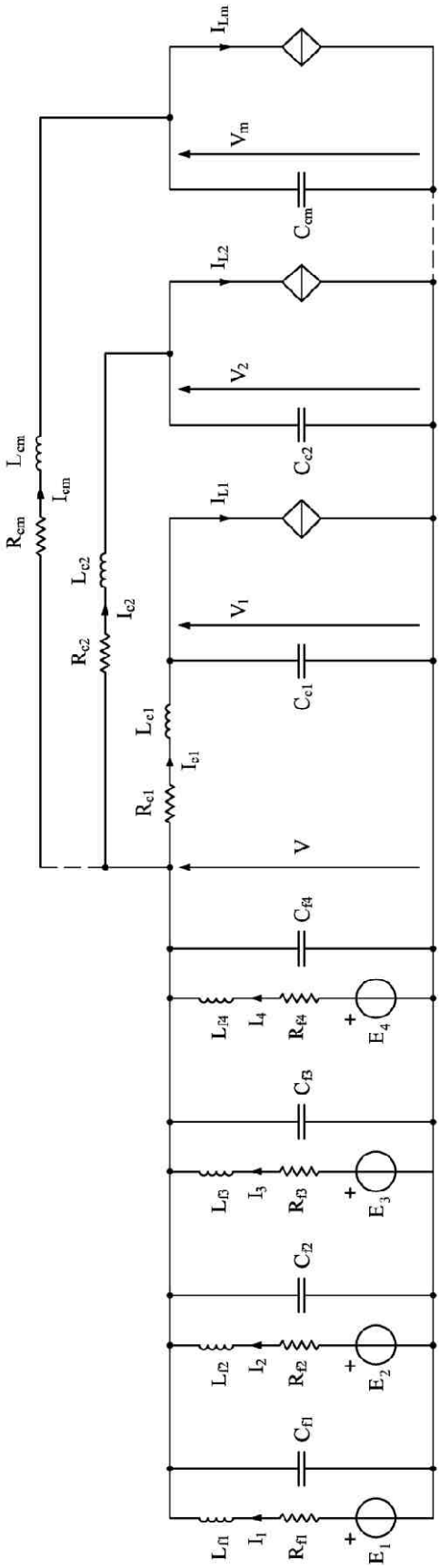

Figure 6.2 Circuit model of the multi-converter MVDC power system.

- each CPL is represented by a current generator $I_{Lh}=P_h/V_h$ ($V_h>0$, $P_h>0$). The generic line h is modeled by means of cable parameters R_{ch}, L_{ch} and possible input filtering capacitor C_{ch}.

Assuming the state variables (the MVDC bus voltage, $V>0$, 4 generators currents, I_k, 9 line currents, I_{ch} and 9 load voltages, V_h >0), the circuit model of Figure 6.2 is described by 23 non-linear differential equations (6.1):

$$\begin{cases} \dfrac{dV}{dt} = \dfrac{1}{C_f}\left(\sum_{k=1}^{4} I_k - \sum_{h=1}^{9} I_{ch}\right) & \\ \dfrac{dI_k}{dt} = \dfrac{1}{L_{fk}}\left(-R_{fk}\cdot I_k - V + E_k\right) & \forall k = 1,2,.....,4 \\ \dfrac{dI_{ch}}{dt} = \dfrac{1}{L_{ch}}\left(-R_{ch}\cdot I_{ch} + V - V_h\right) & \forall h = 1,2,.....,9 \\ \dfrac{dV_h}{dt} = \dfrac{1}{C_{ch}}\left(I_{ch} - \dfrac{P_h}{V_h}\right) & \forall h = 1,2,.....,9 \end{cases} \tag{6.1}$$

where a total capacitor C_f is defined as the sum (parallel) of all filter capacitors C_{fk}

6.4 MVDC equivalent circuit models

Starting from the model of Figure 6.2, it is possible to deduce two equivalent circuits to represent the power system behavior. In particular, the second model will be essential to determine the non-linear function of global LSF strategy.

6.4.1 Simplified model

Considering a common practice for size-limited DC power systems [34,42,52,53,68], it is possible to neglect cable longitudinal parameters $R_{ch,}$ L_{ch} with respect to other longitudinal elements: thus all capacitors and non-linear loads become in parallel, determining an equivalent capacitor C_{eq} and an equivalent load current generator $I_L=P_{eq}/V$ ($V>0$, $P_{eq}>0$).

These assumptions make it possible to define the simplified circuit model (Figure 6.3), which is constituted by 4 DC generating systems, 4 filtering stages and an equivalent CPL. The simplified model, described by 5 non-linear state equations (6.2), will be used to perform simulations and to obtain the 2nd order model (Subsection 6.4.2).

$$\begin{cases} \dfrac{dV}{dt} = \dfrac{1}{C_{eq}}\left(I_1 + I_2 + I_3 + I_4\right) - \dfrac{P_{eq}}{C_{eq}\cdot V} & \\ \dfrac{dI_k}{dt} = -\dfrac{R_{fk}}{L_{fk}} I_k - \dfrac{1}{L_{fk}} V + \dfrac{E_k}{L_{fk}} & \forall k = 1,2,3,4 \end{cases} \tag{6.2}$$

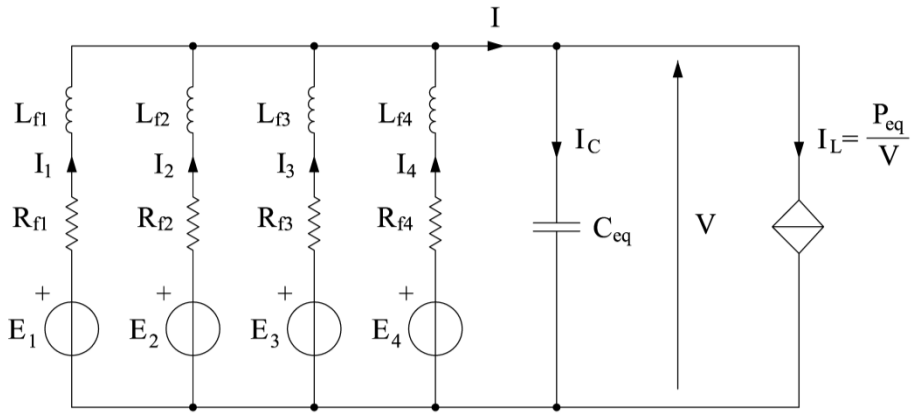

Figure 6.3 Simplified circuit model of the multi-converter MVDC power system.

6.4.2 Second-order model

A suitable design of the generating system filters is assumed (Section 6.6): this implies equal L_{fk}/R_{fk} ratio (with an acceptable approximation) for all proposed filters. Therefore, a time constant T_f can be defined, which will be used in next developments

$$T_f = \frac{L_{fk}}{R_{fk}} \qquad \forall k = 1,2,.....,4 \tag{6.3}$$

A second order non-linear differential equation in the state variable V may be obtained (6.4) deriving the first equation of system (6.2) and substituting in it the four current derivatives:

$$\begin{aligned}\frac{d^2V}{dt^2} = &-\frac{1}{C_{eq}\cdot T_f}\left(I_1+I_2+I_3+I_4\right)-\frac{1}{C_{eq}}\left(\frac{1}{L_{f1}}+\frac{1}{L_{f2}}+\frac{1}{L_{f3}}+\frac{1}{L_{f4}}\right)\cdot V+\\ &+\frac{E_1}{C_{eq}\cdot L_{f1}}+\frac{E_2}{C_{eq}\cdot L_{f2}}+\frac{E_3}{C_{eq}\cdot L_{f3}}+\frac{E_4}{C_{eq}\cdot L_{f4}}+\frac{P_{eq}}{C_{eq}\cdot V^2}\frac{dV}{dt}\end{aligned} \tag{6.4}$$

Considering the following relationships (6.5)-(6.7),

$$\begin{cases} I = I_1+I_2+I_3+I_4 & (6.5)\\ I = I_L+I_C = \dfrac{P_{eq}}{V}+C_{eq}\dfrac{dV}{dt} & (6.6)\\ \dfrac{1}{L_{eq}} = \dfrac{1}{L_{f1}}+\dfrac{1}{L_{f2}}+\dfrac{1}{L_{f3}}+\dfrac{1}{L_{f4}} & (6.7)\end{cases}$$

equation (6.4) can be simplified into (6.8)

$$\frac{d^2V}{dt^2} = -\left(\frac{1}{C_{eq}\cdot L_{eq}}\right)\cdot V - \left(\frac{1}{T_f}\right)\frac{dV}{dt} + \\ + \frac{E_1}{C_{eq}\cdot L_{f1}} + \frac{E_2}{C_{eq}\cdot L_{f2}} + \frac{E_3}{C_{eq}\cdot L_{f3}} + \frac{E_4}{C_{eq}\cdot L_{f4}} - \frac{P_{eq}}{C_{eq}\cdot T_f\cdot V} + \frac{P_{eq}}{C_{eq}\cdot V^2}\frac{dV}{dt} \tag{6.8}$$

which describes a second order non-linear system.

6.5 Global LSF voltage control strategy

Last two addends of equation (6.8) represent system non-linearities. Two control functions f_l and f_d are defined in the following formulas (6.9)-(6.10). Function f_l has the crucial role of compensating for system non-linearities making the system linear (LSF technique), while f_d is chosen in order to realize an analytical pole placement (V_0 represents the steady state bus voltage reference):

$$\begin{cases} f_l = -\dfrac{P_{eq}}{C_{eq}\cdot T_f\cdot V} + \dfrac{P_{eq}}{C_{eq}\cdot V^2}\dfrac{dV}{dt} = -\dfrac{I_L}{C_{eq}\cdot T_f} + \dfrac{I_L}{C_{eq}\cdot V}\dfrac{I-I_L}{C_{eq}} & (6.9) \\ f_d = K_1\cdot(V-V_0) + K_2\dfrac{dV}{dt} = K_1\cdot(V-V_0) + K_2\dfrac{I-I_L}{C_{eq}} & (6.10) \end{cases}$$

It should be underlined that the proposed non-linear state feedback is much more effective than techniques based on small-signal linearization, given that is not affected by a small-signal hypothesis. Once canceled system non-linearities, different type of linear control functions can be applied as f_d.

As an example, in this work, a proportional-differential state-feedback control is utilized in (6.10). It is noteworthy to consider that feedback quantities for f_l and f_d determination can be derived (6.5)-(6.6) from measurements (i.e. I_L, I and V, being I_C=I-I_L). The combined control action of functions f_l and f_d can be split in four contributions F_k over the four generators,

$$F_k = S_k\cdot(f_l + f_d)\cdot C_{eq}\cdot L_{fk} \tag{6.11}$$

using the load sharing coefficients S_k (ΣS_k=1). Thus the desired power sharing among DC/DC converters is provided by the current signal I_L feedback operated by f_l (6.9). Power signals F_k are to be subtracted to the DC/DC converter outputs E_k as in (6.12),

$$\frac{d^2V}{dt^2} = -\left(\frac{1}{C_{eq}\cdot L_{eq}}\right)\cdot V - \left(\frac{1}{T_f}\right)\frac{dV}{dt} + \frac{E_1 - F_1}{C_{eq}\cdot L_{f1}} + \frac{E_2 - F_2}{C_{eq}\cdot L_{f2}} + \\ + \frac{E_3 - F_3}{C_{eq}\cdot L_{f3}} + \frac{E_4 - F_4}{C_{eq}\cdot L_{f4}} - \frac{P_{eq}}{C_{eq}\cdot T_f \cdot V} + \frac{P_{eq}}{C_{eq}\cdot V^2}\frac{dV}{dt} \tag{6.12}$$

in order to obtain a linear system (6.13):

$$\frac{d^2V}{dt^2} + \left(\frac{1}{T_f}\right)\frac{dV}{dt} + \left(\frac{1}{C_{eq}\cdot L_{eq}}\right)\cdot V = \frac{E_1}{C_{eq}\cdot L_{f1}} + \frac{E_2}{C_{eq}\cdot L_{f2}} + \\ + \frac{E_3}{C_{eq}\cdot L_{f3}} + \frac{E_4}{C_{eq}\cdot L_{f4}} - K_2\frac{dV}{dt} - K_1\cdot(V - V_0) \tag{6.13}$$

Control gains K_1 and K_2 make it possible to realize an analytical pole-placement, in accordance to linear control systems theory:

$$\begin{cases} K_1 = \omega_0^2 - \dfrac{1}{C_{eq}\cdot L_{eq}} & (6.14) \\ K_2 = 2\xi\omega_0 - \dfrac{1}{T_f} & (6.15) \end{cases}$$

being ξ and ω_0 the damping factor and the natural frequency of the second order resulting system.

6.6 Filters design

Referring to Figure 5.1, it is well known [27,36,42,65] that CPL stability issue is strongly dependent on converter output filter parameters (R_{fk}, L_{fk} and C_{fk}). In particular, assuming a large filter inductor (i.e. a small current ripple), only a large (but physically bulky) filter capacitor can keep the DC generating system stable when a CPL is fed.

The global LSF control strategy is able to break the relationship between stability and filter design, making possible an independent and feasible selection of limited filter capacitor. This aspect brings important benefits, such as cost and space reduction, system reliability improvement and limitation of discharge current under short-circuit fault conditions [69].

6.6.1 Synthesis

The synthesis of each *k* filter may follow the procedure explained in the previous Chapter (Subsection 5.3.1). Furthermore, assuming some hypotheses about generating

systems (same f_{sk}, same $\Delta P_{\%k}$, same V_{dnk}) and considering an appropriate filters design (same $\Delta I_{\%k}$), the time constant L_{fk}/R_{fk}, expressed by equations (5.3) and (5.5), is identical for each filter k (6.16):

$$\frac{L_{fk}}{R_{fk}} = \frac{1 - D_{nk}}{f_{sk} \cdot \Delta I_{\%k} \cdot \Delta P_{\%k}} = T_{fk} = T_f \tag{6.16}$$

If previous conditions are not verified (i.e. 4 different time constants T_{fk}), it is possible to model the system by means of a unique average time constant T_f, being variations of poles $1/T_{fk}$ irrelevant compared to dominant complex poles. These ones describe the dynamic behavior of each DC generating system as explained below.

6.6.2 CPL stability analysis

As specified in Subsection 5.3.2., the CPL stability can be analyzed by (6.17)-(6.18):

$$\begin{cases} \omega_{0k} = \sqrt{\dfrac{1}{L_{fk} \cdot C_{fk}} \left(1 - \dfrac{R_{fk}}{R_k^0}\right)} & (6.17) \\ \xi_k = \dfrac{1}{2\omega_{0k} \cdot L_{fk} \cdot C_{fk}} \left(C_{fk} \cdot R_{fk} - \dfrac{L_{fk}}{R_k^0}\right) & (6.18) \end{cases}$$

where $R^0{}_k = V_{nk}{}^2/P_{nk}$ is the absolute value of the negative incremental resistance. In equation (6.18), the damping factor ξ_k, which depends both on the filter parameters and on the loading level P_{nk}, is of very important because it provides an index of k system CPL instability.

6.6.3 Design

As seen in equations (5.1)-(5.7), the specifications about power losses $\Delta P_{\%k}$, current ripple $\Delta I_{\%k}$ and voltage ripple $\Delta V_{\%k}$ are to be used for designing filters. In particular, the third specification is chosen in accordance to the IEEE Standard [13], which states an rms value of ripple lower than 5% per unit.

The filters design may be summarized by Table 6.1, which reports the parameters values and the voltage instability index ξ_k for each DC generating system. Regarding Table 6.1 it is possible to notice the low current ripple (30%): considering the relevant non-linear powers P_{nk}, this current requirement would impose to use a large capacitor (i.e. a very low voltage ripple) in order to maintain a positive damping factor (6.18) in absence of LSF control. Instead, by directly cancelling the CPL' non-linearities, the proposed global LSF strategy may overtake this tight design constraint, allowing the choice of a reasonable $\Delta V_{\%k}$ (3%) (i.e. a limited capacitor with its lower cost, space and discharge current). In effect, the loop-cancellation guarantees system stability also in this critical situation, even in presence of very negative damping factor.

	BF1/BF3	BF2/BF4
P_{nk} [MW]	15.75	10.50
V_{dnk} [V]	8910	8910
V_{nk} [V]	6000	6000
D_{nk}	0.67	0.67
I_{nk} [A]	2494	1662
f_{sk} [Hz]	1500	1500
$\Delta P_{\%k}$	5	5
$\Delta V_{\%k}$	3	3
$\Delta I_{\%k}$	30	30
R^0_k [Ω]	2.3	3.4
R_{fk} [mΩ]	126.6	189.9
L_{fk} [mH]	1.7	2.6
C_{fk} [μF]	346.3	230.9
ω_{0k} [rad/s]	1250	1250
ξ_k	-0.48	-0.48

Table 6.1 Filters design (global LSF).

6.7 LSF sensitivity analysis

Due to system parameters mismatch (ΔT_f, ΔL_{eq} and ΔC_{eq}), the linearizing function f_l could be able to cancel the CPL non-linearities only partially. It is of interest in this Section to evaluate how much this partial linearization affects system stability.

The study considers design data T_f, L_{eq} and C_{eq} (Table 6.1) in evaluating the linearizing function f_l, while controlled power system presents actual parameters T_f^*, L_{eq}^* and C_{eq}^* ($T_f^*=T_f+\Delta T_f$, $L_{eq}^*=L_{eq}+\Delta L_{eq}$ and $C_{eq}^*=C_{eq}+\Delta C_{eq}$). Further hypotheses regard the control feeding back variables (I_L, I and V), which are assumed known without errors and delays [69]. Starting from (6.8), equation (6.19) is derived setting to zero the DC/DC converter outputs E_k and adding the function f_l (6.9):

$$\frac{d^2V}{dt^2}+\left(\frac{1}{T_f^*}\right)\frac{dV}{dt}+\left(\frac{1}{C_{eq}^*\cdot L_{eq}^*}\right)\cdot V+\left(-\frac{1}{C_{eq}\cdot T_f}+\frac{1}{C_{eq}^*\cdot T_f^*}\right)\cdot I_L+ \\ +\left(\frac{1}{C_{eq}^2}-\frac{1}{C_{eq}^{*2}}\right)\frac{I_L\cdot I}{V}-\left(\frac{1}{C_{eq}^2}-\frac{1}{C_{eq}^{*2}}\right)\frac{I_L^2}{V}=0 \tag{6.19}$$

The last three addends of equation (6.19) are the remaining system non-linearities due to parameters mismatch. A small-signal analysis is performed by linearizing equation (6.19) in the operating point (V_0, I_0), where $I_0=P_{eq}/V_0$ (Section 2.3).

$$\frac{d^2\Delta V}{dt^2}+\left(\frac{1}{T_f^*}\right)\frac{d\Delta V}{dt}+\left(\frac{1}{C_{eq}^*\cdot L_{eq}^*}\right)\cdot\Delta V+\left(-\frac{1}{C_{eq}\cdot T_f}+\frac{1}{C_{eq}^*\cdot T_f^*}\right)\cdot\Delta I_L+$$
$$+\left(\frac{1}{C_{eq}^2}-\frac{1}{C_{eq}^{*2}}\right)\cdot\left[\frac{I_0}{V_0}\Delta I_L+\frac{I_{L0}}{V_0}\Delta I-\frac{I_{L0}\cdot I_0}{V_0^2}\Delta V\right]+ \tag{6.20}$$
$$-\left(\frac{1}{C_{eq}^2}-\frac{1}{C_{eq}^{*2}}\right)\cdot\left[\frac{2I_{L0}}{V_0}\Delta I_L-\frac{I_{L0}^2}{V_0^2}\Delta V\right]=0$$

Using following relationships [27],

$$\begin{cases} I_{L0}=I_0=\dfrac{P_{eq}}{V_0} & (6.21)\\ \Delta I_L=-\left(\dfrac{P_{eq}}{V^2}\right)_0\Delta V=\dfrac{\Delta V}{-R^0} & (6.22)\\ \Delta I=\Delta I_C+\Delta I_L=C_{eq}^*\dfrac{d\Delta V}{dt}+\dfrac{\Delta V}{-R^0} & (6.23)\end{cases}$$

it is possible to simplify (6.20) into (6.24):

$$\frac{d^2\Delta V}{dt^2}+\left(\frac{1}{T_f^*}\right)\frac{d\Delta V}{dt}+\left(\frac{1}{C_{eq}^2}-\frac{1}{C_{eq}^{*2}}\right)\frac{C_{eq}^*}{R^0}\frac{d\Delta V}{dt}+$$
$$+\left(\frac{1}{C_{eq}^*\cdot L_{eq}^*}\right)\cdot\Delta V+\left(\frac{1}{C_{eq}\cdot T_f}-\frac{1}{C_{eq}^*\cdot T_f^*}\right)\frac{\Delta V}{R^0}=0 \tag{6.24}$$

Considering the resulting characteristic equation (6.25) and the usual notation for second-order system (6.26),

$$s^2+\left[\frac{1}{T_f^*}+\frac{C_{eq}^*}{C_{eq}^2\cdot R^0}-\frac{1}{C_{eq}^*\cdot R^0}\right]s+\left[\frac{1}{C_{eq}^*\cdot L_{eq}^*}+\frac{1}{C_{eq}\cdot T_f\cdot R^0}-\frac{1}{C_{eq}^*\cdot T_f^*\cdot R^0}\right]=0 \tag{6.25}$$

$$s^2+2\xi_t\omega_{0t}s+\omega_{0t}^2=0 \tag{6.26}$$

the total damping factor ξ_t is easily determined which is assumed from classical control theory as a stability index.

Assuming a rough knowledge of system parameters T_f^*, L_{eq}^* and C_{eq}^*, the proposed sensitivity study may be used to evaluate the impact of parameters variations or uncertainties on stability in a worst case scenario (i.e. deactivating control function f_d contribution).

6.8 Model implementation

In order to implement the global LSF strategy, an AVM simulation arrangement is used. As seen before (Sections 6.4 and 6.5), the AVM is utilized to determine the linearizing function f_l as well as the control gains K_1 and K_2 in function f_d. The dynamic results obtained by AVM simulation will be finally validated by the results of a different simulation platform [67].

The block scheme of Figure 6.4 describes the system AVM. Assuming the diode converters output voltages V_{dnk} constant during load supply, DC/DC converters can be modeled by means of the gain value $K_{ck}=V_{dnk}$ (k=1,2,…4). These DC/DC power converters are therefore considered as "voltage actuators" with a negligible dynamics. The multi-converter MVDC system's voltage operating point is reached thanks to an outer integral controller (integral gain K_I), which processes the bus voltage V feedback and generates the operating point command D for the converters duty cycle. This integral control loop is designed with a slow dynamics, with respect to the fast action of the inner control loops.

Control functions, f_l and f_d (6.9)-(6.11) are implemented by the LSF voltage controller blocks, whose output commands are added to D in order to generate the duty cycle commands D_k*. Figure 6.4 highlights (red lines) the CPL non-linear part canceled by f_l. From a practical point of view, the generators load sharing realized by the four contributions F_k (6.11) may be affected by steady state errors in case of unrefined approximated time constant T_f: in this case additional generator current control loops could be used to regulate load sharing coefficients S_k in order to assure the correct steady state power sharing.

6.9 Simulation results

A sudden generating system disconnection actually represents a worst-case scenario in shipboard power systems; therefore such perturbation is chosen to validate the global LSF strategy.

6.9.1 Case of study

At the initial steady-state, a multi-converter MVDC system having the layout of Figure 6.3 and parameters of Table 6.1 is assumed to supply a CPL (P_{eq}=18.5 MW), through 3 DC generating system (B1, B2, B3) whose total rated power is P_n=(15.75*2+10.5)=42 MW. Operating point is maintained, at steady state, feeding the CPL.

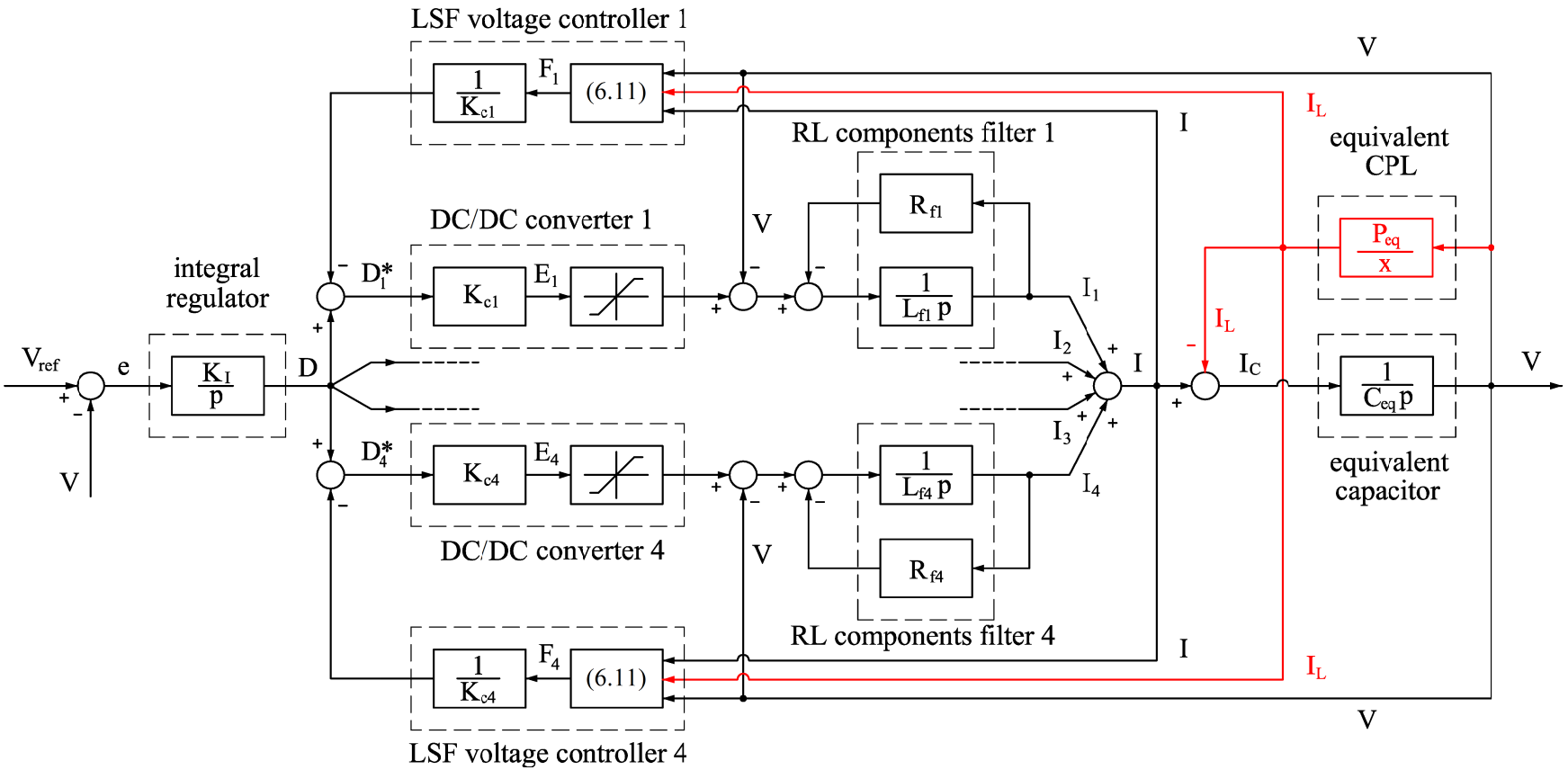

Figure 6.4 Block scheme of the multi-convert MVDC system (global LSF).

At t=6 s, CB3 opens to simulate the loss of B3, therefore the total rated power becomes P_n=26.25 MW. The load sharing coefficients S_k are automatically calculated and adapted in order to re-share the load over the two remaining DC generating system. After B3 disconnection, the remaining converters' output powers result about 70% of their rated ones (P_{nk}). The slow dynamics of the outer integral control loop is characterized by an equivalent time constant of 0.5 s, whereas the control gains K_1 and K_2 are set with ξ=0.3 and ω_0=1500 rad/s: thus the outer voltage control loop results dynamically decoupled from the inner ones.

6.9.2 Results

For the initial system (f_l and f_d deactivated), the total damping factor (calculated by linearizing (6.8) in correspondence of P_{eq}) results ξ_t=-0.32, which is characteristic of an unstable system. Therefore, the necessary application of the global LSF control strategy application is commented in the following.

Assuming the activation of the linearizing function f_l and of the control function f_d, three transients are represented in Figures 6.5-6.7 in order to highlight the power system dynamic behavior after the generating system disconnection. Bus voltage (Figure 6.5), generators currents (Figure 6.6) and CPL current (Figure 6.7) are characterized by a stable evolution with the desired dynamic imposed by f_d. On the other hand, the transient depicted in Figure 6.8 confirms the role of f_l in keeping the system stability. The uncompensated CPL non-linearity (f_l off) creates wide unstable oscillations: this would determine a consequent voltage protections intervention in a real plant [13,65].

Assuming a worst case scenario (deactivation of f_d), the sensitivity (small-signal) analysis theorized in Section 6.7 is used to verify stability effects due to system parameters mismatching. Figures 6.9-6.10 show the system damping factor ξ_t in case of real system-design discrepancy: the stability issue results strictly linked to system capacitor mismatching ΔC_{eq}, while ΔT_f and ΔL_{eq} cause an irrelevant effect on ξ_t. Considering f_l synthesis on designed parameters (Figure 6.9), the global LSF strategy is unable to guarantee stability (i.e. ξ_t<0) if C_{eq}^*/C_{eq} is approximately smaller than 0.95. In order to prevent this critical unstable situation an over-linearization strategy [52] is applied, calculating f_l as a function of a reduced equivalent capacitor (chosen, as an example, equal to $0.8 \cdot C_{eq}$): thanks to this strategy the system stability is augmented (Figure 6.10). With reference to the variation of C_{eq}^* only (the most sensitive parameter), the same conclusions can be drawn by evaluating the root-loci in the two cases (standard linearization, Figure 6.11, and over-linearization, Figure 6.12).

The AVM results obtained from the averaged model are coherent with detailed model results (Figures 6.13-6.15) available in literature [67].

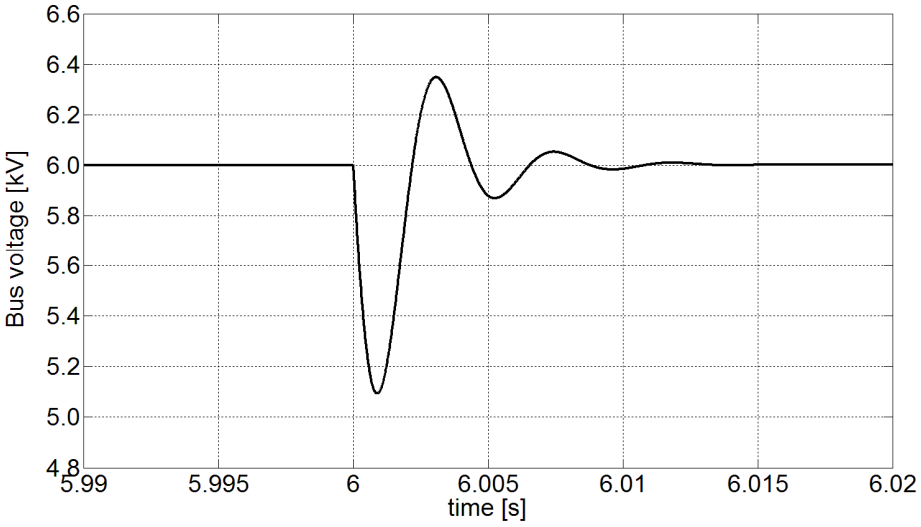

Figure 6.5 Bus voltage transient (f_l on, f_d on, averaged model result)

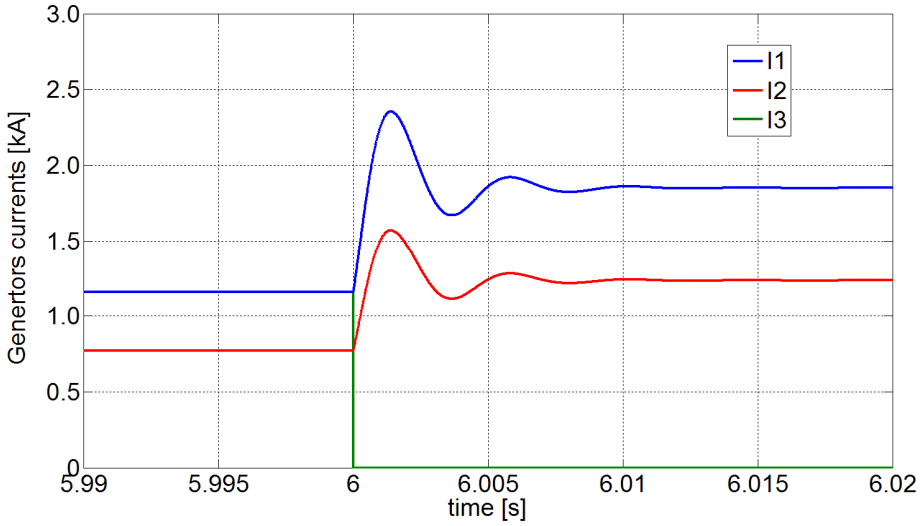

Figure 6.6 Generators currents transient (f_l on, f_d on, averaged model result).

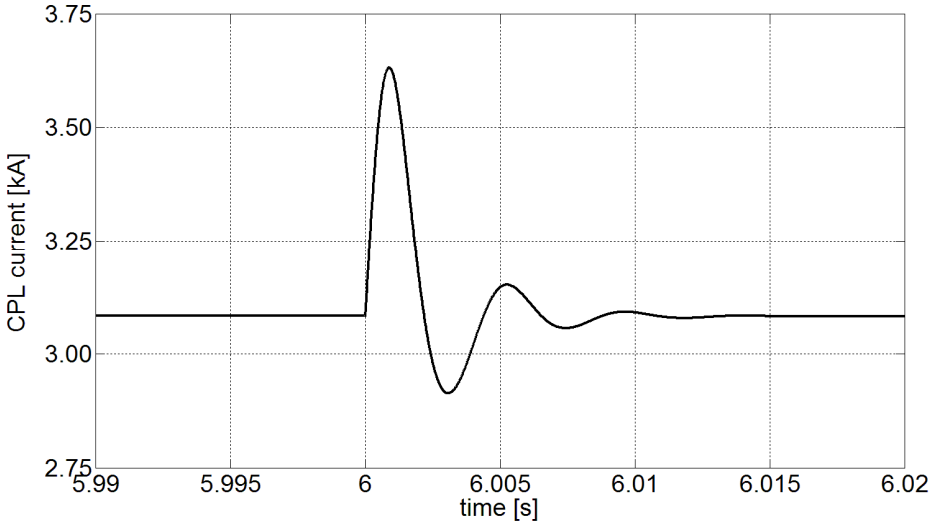

Figure 6.7 CPL current transient (f_l on, f_d on, averaged model result).

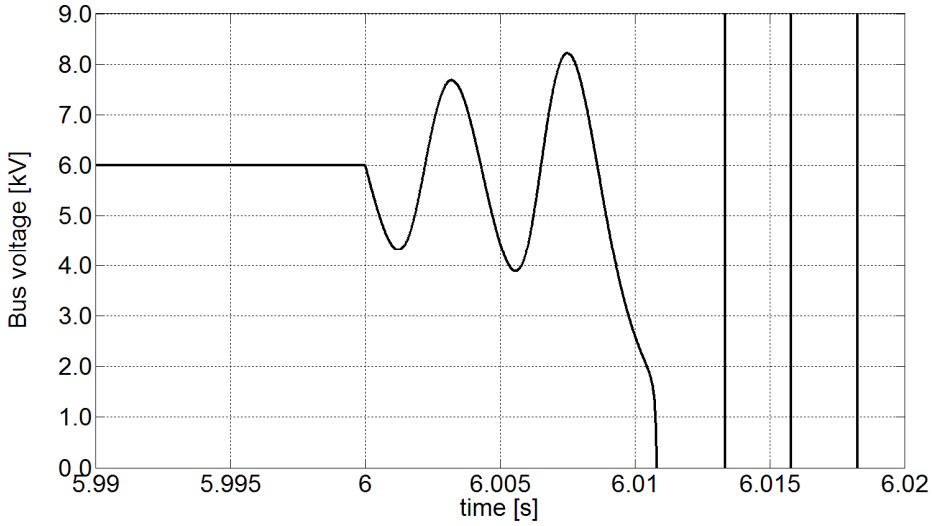

Figure 6.8 Bus voltage transient (f_l off, f_d on, averaged model result).

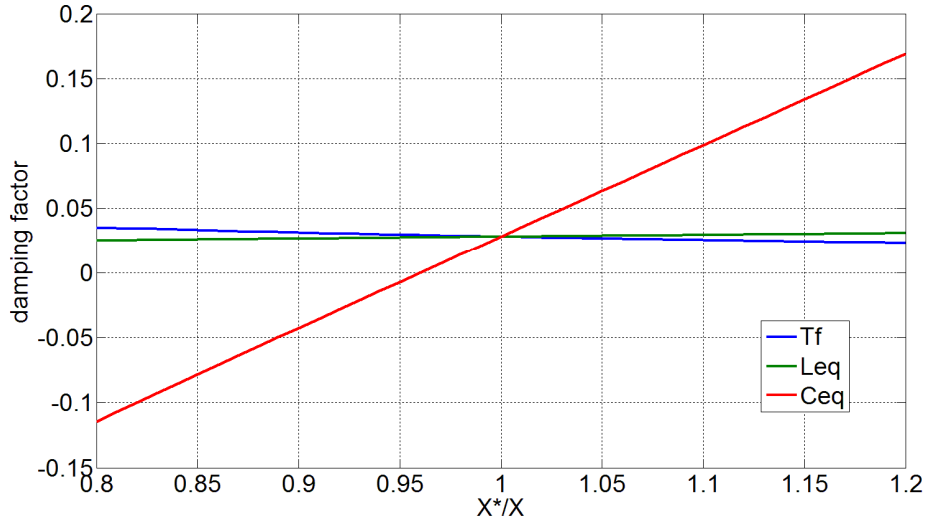

Figure 6.9 Sensitivity analysis (f_l on, f_d off).

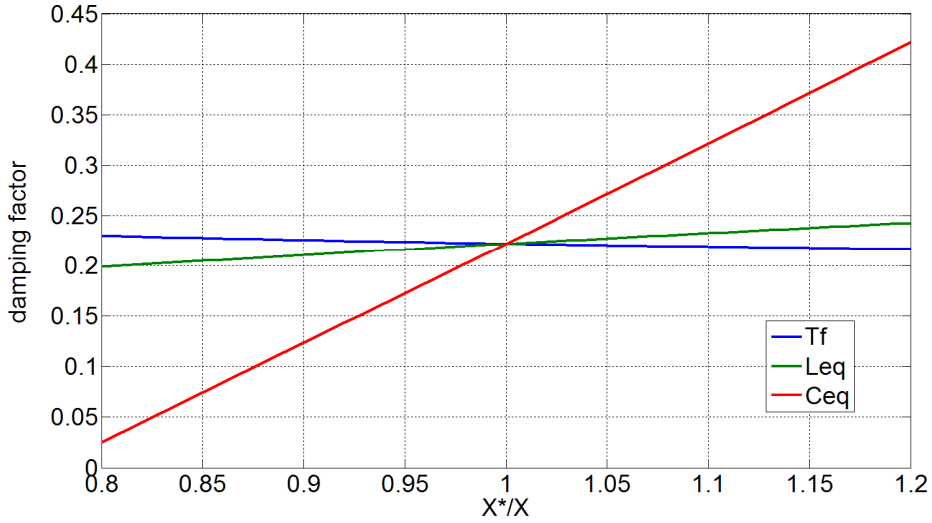

Figure 6.10 Sensitivity analysis (f_l on, f_d off, over-linearization).

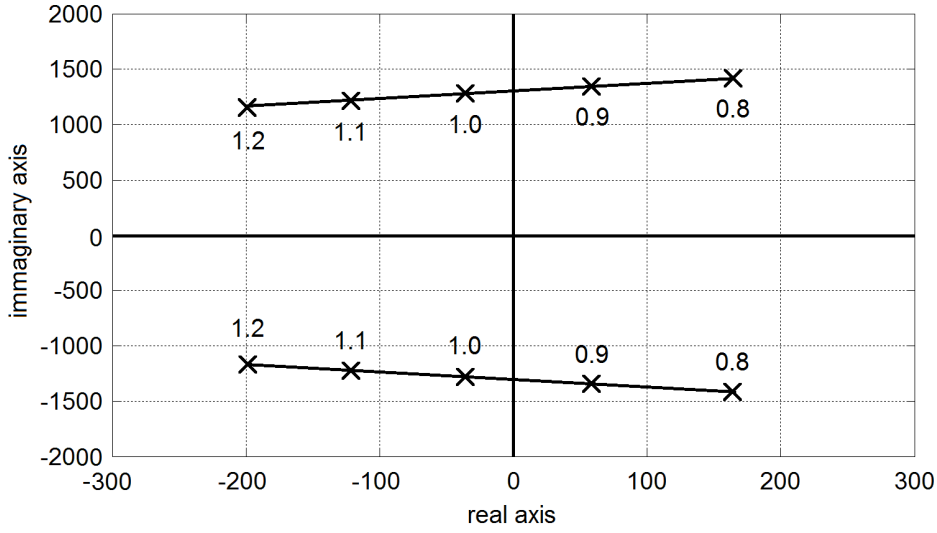

Figure 6.11 Root-locus by varying C_{eq}^{*}/C_{eq} (f_l on, f_d off).

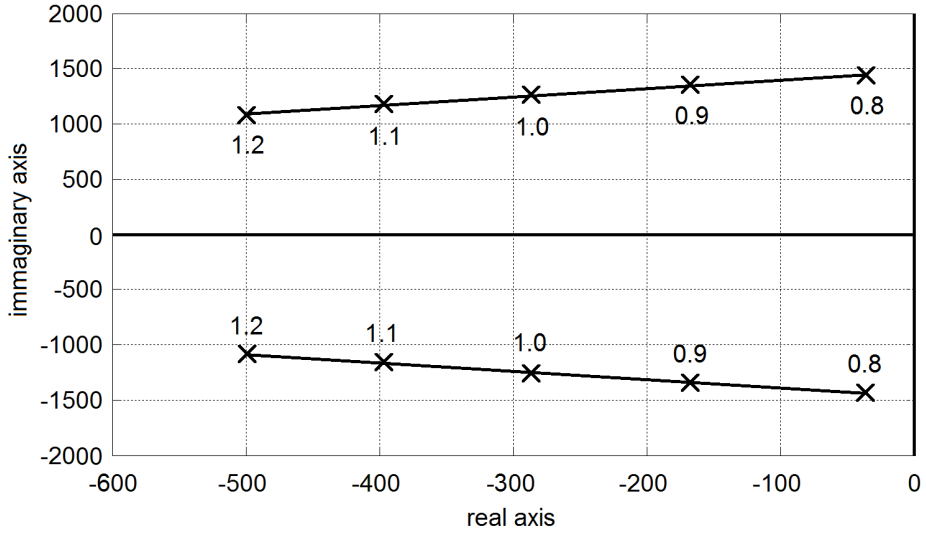

Figure 6.12 Root-locus by varying C_{eq}^{*}/C_{eq} (f_l on, f_d off, over-linearization).

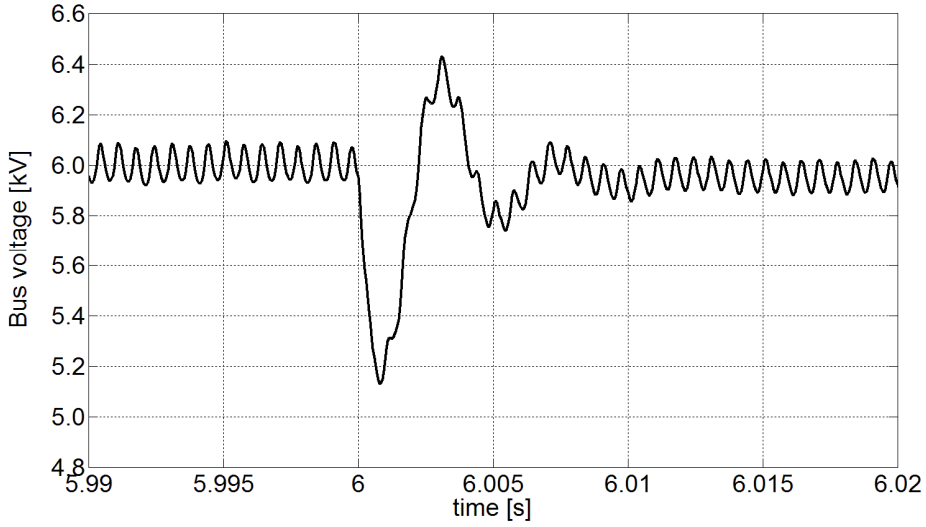

Figure 6.13 Bus voltage transient (f_l on, f_d on) [67].

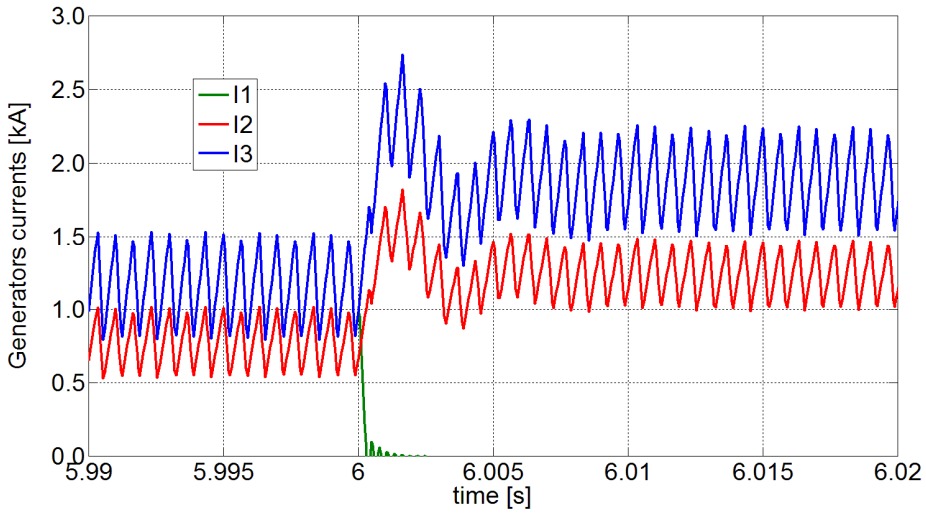

Figure 6.14 Generators currents transient (f_l on, f_d on) [67].

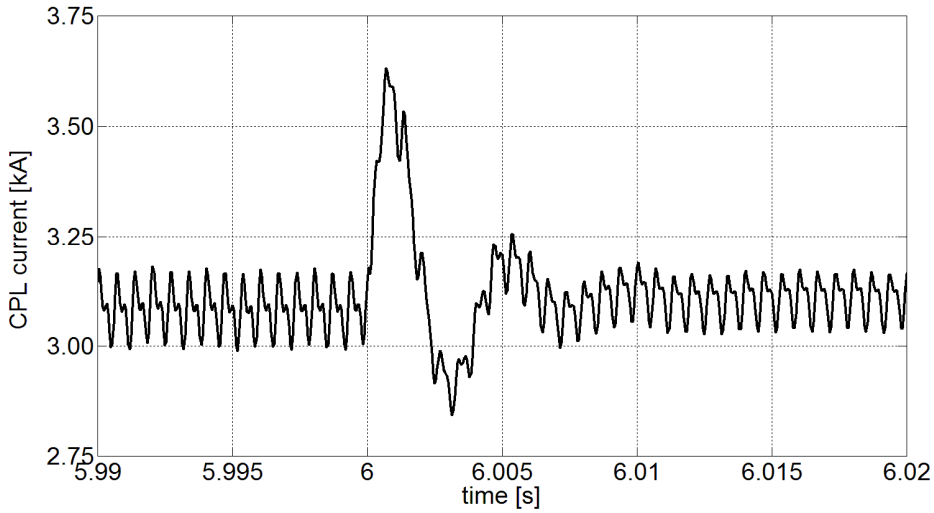

Figure 6.15 CPL current transient (f_l on, f_d on) [67].

6.10 Conclusions

Chapter 6 has presented a voltage control design procedure for multi-converter MVDC power system. The control design is based on the global LSF strategy and it is aimed at solving the Constant Power Load stability issue. The proposed control is applied to the model of a possible MVDC power system, which is derived from an originally actual All Electric Ship AC power system.

A complete voltage control design procedure has been provided taking advantage from an original system model simplification. It has been demonstrated how, under acceptable design assumptions, a complex multi-converter DC system can be represented by an equivalent non-linear 2nd order model. Then, this system is made linear using the LSF technique and, after that, it can be easily controlled according to traditional linear systems theory.

The proposed control design has also taken into account implementation aspects, in order to meet the shipboard plant requirements. Among gained advantages, it is possible to notice:

- the feedback quantities (to be measured and elaborated in order to calculate control signals) have been considered normally available from on-board measurements (generating converters currents, bus voltage, load converters currents);
- besides MVDC bus voltage control, a dynamic power sharing has been obtained among generating systems, which are in charge of providing load power and stabilizing power;
- the global LSF strategy, supplemented by a suitable filters design, has provided stability while keeping limited the capacitors size of the converters

output stages. This contributes in reducing fault current levels in case of short circuit on the MVDC bus;

- sensitivity (small-signal) analysis has verified the overall design, evaluating control robustness in case of parameters uncertainties and emphasizing most sensitive parameters. An over-linearization technique has been also proposed to augment the system robustness.

Results available in literature [67] confirm the ones obtained by AVM. The control action of the LSF strategy has been tested by means of time-domain transient responses (bus voltage, generators currents and equivalent CPL current) in presence of a relevant perturbation (loss of one generator out of three running).

The context of the work (future MVDC shipboard power systems) represents a challenging case of DC grid, limited for extension but very dense in load power, generation capacity, power electronics and interacting controls to be managed in an intelligent way. As DC microgrids in islanding mode can be considered to be very similar to shipboard context, developments gained are believed to be also valuable for application to land DC grids design and control.

7. Conclusions

During the last twenty-five years, the development and diffusion of power electronics has determined the beginning of a new large ship concept, the All Electric Ship (AES) paradigm. AESs, which nowadays represent 100% of modern cruise ships, are electrically propelled and equipped with an Integrated Power System (IPS), in order to feed propulsion system and ship service loads. In this context the innovative Medium Voltage DC distribution represent a new possibility to renew the IPS, considering the important advantages provided by MVDC enabling technology.

Unfortunately, MVDC power systems are characterized by the important problem of CPL voltage instability which is a relevant issue not only from a theoretical point of view, but also in practical power system applications. To solve the instability, different approaches may be followed. For example, the voltage actuator approach is a reliable possibility to compensate for the destabilizing effect of CPLs. In this context the non-linear loads compensation is strictly dependent on the dynamics imposed by voltage control, therefore the voltage control techniques (SF, AD, LSF) have to guarantee notable performance.

Control techniques are widely analyzed in the thesis, highlighting pros and cons. In particular, neglecting the simplest State Feedback, control capability provided by Active Damping and Linearization via State Feedback has appeared sufficient in CPL solution. The AD is a control method to damp the voltage oscillations, by transiently increasing the filter resistances, whereas LSF is a non-linear technique to cancel the effect of CPLs. Being AD a basic technique, the implementation is quite simple on digital controllers, whereas its limited control performance avoids the practical use in stabilizing adverse systems (i.e. small filter capacitances, large CPLs). To guarantee the stability of such critical power systems, an effective option is represented by complex LSF technique, which is able to offer remarkable results also in heavy conditions.

Considering the positive aspects of each control technique and a realistic multi-converter MVDC power system, two final studies have proposed control strategies to face instability. A former analysis tries to exploit the advantages of both AD and LSF. Such techniques are utilized to solve the CPL issue, by utilizing generating DC/DC converters (global AD controlled) and load converters (local LSF controlled). Whereas, in the last Chapter a second study has been presented, foreseeing to realize a global LSF strategy to stabilize an equivalent CPL. By representing the power system behavior by means an equivalent non-linear 2^{nd} order model and actuating a proper non-linear

function, the multi-converter MVDC power system may be made linear, therefore controllable by standard linear systems theory. Designed voltage controls have been validated by dedicated simulations, which have been realized by numerical simulators. Results obtained have demonstrated the control effectiveness in solving CPL oscillations.

By observing the last sensitivity analysis, further developments will be aimed in developing robust controls. This technique will be very useful to overcome the problem of LSF, which tends to fail the loop-cancellation in presence of parameters uncertainties. In the future, experimental validations will be also realized on Medium Voltage DC power system's test-bed.

Bibliography

[1] G. Sulligoi, “All Electric Ships: Present and Future after 20 Years of Research and Technical Achievements”, *EERR Electrical Engineering Research Report*, vol. 1, no. 27, December 2011.

[2] J. S. Thongam, M. Tarbouchi, A. F. Okou, D. Bouchard and R. Beguenane, “All-Electric Ships-A review of the Present State of the Art”, *IEEE Ecological Vehicles and Renewable Energies Conference (EVER) 2013*, pp. 1-8, March 27-30, 2013, Monaco.

[3] S. D. Sudhoff, “Currents of Change”, *IEEE Power and Energy Magazine*, vol. 9, no. 4, pp. 30-37, July-August 2011.

[4] R. Hepburn, “Why a Naval Architect Likes an Electric Ship”, *IEEE International Symposium on Power Electronics, Electrical Drives, Automation and Motion (SPEEDAM) 2008*, pp. 591-593, June 11-13, 2008, Ischia (Italy).

[5] V. Arcidiacono, R. Menis, G. Sulligoi, “Improving Power Quality in All Electric Ships Using a Voltage and VAR Integrated Regulator”, *IEEE Electric Ship Technologies Symposium (ESTS) 2007*, pp. 322-327, May 21-23, 2007, Arlington (VA), USA.

[6] D. Bosich, M. Filippo, D. Giulivo, G. Sulligoi, A. Tessarolo. “Thruster motor start-up transient in an all-electric cruise-liner: Numerical simulation and experimental assessment”, *IEEE International Conference on Electrical Systems for Aircraft, Railway and Ship Propulsion (ESARS) 2012*, pp. 1-5, October 16-18, 2012, Bologna (Italy).

[7] J. V. Meer, A. Bendre, S. Krstic and D. Divan, “Improved ship power system - generation, distribution, and fault control for electric propulsion and ship service”, *IEEE Electric Ship Technologies Symposium (ESTS) 2005*, pp. 284-291, July 25-27, 2005, Philadelphia (PA), USA.

[8] S. Castellan, S. Quaia, P. Scialla, G. Sulligoi, “All-electric Mega-Yachts: Integrated power system operation and its interaction with propulsion converters”, *IEEE International Symposium on Power Electronics, Electrical Drives, Automation and Motion (SPEEDAM) 2006*, pp. 317-322, May 23-26, 2006, Taormina (Italy).

[9] V. Bucci, A. Marinò, S. Castellan, G. Sulligoi, “Innovative design concepts for the yachting market: expedition yachts and electric propulsion”, *5th International Congress of Maritime Technological Innovations and Research*, November 21-23, 2007, Barcelona (Spain).

[10] G. Sulligoi, S. Castellan, M. Aizza, D. Bosich, L. Piva, G. Lipardi, "Active front-end for shaft power generation and voltage control in FREMM frigates integrated power system: Modeling and validation", *IEEE International Symposium on Power Electronics, Electrical Drives, Automation and Motion (SPEEDAM) 2012*, pp. 452-457, June 20-22, 2012, Sorrento (Italy).

[11] G. Sulligoi, D. Bosich, T. Mazzuca, L. Piva, "The FREMM simulator: A new software tool to study electro-mechanic dynamics of the shipboard integrated power system", *IEEE International Conference on Electrical Systems for Aircraft, Railway and Ship Propulsion (ESARS) 2012*, pp. 1-5, October 16-18, 2012, Bologna (Italy).

[12] G. Sulligoi, D. Bosich, A. Vicenzutti, L. Piva, G. Lipardi, T. Mazzuca, "Studies of electromechanical transients in FREMM frigates integrated power system using a time-domain simulator", *IEEE Electric Ship Technologies Symposium (ESTS) 2013*, pp. 429-433, April 22-24, 2013, Arlington (VA), USA.

[13] IEEE Std. 1709-2010, "IEEE Recommended Practice for 1 kV to 35 kV Medium-Voltage DC Power Systems on Ships", *IEEE Industry Applications Society, Petroleum & Chemical Industry Committee*, November 2010.

[14] S. B. Leeb, J. L. Kirtley, Jr., W. Wichakool, Z. Remscrim, C. N. Tidd, J. A. Goshorn, K. Thomas, R. W. Cox and R. Chaney, "How Much DC Power Is Necessary?", *American Society of Naval Engineers*, 2010.

[15] N. Doerry and J. Amy, "Functional decomposition of a medium voltage DC integrated power system", *ASNE Shipbuilding in Support of the Global War on Terrorism Conference*, April 14-17, 2008, Biloxi (MS), USA.

[16] N. Doerry and K. McCoy, "Next Generation Integrated Power System, NGIPS Technology Development Roadmap", *Naval Sea Systems Command*, 2007.

[17] N. Doerry and J. Amy, "Implementing Quality of Service in Shipboard Power System Design", *IEEE Electric Ship Technologies Symposium (ESTS) 2011*, pp. 1-8, April 10-13, 2011, Alexandria (VA), USA.

[18] IEEE Std. 1826-2012, "IEEE Standard for Power Electronics Open System Interfaces in Zonal Electrical Distribution Systems Rated Above 100 kW", *IEEE Industry Applications Society, Petroleum & Chemical Industry Committee*, June 2012.

[19] G. Sulligoi, "Stato dell'arte e ricerca nelle applicazioni elettriche navali", *AEIT magazine*, no. 3, pp. 6-11, March 2009.

[20] T. Ericsen, "The ship power electronic revolution: Issues and answers", *IEEE Petroleum and Chemical Industry Technical Conference (PCIC) 2008*, pp. 1-11, September 22-24, 2008, Cincinnati (OH), USA.

[21] Y. Khersonsky, "New IEEE Standards for Ships", *IEEE Electric Ship Technologies Symposium (ESTS) 2011*, pp. 424-429, April 10-13, 2011, Alexandria (VA), USA.

[22] T. Ericsen, N. Hingorani and Y. Khersonsky, "Power Electronics and Future Marine Electrical Systems", *IEEE Transactions on Industry Applications*, vol. 42, no. 1, pp. 155-163, January/February 2006.

[23] T. Ericsen, "The Second Electronic Revolution (It's All About Control)", *IEEE Transactions on Industry Applications*, vol. 46, no. 5, September/October 2010.

[24] P. Kundur et al., “Definition and Classification of Power System Stability”, *IEEE Transactions on Power Systems*, vol. 19, no. 2, May 2004.

[25] E. Zivi, “Design of robust shipboard power automation systems”, *Annual Reviews in Control*, Elsevier, vol. 29, pp. 261–272, 2005.

[26] C. G. Hodge, J. O. Flower, A. Macalindin, “DC power system stability”, *IEEE Electric Ship Technologies Symposium (ESTS) 2009*, pp. 433-439, April 20-22, 2009, Baltimore (MD), USA.

[27] V. Arcidiacono, A. Monti and G. Sulligoi, “Generation control system for improving design and stability of medium-voltage DC power systems on ships”, *IET Electrical Systems in Transportation*, vol. 2, no. 3, pp. 158-167, September 2012.

[28] M. Belkhayat, R. Cooley, A. Witulski, “Large Signal Stability Criteria For Distributed Systems with Constant Power Loads”, *26th IEEE Annual Power Electronics Specialists Conference 1995*, vol. 2, pp. 1333-1338, June 18-22, 1995, Atlanta (GA), USA.

[29] S. D. Sudhoff, D. H. Schmucker, R. A. Youngs, H. J. Hegner, “Stability analysis of DC distribution systems using admittance space constraints”, *The Institute of Marine Engineers, All Electric Ship Symposium 1998*, September 29-30, 1998, London (UK).

[30] S. D. Sudhoff, S. F. Glover, “Three-Dimensional Stability Analysis of DC Power Electronics Based Systems”, *31st IEEE Annual Power Electronics Specialists Conference (PESC) 2000*, vol. 1, pp. 101-106, June 18-23, 2000, Galway (Ireland).

[31] S. D. Sudhoff, S. F. Glover, P. T. Lamm, D. H. Schmucker and D. E. Delisle, “Admittance Space Stability Analysis of Power Electronic Systems”, *IEEE Transactions on Aerospace and Electronic Systems*, vol. 36, no. 3, pp. 965-973, July 2000.

[32] S. D. Sudhoff and J. M. Crider, “Advancements in Generalized Immittance Based Stability Analysis of DC Power Electronics Based Distribution Systems”, *IEEE Electric Ship Technologies Symposium (ESTS) 2011*, pp. 207-212, April 10-13, 2011, Alexandria (VA), USA.

[33] A. Riccobono and E. Santi, “Stability analysis of an all-electric ship MVDC Power Distribution System using a novel Passivity-Based Stability Criterion”, *IEEE Electric Ship Technologies Symposium (ESTS) 2013*, pp. 411-419, April 22-24, 2013, Arlington (VA), USA.

[34] C. H. Rivetta, A. Emadi, G. A. Williamson, R. Jayabalan and B. Fahimi, “Analysis and Control of a Buck DC-DC Converter Operating With Constant Power Load in Sea and Undersea Vehicles”, *IEEE Transactions on Industry Applications*, vol. 42, no. 2, pp. 559-572, March/April 2006.

[35] A. Emadi, A. Khaligh, C. H. Rivetta and G. A. Williamson, “Constant Power Loads and Negative Impedance Instability in Automotive Systems: Definition, Modeling, Stability, and Control of Power Electronic Converters and Motor Drives”, *IEEE Transactions on Vehicular Technology*, vol. 55, no. 4, July 2006.

[36] A. Kwasinski and C. N. Onwuchekwa, “Dynamic Behavior and Stabilization of DC Microgrids With Instantaneous Constant-Power Loads”, *IEEE Transactions on Power Electronics*, vol. 26, no. 3, March 2011.

[37] P. Bolzern, R. Scattolini and N. Schiavoni, “Fondamenti di Controlli Automatici”, *McGraw-Hill*, 2003.

[38] H. K. Khalil, “Nonlinear systems”, *Prentice-Hall, Inc.*, 2002.

[39] C. Tunc and E. Tunc, “On the asymptotic behavior of solutions of certain second-order differential equations”, *Journal of the Franklin Institute*, El Sevier, 344, pp. 391-398, February 2006.

[40] C. J. Sullivan, S. D. Sudhoff, E. L. Zivi and S. H. Żak, “Methods of Optimal Lyapunov Function Generation with Application to Power Electronic Converters and Systems”, *IEEE Electric Ship Technologies Symposium (ESTS) 2007*, pp. 267-274, May 21-23, 2007, Arlington (VA), USA.

[41] S. F. Glover and S. D. Sudhoff, “An experimentally validated nonlinear stabilizing control for power electronics based power systems”, *Society of Automotive Engineers*, 981255, 1997.

[42] S. D. Sudhoff, K. A. Corzine, S. F. Glover, H. J .Hegner and H. N. Robey, Jr., “DC link stabilized field oriented control of electric propulsion systems”, *IEEE Transactions on Energy Conversion*, vol. 13, no. 1, March 1998.

[43] R. Marconato, “Electric power systems”, *CEI, Italian Electrotechnical Committee*, 2002-2004.

[44] IEEE Std. 421.5-2005, “IEEE Recommended Practice for Excitation System Models for Power System Stability Studies”, *IEEE Power and Energy Society*, August 2002.

[45] N. Mohan, T. M. Undeland and W. P. Robbins, “Power electronics: converters, applications and design", *John Wiley & Sons, Inc.*, 1995.

[46] F. Saccomanno, “Electric Power Systems: Analysis and Control”, *IEEE Press Series on Power Engineering*, 2003.

[47] B. P. Loop, S. D. Sudhoff, S. H. Zak and E. L. Zivi, “Estimating regions of asymptotic stability of power electronics systems using genetic algorithms”, *IEEE Transactions on Control Systems Technology*, vol. 18, no. 5, pp. 1011-1022, September 2010.

[48] A. M. Rahimi and A. Emadi, “Active damping in DC/DC power electronic converters: a novel method to overcome the problems of constant power loads”, *IEEE Transactions on Industrial Electronics*, vol. 56, no. 5, pp. 1428–1439, May 2009.

[49] D. Bosich and G. Sulligoi, “Voltage control on a refitted luxury yacht using hybrid electric propulsion and LVDC distribution”, *IEEE Ecological Vehicles and Renewable Energies Conference (EVER) 2013*, pp. 1-6, March 27-30, 2013, Monaco.

[50] J. G. Ciezki and R.W. Ashton, “The Design of Stabilizing Controls for Shipboard DC-to-DC Buck Choppers Using Feedback Linearization Techniques”, *29th Annual IEEE Power Electronics Specialists Conference (PESC) 1998*, vol. 1, pp. 335-341, May 17-22, 1998, Fukuoka (Japan).

[51] J. G. Ciezki and R.W. Ashton, “The application of feedback linearization techniques to the stabilization of DC-to-DC converters with constant power loads”, *IEEE International Symposium on Circuits and Systems (ISCAS) 1998*, vol. 3, pp. 526-529, May 31-June 3, 1998, Monterey (CA), USA.

[52] A. M. Rahimi, G. A. Williamson and A. Emadi, “Loop cancellation technique: a novel nonlinear feedback to overcome the destabilizing effect of constant-power loads”, *IEEE Transactions on Vehicular Technology*, vol. 59, no. 2, pp. 650-661, February 2010.

[53] G. Sulligoi, D. Bosich, L. Zhu, M. Cupelli and A. Monti, “Linearizing control of shipboard multi-machine MVDC power systems feeding constant power loads”, *IEEE Energy Conversion Congress and Exposition (ECCE) 2012*, pp. 691-697, September 15-20, 2012, Raleigh (NC), USA.

[54] W. S. Levine, “Control system advanced methods”, *CRC Press*, 2011.

[55] G. Sulligoi, D. Bosich and G. Giadrossi, "Linearizing voltage control of MVDC power systems feeding constant power loads: stability analysis under saturation”, *IEEE Power and Energy Society (PES) General Meeting 2013*, pp. 1-5, Jul. 21-25, 2013, Vancouver (BC), Canada.

[56] V. Arcidiacono, S. Castellan, R. Menis and G. Sulligoi, “Integrated Voltage and Reactive Power Control for All Electric Ship Power Systems”, *IEEE International Symposium on Power Electronics, Electrical Drives, Automation and Motion (SPEEDAM) 2006*, pp. 878-882, May 23-36, 2006, Taormina (Italy).

[57] A. Vicenzutti, D. Bosich and G. Sulligoi, “MVDC Power System Voltage Control through Feedback Linearization Technique: application to different Shipboard Power Conversion Architectures”, *IEEE Electric Ship Technologies Symposium (ESTS) 2013*, pp. 303-307, April 22-24, 2013, Arlington (VA), USA.

[58] G. Sulligoi, A. Tessarolo, V. Benucci, M. Baret, A. Rebora and A. Taffone, “Modeling, Simulation, and Experimental Validation of a Generation System for Medium-Voltage DC Integrated Power Systems”, *IEEE Transactions on Industry Applications*, vol. 46, no. 4, pp. 1304-1310, July/August 2010.

[59] G. Sulligoi, A. Tessarolo, V. Benucci, A. M. Trapani, M. Baret, F. Luise, “Design, Implementation and Testing of a Ship-Board Medium-Voltage DC Generation System Based on a Ultra-High Speed 12-Phase Alternator”, *IEEE Electric Ship Technologies Symposium (ESTS) 2011*, pp. 388-395, April 10-13, 2011, Alexandria (VA), USA.

[60] M. Aizza, D. Bosich, S. Castellan, R. Menis, G. Sulligoi and A. Tessarolo, “Coordinated speed and voltage regulation of a DC POWER generation system based on a woundfield split-phase generator supplying multiple rectifiers”, *6th IET International Conference on Power Electronics, Machines and Drives (PEMD) 2012*, pp. 1-6, March 27-29, 2012, Bristol (UK).

[61] A. Tessarolo, “Experimental performance assessent of multiphase alternators supplying multiple AC/DC power converters”, *5th IET International Conference on Power Electronics, Machines and Drives (PEMD) 2010*, pp. 1-6, April 19-21, 2010, Bristol (UK).

[62] A. Tessarolo, “Benefits of increasing the number of stator phases in terms of winding construction technology in high-power electric machines”, *5th IET International Conference on Power Electronics, Machines and Drives (PEMD) 2010*, pp. 1-6, April 19-21, 2010, Bristol (UK).

[63] I. Kondratiev and R. A. Dougal, “Synergetic control strategies for shipboard DC power distribution systems”, *American Control Conference 2007*, pp. 4744-4749, July 9-13, 2007, New York City (NY), USA.

[64] I. Kondratiev and R. A. Dougal, “Invariant based ship DC power system design”, *IEEE Electric Ship Technologies Symposium (ESTS) 2011*, pp. 15-20, April 10-13, 2011, Alexandria (VA), USA.

[65] G. Sulligoi, D. Bosich, V. Arcidiacono and G. Giadrossi, “Considerations on the design of voltage control for multi-machine MVDC power systems on large ships”, *IEEE Electric Ship Technologies Symposium (ESTS) 2013*, pp. 314–319, April 22-24, 2013, Arlington (VA), USA.

[66] V. Arcidiacono, E. Ferrari, R. Marconato, J. D. Ghali and D. Grandez, “Evaluation and Improvement of Electromechanical Oscillation Damping By Means of Eigenvalue-Eigenvector Analysis. Practical Results in the Central Peru Power System”, *IEEE Transactions on Power Apparatus and Systems*, vol. PAS-99 , no. 2, pp. 769-778, March 1980.

[67] G. Sulligoi, D. Bosich, G. Giadrossi, L. Zhu, M. Cupelli and A. Monti, “Multi-Converter Medium Voltage DC Power Systems on Ships: Constant-Power Loads Instability Solution using Linearization via State Feedback Control”, *IEEE Transactions on Smart Grid*, submitted.

[68] L. Zhu, J. Liu, M. Cupelli and A. Monti, “Decentralized linear quadratic gaussian control of multi-generator MVDC shipboard power system with constant power loads”, *IEEE Electric Ship Technologies Symposium (ESTS) 2013*, pp. 308-313, April 22-24, 2013, Arlington (VA), USA.

[69] F. Barati, D. Li and R. A. Dougal, “Voltage regulation in medium voltage DC systems”, *IEEE Electric Ship Technologies Symposium (ESTS) 2013*, pp. 372-378, April 22-24, 2013, Arlington (VA), USA.

Papers

[6] D. Bosich, M. Filippo, D. Giulivo, G. Sulligoi, A. Tessarolo. “Thruster motor start-up transient in an all-electric cruise-liner: Numerical simulation and experimental assessment”, *IEEE International Conference on Electrical Systems for Aircraft, Railway and Ship Propulsion (ESARS) 2012*, pp. 1-5, October 16-18, 2012, Bologna (Italy).

[10] G. Sulligoi, S. Castellan, M. Aizza, D. Bosich, L. Piva, G. Lipardi, “Active front-end for shaft power generation and voltage control in FREMM frigates integrated power system: Modeling and validation”, *IEEE International Symposium on Power Electronics, Electrical Drives, Automation and Motion (SPEEDAM) 2012*, pp. 452-457, June 20-22, 2012, Sorrento (Italy).

[11] G. Sulligoi, D. Bosich, T. Mazzuca, L. Piva, “The FREMM simulator: A new software tool to study electro-mechanic dynamics of the shipboard integrated power system”, *IEEE International Conference on Electrical Systems for Aircraft, Railway and Ship Propulsion (ESARS) 2012*, pp. 1-5, October 16-18, 2012, Bologna (Italy).

[12] G. Sulligoi, D. Bosich, A. Vicenzutti, L. Piva, G. Lipardi, T. Mazzuca, “Studies of electromechanical transients in FREMM frigates integrated power system using a time-domain simulator”, *IEEE Electric Ship Technologies Symposium (ESTS) 2013*, pp. 429-433, April 22-24, 2013, Arlington (VA), USA.

[49] D. Bosich and G. Sulligoi, “Voltage control on a refitted luxury yacht using hybrid electric propulsion and LVDC distribution”, *IEEE Ecological Vehicles and Renewable Energies Conference (EVER) 2013*, pp. 1-6, March 27-30, 2013, Monaco.

[53] G. Sulligoi, D. Bosich, L. Zhu, M. Cupelli and A. Monti, “Linearizing control of shipboard multi-machine MVDC power systems feeding constant power loads”, *IEEE Energy Conversion Congress and Exposition (ECCE) 2012*, pp. 691-697, September 15-20, 2012, Raleigh (NC), USA.

[55] G. Sulligoi, D. Bosich and G. Giadrossi, "Linearizing voltage control of MVDC power systems feeding constant power loads: stability analysis under saturation”, *IEEE Power and Energy Society (PES) General Meeting 2013*, pp. 1-5, Jul. 21-25, 2013, Vancouver (BC), Canada.

[57] A. Vicenzutti, D. Bosich and G. Sulligoi, “MVDC Power System Voltage Control through Feedback Linearization Technique: application to different Shipboard Power Conversion Architectures”, *IEEE Electric Ship Technologies Symposium (ESTS) 2013*, pp. 303-307, April 22-24, 2013, Arlington (VA), USA.

[60] M. Aizza, D. Bosich, S. Castellan, R. Menis, G. Sulligoi and A. Tessarolo, “Coordinated speed and voltage regulation of a DC POWER generation system based on a woundfield split-phase generator supplying multiple rectifiers”, *6th IET International Conference on Power Electronics, Machines and Drives (PEMD) 2012*, pp. 1-6, March 27-29, 2012, Bristol (UK).

[65] G. Sulligoi, D. Bosich, V. Arcidiacono and G. Giadrossi, “Considerations on the design of voltage control for multi-machine MVDC power systems on large ships”, *IEEE Electric Ship Technologies Symposium (ESTS) 2013*, pp. 314–319, April 22-24, 2013, Arlington (VA), USA.

[67] G. Sulligoi, D. Bosich, G. Giadrossi, L. Zhu, M. Cupelli and A. Monti, “Multi-Converter Medium Voltage DC Power Systems on Ships: Constant-Power Loads Instability Solution using Linearization via State Feedback Control”, *IEEE Transactions on Smart Grid*, submitted.